Development of a β-catenin stability sensor

Dissertation

Katrin Prost

Fakultät für
Chemie und Chemische Biologie
der Technischen Universität Dortmund

Vorgelegt im Mai 2015

von Katrin Prost

Gutachter:
Prof. Dr. Philippe Bastiaens
Prof. Dr. Jan Hengstler

Work presented in this dissertation was performed in the laboratory of
Prof. Dr. Philippe Bastiaens at the Max-Planck-Institute of Molecular Physiology,
Dortmund, Germany.

Eidesstattliche Versicherung

Ich versichere hiermit an Eides statt, dass die vorgelegte Dissertation von mir selbständig und unter Angabe aller verwendeten Quellen angefertigt wurde.

Dortmund, den …….. …….……

(Unterschrift)

Erklärung

Ich erkläre, dass meine Dissertation in der gegenwärtigen oder einer anderen Fassung weder an der Technischen Universität noch an einer anderen Hochschule im Zusammenhang mit einer staatlichen oder akademischen Prüfung vorgelegt wurde. Ich habe mich an keiner anderen Hochschule einer Promotionsprüfung unterzogen.

Dortmund, den …….. …….……

(Unterschrift)

Contents

1 Abstract

Wnt/β-catenin signalling plays a major role in almost all biological processes like embryogenesis, development and homeostasis. Therefore, countless studies over the past decades from multiple research fields unravelled the structure of β-catenin and its interaction partners as well as the kinetics of Wnt-dependent and -independent β-catenin activation. However, surprisingly, there is still a lack of knowledge about the spatio-temporal β-catenin activation, as the key player in Wnt/β-catenin signalling. The correlation of β-catenin structure and function with its activation in time and space will provide insight into the dynamic regulation of β-catenin at the single cell level.

One possible tool, an intramolecular biosensor monitoring the stability of β-catenin in single living cells, is presented in this thesis. The basic principle, used to measure the relative stability of the sensor molecule, is the difference in maturation kinetics of a FRET pair of two fluorophores. With this, the sensor molecule contains an intramolecular "concentration" and a "half-lifetime" marker.

In addition, genetic modifications of β-catenin yield a sensor (1) specific for monitoring only Wnt-dependent (canonical Wnt/β-catenin pathway) ß-Catenin activation, as well as (2) it does not report on β-catenin stability changes mediated via growth factor stimulation of RTKs and is (3) inert for downstream transcriptional activation. Therefore, the biosensor neither interferes with the degradation kinetics of endogenous β-catenin nor the downstream effectors or the induction of feedback loops. These modifications ensure, that fold change by stabilization upon Wnt ligand induction were recorded by the stability sensor.

Wnt stimulation induced stabilization of the sensor molecules within hours after application, measurable with FLIM and ratiometric widefield imaging. Comparison with available transcriptional reporter systems revealed a faster response time for the sensor molecules on single-cell level. Thus, the sensor, but not reporters with delayed response times, enables the detection of early Wnt-dependent signalling events as well as cell history and fate with live cell imaging.

2 Zusammenfassung

Der Wnt/β-catenin Signalweg spielt in nahezu allen biologischen Prozessen, wie der Embryogenese, Entwicklung aber auch der Homöostase, eine essentielle Rolle. Studien mit unterschiedlichsten Schwerpunkten untersuchten daher in den letzten Jahrzenten sowohl die Struktur und Funktion von β-catenin und einer Anzahl Interaktionspartner, wie auch die Aktivierung der Wnt Signalwege. Die Verknüpfung der Struktur und Funktion von β-catenin mit der räumlich-zeitlichen Aktivierung wird Einblicke in die dynamische Regulation von β-catenin auf Einzelzellniveau liefern.

In der vorliegenden Arbeit wird zu diesem Zweck ein intramolekularer, genetisch codierter Biosensor für die Stabilität von β-catenin in einzelnen lebenden Zellen präsentiert. Für die Entwicklung dieses neuartigen Sensors wurde ein FRET Paar fluoreszenter Proteine mit unterschiedlichen Chromophor-Reifungszeiten verwendet, um die relative Stabilität des Sensors zu definieren. Zusätzlich ergeben genetische Modifikationen einen Sensor, der (1) spezifisch für Wnt induzierte β-catenin Aktivierung ist, (2) nicht die Änderung in der Stabilität vermittelt durch RTK Aktivierung anzeigt und (3) keine transkriptionelle Aktivität besitzt. Dadurch verändert der Sensor weder die Degradationskinetik des endogenen β-catenin, noch die transkriptionelle Aktivität oder die Aktivierung von *feedback* Schleifen. Es wird durch den Sensor die Stabilisierung des β-catenins nach Stimulation mit Wnt Liganden angezeigt.

In FLIM und konventionellen Fluoreszenzmikrokopischen Messungen konnte die Wnt induzierte Stabilisierung des Biosensors innerhalb weniger Stunden nach Induktion nachgewiesen werden. Der Vergleich mit publizierten β-catenin Transkriptionsreportern zeigt, dass der β-catenin Stabilitätssensor deutlich schneller und auf Einzelzellniveau die Aktivierung des Wnt Signalweg anzeigt. Mit diesem β-catenin Stabilitätssensor sind wir nun in der Lage, Ursprung und Schicksal einzelner Zellen nach Wnt Stimulation mit der Stabilisierung von β-catenin zu korrelieren und live in lebenden Zellen zu verfolgen.

3 Introduction

The β-catenin protein is highly conserved throughout all metazoans and involved in a variety of signalling pathways, converging input from different signalling cascades[1]. Studies over the past decades revealed a complex interplay with other proteins as well as tight regulations of β-catenin in order to keep signalling pathways in check. Misbalances following mutations, deletions or overexpression of β-catenin have a severe impact on development and homeostasis, often resulting in cancer and metastasis[2]. Conditional as well as conventional knock-out studies addressed the systemic and tissue-specific relevance of β-catenin and highlighted β-catenin as a signalling hub for a list of developmental processes as well as the balance between proliferation and differentiation[3].

3.1 β-catenin activation sites in the cell

Throughout the cell, different pools of β-catenin mediating signalling or contributing to the cytoskeleton exist (Figure 1). At the plasma membrane, more specific at the site of adherens junctions, β-catenin interacts with E-cadherin and α-catenin, thereby influencing the actin cytoskeleton. This interaction can be disassembled during cytoskeleton rearrangements, but also through receptor tyrosine kinase activity, releasing the β-catenin into the cytosol. In the cytosol, β-catenin becomes phosphorylated and degraded by the destruction complex, in the Wnt "Off" state of the Wnt/β-catenin pathway (discussed below). A small fraction remains soluble but protected from degradation by interaction with APC. In presence of Wnt ligand, the destruction complex is inhibited and β-catenin becomes stabilized. Nuclear β-catenin interacts with TCF/Lef family of transcription factors regulating target gene induction, a general signalling output of any Wnt signalling cascade. At the centrosome, β-catenin and other components of the Wnt pathway accumulate and regulate microtubule growth[4].

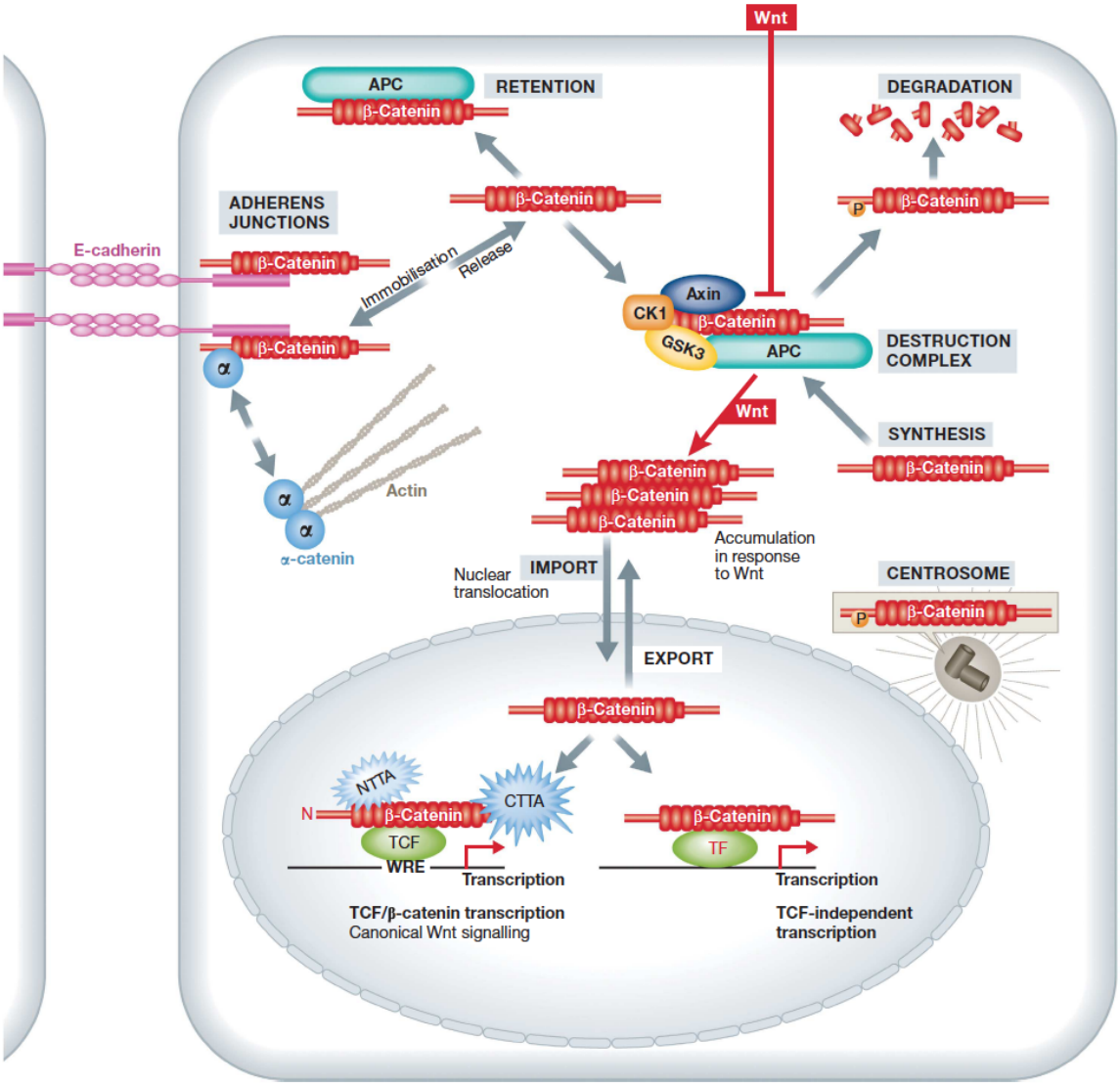

Figure 1: **Current model of β-catenin interactions and signalling activities throughout the cell.** At the site of adherens junctions, β-catenin interacts with E-cadherin and influences the actin cytoskeleton via α-catenin. β-catenin becomes phosphorylated and degraded by the destruction complex, although a small fraction remains soluble protected by APC interaction. In presence of Wnt ligand, the destruction complex is inhibited and β-catenin stabilized. β-catenin translocates to the nucleus and interacts with TCF/Lef family of transcription factors. At the centrosome, β-catenin and other components of the Wnt pathway accumulate and regulate microtubule growth[4]. CTTA, C-Terminal Transcriptional Activators, NTTA, N-Terminal Transcriptional Activators.

3.2 Structural features of β-catenin

Human β-catenin consists of 781 aa residues, aa 138–664 represent the 12 central armadillo (ARM) repeats[5,6]. ARM repeats are repetitive sequences of 42 aa which form 3 α–helices ordered in a triangular shape, leading to a right-handed superhelix with a positive charge at the inner groove[6]. This positively charged

groove provides an interaction platform for the majority of β-catenin interaction partners with highly overlapping interaction sites. At the N-terminal domain (NTD) of β-catenin, regulatory serine (S) and threonine (T) residues determine the ubiquitination or the interaction with α–catenin[7-11], respectively. Therefore these sites are involved in the regulation towards the proteasomal degradation machinery or interactions with the adherens junctions. At the C-terminal end a conserved helix structure is located between the last ARM repeat and the flexible C-terminal domain (CTD) (aa 667-683)(Figure 2).

Figure 2: **Domain structure of β-catenin.** The flexible N-terminal domain contains regulatory S/T residues, targeted for ubiquitination upon phosphorylation by GSK3β and CK1. The central 12 rigid helical ARM repeats (1-12) provide an interaction platform with a positively charged groove, followed by a C-terminal α-helix (C) and a flexible C-terminal domain[4].

As a central interaction platform, β-catenin provides competitive binding sites for multiple proteins (Figure 3). Therefore, interactions with E-cadherin, APC, as well as TCF/Lef family transcription factors are mutually exclusive, leading to an additional level of signal transmission regulation. The three major roles of β-catenin within the cell can not be transduced by the same molecule at the same time. Most nuclear interaction partners of β-catenin interact with the last two ARM repeats and the C-terminal domain of β-catenin, predominantly mediating interactions with the transcription complex, including proteins that rearrange histones, remodel chromatin structures and provide interaction platforms with the DNA. The nuclear interaction partners lead to retention of β-catenin in the nucleus and prolong the half-lifetime of the molecule. Thus, truncated versions of β-catenin, lacking C-terminal parts or the entire C-terminal domain, exhibit reduced half-lifetimes as well as reduced transcriptional activity[12,13].

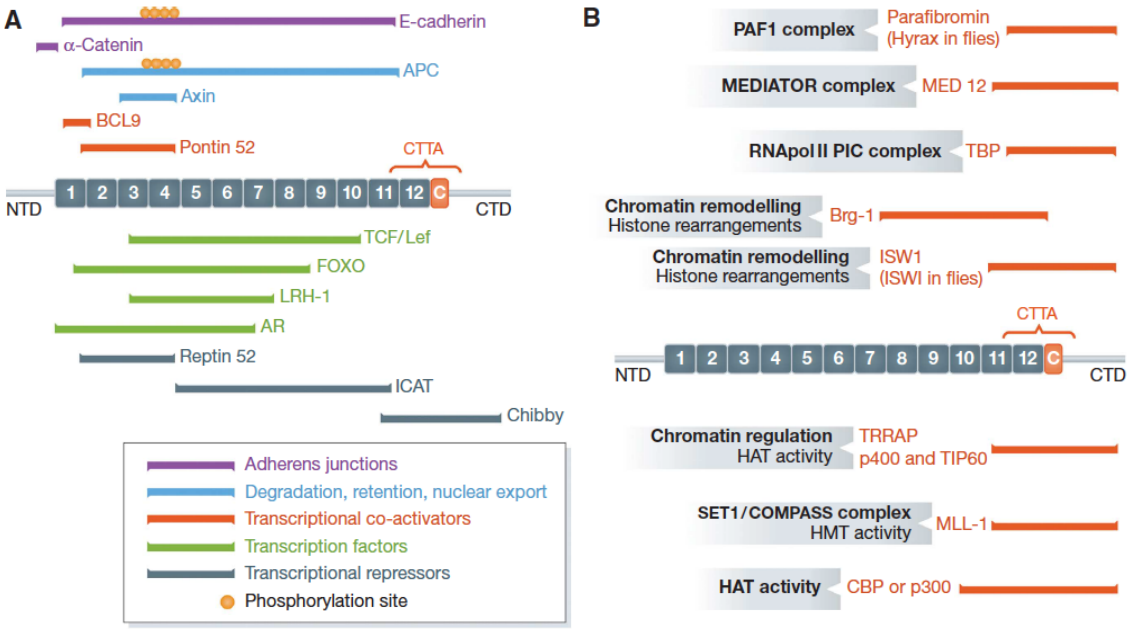

Figure 3: **Interaction partners of β-catenin.** A. Schematic description of interaction sites on β-catenin. High overlap of interactions sites within the armadillo repeats. B. Signal transduction complex formation platform at the C-terminal domain of β-catenin[4].

A plethora of post-transcriptional modifications on β-catenin have been identified until now (Figure 4). Most of which mediate signalling or are related to the degradation machinery. In addition, there are also some modifications connected to adherens junctions via E-cadherin or alpha-catenin binding. By phosphorylation/dephosphorylation or other posttranslational modifications of amino acid residues in the ARM repeats certain binding partners are favoured, as discussed below.

MODIFICATION	SITES	ENZYME	FUNCTION (enhancement of)	REFERENCES
Ser/Thr phosphorylation	S33, S37	GSK3	Degradation, provides sites for β-TrCP	Winston *et al* (1999) Liu *et al* (1999)
	T41	GSK3	Degradation, phosporylation relay site	Wu and He (2006)
	S45	CK1	Degradation, priming for GSK3	Liu *et al* (2002)
	T112	CK2	Adhesion, promotes α-catenin binding	Bek and Kemler (2002)
	T120	PKD1	Inhibition of signalling by immobilization of β-catenin in trans-Golgi	Du *et al* (2009) Du *et al* (2012)
	S191	JNK2	Nuclear translocation	Wu *et al* (2008)
	S246	Cdk5	Inhibition of APC binding (via Pin 1)	Muñoz *et al* (2007)
	T393	CK2	Signalling, promotes stability	Song *et al* (2003)
	S552	Akt, PKA	Signalling	Fang *et al* (2007)
	S605	JNK2	Nuclear translocation	Wu *et al* (2008)
	S675	PKA	Signalling, enhancement of CBP binding	Fang *et al* (2007) van Veelen *et al* (2011)
	S675	PAK (p21 activ. kinase)	Signalling, promoting stability and transcription	Zhu *et al* (2012)
	S23, S29	CK2 (?)	Stability (?)	van Noort *et al* (2002)
	(?) (in *Drosophila*)	Hipk, HipK2	Promoting stability of Armadillo (opposite in other system reported)	Lee *et al* (2009) Kim *et al* (2010)
	S764, S802, S827 (sites not in vertebrates)	NLK	Connecting Armadillo–E-cadherin complex with Wnt/PCP pathway	Mirkovic *et al* (2011)
Tyr phosphorylation	Y654	Src	Signalling, reduces cadherin binding allows TBP binding	Huber and Weis, (2001) van Veelen *et al* (2011)
	Y142	Fer/Fyn; Met	Signalling, reduces α-catenin binding	Brembeck *et al* (2004) Bustos *et al* (2006)
	Y86, Y654	Bcr-Abl, Abl	Signalling, stabilizing β-catenin	Coluccia *et al* (2007)
	Y333	Src (EGFR mediated)	Signalling, promotes nuclear function in response to EGF (Wnt independent)	Yang *et al* (2011 b)
	Y489	Abl	Signalling, disrupts binding to N-cadherin	Rhee *et al* (2007)
	Y654, Y670	Met (?)	Signalling, HFG-mediated release from membrane	Zeng *et al* (2006)
Ubiquitylation	K19	SCF ubiquitin ligase	Degradation	Wu *et al* (2003)
	K666, K671	Siah-1	Degradation, block of signalling	Dimitrova *et al* (2010)
Acetylation	K49	CBP	Signalling, enhancement of target specific β-catenin transcription *(c-myc)*	Wolf *et al* (2002)
	K345	p300	Signalling, increases binding of TCF, reduces binding to AR	Lévy *et al* (2004)
Glycosylation	(?)	O-GlcNAc transferase	Reduces nuclear localization	Sayat *et al* (2008)

Figure 4: **Post-translational modifications of β-catenin.** Phosphorylation and other post-translational modifications of β-catenin regulate its binding affinities and therefore signalling activity and trafficking[4].

Certain sites were identified being involved predominantly in Wnt-independent β-catenin stabilising pathways and transcriptional activation. Growth factor induced activation of c-src via the epithelial growth factor receptor (EGFR) for example, leads to phosphorylation of β-catenin at tyrosine 333, allowing pyruvate kinase M2 (PKM2) binding to β-catenin in the nucleus[14]. Upon PKM2 binding CyclinD1 expression is facilitated. Although this interaction is so far only reported for EGFR-promoted β-catenin transactivation in proliferation and tumorigenesis of cancer tissue, it could be a general mechanism of Wnt independent β-catenin signalling. It is highly likely, that this mechanism is not restricted to EGFR but would occur with other receptor tyrosine kinase (RTK) activation as well[14]. The p21-activated kinase 1 (PAK-1), a Rac1 effector, interacts with β-catenin and

phosphorylates it at serine 675 in the C-terminal domain, stabilizing it and promoting transcriptional activation[15]. This activation is reported to occur subsequent to K-ras induction in colorectal cancer in a Wnt independent way. Serine 552 as direct target of Akt-1/PKB, becomes phosphorylated subsequent to growth factor induced PI3K activation[16]. β-catenin phosphorylated at S552 results in nuclear translocation and stabilization of β-catenin. E-cadherin binds to β-catenin in adherens junctions at the plasma membrane. Upon growth factor stimulation, β-catenin is phosphorylated at tyrosine 654 by RTKs and released from the E-cadherin complex[17]. Thereby Wnt independent activation of β-catenin translocation and transcription is induced, due to a massive fold-change in cytosolic β-catenin levels..

3.3 Wnt signalling

β-catenin plays a key role in Wnt signalling, which organizes and regulates a whole set of events in cells, as well as tissues, organs and organisms. During early stage development, Wnt gradients trigger the formation of the body axis, but also cause partitioning of tissue and organ structure. Besides the Wnt/β-catenin pathway, also called "canonical" Wnt pathway, Wnt ligands can induce the "non-canonical" Wnt/RTK (RYK/ROR) pathway, the Ca^{2+} dependent and G-protein coupled receptor-dependent Wnt pathways[18].

3.3.1 Wnt ligands and receptors

Wnt ligands are secreted, cysteine-rich glycol-lipoproteins of approximately 400 aa length. 19 Wnt ligands are known in mammals, but generally all metazoans express some. The first purified and biochemically characterized Wnt ligand was murine Wnt3a[19], since Wnt3a is more efficiently secreted than other Wnt ligands. Wnt3a is palmitoylated at cysteine 77 as well as serine 209[19,20]. In addition it is N-linked glycosylated[21]. While glycosylation and S209 palmitoylation is mandatory for secretion, C77 palmitoylation is required for Wnt/β-catenin activation (Figure 5).

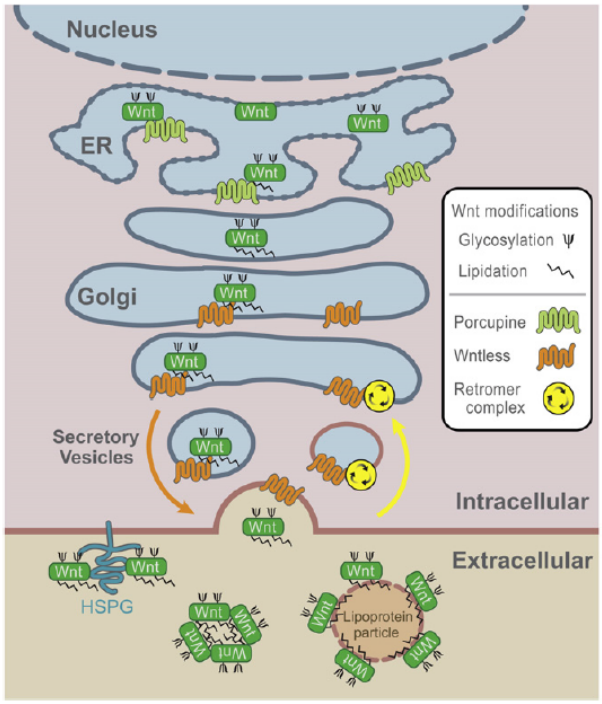

Figure 5: **Wnt ligand secretion.** The current model of posttranslational modification of Wnt3a ligand describes the N-linked glycosylation, followed by Porcupine catalysed S209 palmitoylation in the ER. The carrier protein Wntless (WLS) recognizes modified Wnt3a for trafficking to the plasma membrane. [22]

These lipidations lead to poor solubility and secretion of Wnt3a and most other Wnt ligands. Porcupine, an ER-resident, membrane-bound O-acetyltransferase, catalyzes S209 palmitoylation of Wnt3a[20]. This modification is required for the carrier Wntless to bind the ligand and subsequent trafficking to the plasma membrane (PM). Where and by which enzyme C77 becomes palmitoylated remains unknown.

Once secreted, Wnt ligands can act as morphogens over long and short distances. A proposed model for short range Wnt activity is the "loading" of a neighbouring cell by a Wnt secreting cell, rather than free diffusion through the extracellular space. This mechanism was called "restricted diffusion", since it depends on the interaction with receptor and lipoproteins on the cell surface in the extracellular space[23]. For long distances Wnt ligands could interact with each other via their lipid modifications and therefore become more soluble. In addition, Wnt ligand interaction with lipoproteins, especially heparan sulphate proteoglycans, promotes stability and homing of Wnt ligands to membranes[24]. These effects are reflected by a higher stability and activity of purified Wnt3a, when the protein is solubilized in artificial liposomes[25]; either due to enhanced solubility or by direct

recruitment to membranes, since liposomes interact with the plasma membrane via hydrophobic interactions.

Two families of receptors are responsible for Wnt ligand recognition in Wnt/β-catenin signalling (Figure 6). In mammalian cells Frizzled (Fz), a family of 10 7-transmembrane-receptors, and Low-density lipoprotein receptor related protein (LRP) 5 or 6 as co-receptor form heterodimers [26,27]. These 10 Fz variants have diverse specificities for the 19 different Wnt ligands and vary in their capacity to induce Wnt/β-catenin signalling activity[28]. LRP5, though important for adult bone homeostasis, is dispensable for embryogenesis; while LRP6 as the more dominant co-receptor of Fz is always essential. Both LRP5 and 6 are required for mouse gastrulation[27]. Induced by Wnt3a stimulation, Fz and LRP5/6 form a heterodimeric complex, which requires palmitoylation of Wnt3a on C77[21,29]. In contrast to its role in Wnt/β-catenin signalling, LRP6 is inhibitory for non-canonical Wnt pathways, possibly by competition for Wnt ligand binding[30].

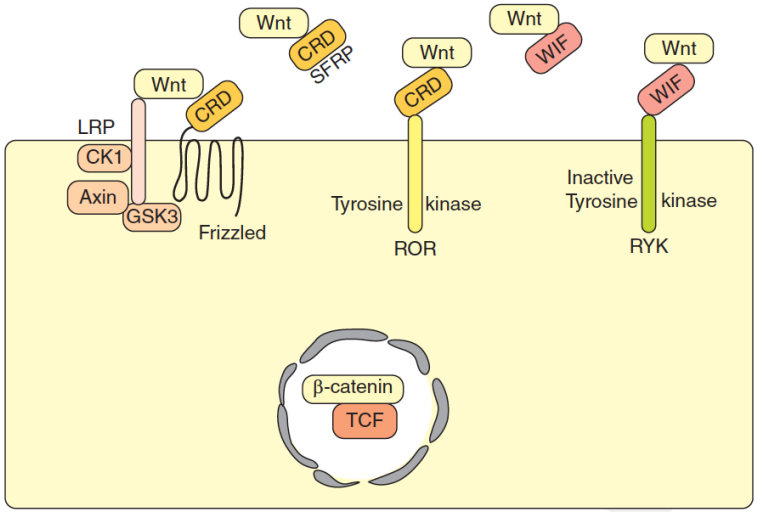

Figure 6: **Model of Wnt receptors.** Beside Wnt/β-catenin receptors FZ/LRP, ROR and Ryk RTKs can bind Wnt ligands as part of the non-canonical Wnt pathway activation.[31]

Two receptor tyrosine kinases, Ryk and ROR, have been identified as Wnt receptors in the Wnt/RTK pathway (reviewed in [18,31]) (Figure 6). Ryk, a catalytically inactive RTK, contains an extracellular Wnt inhibitory factor (WIF) domain that binds to Wnt ligands with high affinity[32-35]. The intracellular domain of Ryk was reported to be dispensable for functionality of the receptor, whereas the extracellular WIF domain is essential[34,36]. This qualifies Ryk rather as a co-receptor than a signalling receptor. One possible interaction partner is Fz, since it

has been shown that Ryk stimulates Fz activity in neurite outgrowth of mammalian cells in cell culture and *in vivo* independent of Wnt/β-catenin signalling[37]. Recently, Ryk, although shown to be dispensable for Wnt/β-catenin signalling before, has been reported to enhance/activate β-catenin signalling in dependence of its interaction partner Mindbomb1[38].

Another alternative receptor family is the single transmembrane receptor tyrosine kinase ROR, as represented by ROR1 and ROR2. Like Fz receptors and secreted Fz related proteins (sFRP), they have an extracellular cysteine rich domain for Wnt binding[39-41]. ROR1 and ROR2 are evolutionary conserved through vertebrate and invertebrate species and found to be overlapping expressed in various tissues during embryonic development in mice. The expression of ROR2 drops down directly before birth, while ROR1 remains expressed on a lower level in adult tissue[41,42]. In contrast to Ryk, ROR2 has an active tyrosine kinase domain. Autonomous activation through ROR2 forced dimerization leads to tyrosine phosphorylation, while native ligand binding induces tyrosine as well as serine/threonine phosphorylation[43]. Wnt5a is a known ligand for ROR2. The proposed mechanism of native ligand activation is the formation of a ROR2/Fz heterodimer, followed by an activation of the Wnt/β-catenin signalling cascade. Since Wnt5a is discussed to be inhibitory for Wnt/β-catenin signalling[31], these findings strengthen the model that Wnt ligand identity might determine, which pathway is activated, rather than a certain receptor. ROR1 is lacking tyrosine kinase activity and most likely functions as a pseudokinase, similar to Ryk.

3.3.2 Natural Wnt agonists and antagonists

R-spondin proteins act similar to Wnt ligands, through direct binding to LRP5/6, as well as Fz receptors. R-spondin genes are often co-expressed with Wnt and are dependent on Wnt expression itself, maybe due to a positive feedback accelerating Wnt activation[44]. Norrin, which regulates vascularization of the vertebrate retina and ear during development, is specific for Fz4 and induces Wnt signalling through Fz4/LRP5/6 heterodimerization[44,45].

In general, secreted Fz related proteins (sFRP) and Wnt inhibitory factor (WIF) bind to Wnt, sFRPs and to Fz, thereby blocking Wnt signalling through competition for binding sites [46]. WIF is secreted and binds to Wnt ligands in the extracellular

space, thus inhibiting receptor binding (Semënov et al., 2001). Downstream effects of WIF administration were described as a reduction in Wnt dependent gene expression (Hsieh et al., 1999). Proteins of the Dickkopf family and WISE/SOST family are more specific for Wnt/β-catenin signalling inhibition since they disrupt Fz-LRP complex formation, induced by Wnt [47-50]. Shisa interacts (among others) with immature Fz receptors in the ER, preventing posttranslational maturation of these receptors and their trafficking to the plasma membrane. Other proteins interacting either with Wnt ligands, Fz or LRP5/6 receptors are bone morphogenic protein and Insulin-like growth factor binding protein-4 both of which antagonise Wnt activity[51,52].

3.3.3 Wnt/β-catenin signalling

For historical reasons, the Wnt/β-catenin signalling, initiated by the activation of a LRP5/6 and Frizzled receptor heterodimer upon Wnt ligand binding, is termed the canonical Wnt signalling pathway. Subsequent recruitment of the destruction complex (see below) to the LRP5/6 complex results in β-catenin stabilization in the cytosol. This leads to a prolonged half-lifetime of β-catenin as the most abundant key player in Wnt/β-catenin signalling.

In absence of Wnt/β-catenin signalling, the destruction complex, consisting of Axin, *adenomatous polyposis coli* (APC), glycogen synthase kinase 3-β (GSK3β), and casein kinase 1 (CK1), is formed (Figure 7). The scaffold protein Axin binds to GSK3β, CK1, APC, and β-catenin via separate domains. This binding coordinates phosphorylation of β-catenin residue serine 45 by CK1, priming the β-catenin for subsequent phosphorylation at threonine 41, serine 37 and serine 33 by GSK3β[53]. The β-catenin S37 and S33 phosphorylation provide an interaction site for the β-transducin repeat containing E3 ubiquitin protein ligase (β-Trcp). Ubiquitination leads to proteasomal degradation of β-catenin. Mutations in the N-terminal domain or N-terminal truncations of β-catenin often result in a disruption of the β-Trcp interaction, causing stabilization of β-catenin and affecting cancer development. Mutations of the tumour suppressor genes Axin and APC, leading to truncated and less efficient scaffold proteins, are also correlated with tumour formation, most notably in colorectal cancer[54,55].

In addition to β-catenin phosphorylation, the kinases GSK3β and CK1 phosphorylate Axin and APC, which leads to a higher binding affinity for β-catenin and acceleration of β–catenin phosphorylation and degradation[53,56]. Wilms tumour suppressor protein also facilitates Axin binding to β-catenin, although little is known about the mechanism[57]. Diversin can recruit CK1ε to the complex to enhance β-catenin phosphorylation and degradation[58].

Protein phosphatase 1 (PP1) dephosphorylates Axin, counteracting GSK3β and CK1, while β-catenin is dephosphorylated by protein phosphatase 2 A (PP2A)[59,60]. PP2A also associates with Axin, as the scaffold protein in the degradation complex. The interaction of β-catenin with APC might protect β-catenin from PP2A dephosphorylation as one mechanism for β-catenin retention in the cytosol. Upon APC phosphorylation by CK1 and GSK3β, phosphorylated APC competes with Axin for the same binding site on β-catenin thus leading to „unloading" of phosphorylated β-catenin from the degradation complex. The phosphorylated β-catenin is now recognized by β-Trcp for ubiquitination and the degradation complex free for another β-catenin phosphorylation cycle[53,61].

Both Axin and APC control their expression levels in a bilateral way. If APC is highly expressed it promotes Axin degradation[62]. In case of low APC, Axin levels are elevated[63]. Axin overexpression on the other hand facilitates APC degradation[64]. Neither for Axin nor for APC proteasomal degradation mechanisms have been described yet.

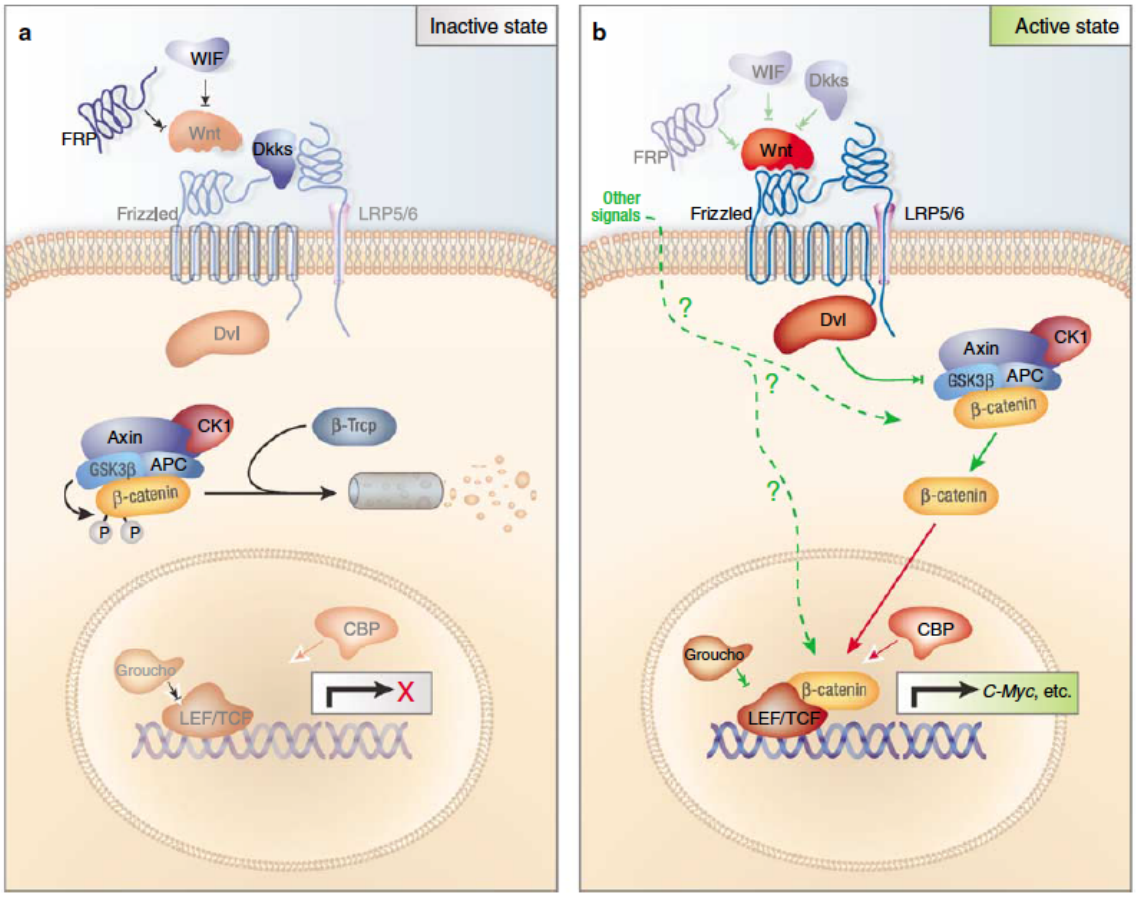

Figure 7: **Wnt/β-catenin signalling.** A. In absence of Wnt ligand, β-catenin is constantly targeted by the APC/Axin/GSK3-β/CK-1 complex. After S45 phosphorylation by CK-1, β-catenin is primed for GSK3-β phosphorylation at S33/S37/T41, thus generating the binding site for β-TrCP, an E3 ligase. Subsequent ubiquitination and proteasomal degradation constantly keep β-catenin levels low. B. Upon Wnt ligand binding, Dishevelled is recruited to Fz receptor. Phosphorylated LRP5/6 recruits Axin to the plasma membrane and β-catenin is stabilized and translocates to the nucleus, where it associates with TCF/Lef family transcription factors and thereby regulates target gene transcription[65].

In presence of Wnt/β–catenin signalling, the Wnt receptors Fz and LRP5/6 are recruited in a Wnt induced complex. LRP5/6 is dually phosphorylated after Wnt ligand binding on each of its five intracellular PPPSPxS motifs by GSK3β and CK1. The first phosphorylation seems to be PPPS by GSK3β in the GSK3β-Axin complex, followed by phosphorylation of xS by CK1[66-68]. Phosphorylated LRP5/6 recruits Axin in complex with GSK3β to the PM, pointing to a feed forward loop enhancing LRP5/6 phosphorylation[56]. Wnt signalling can be efficiently inhibited by a membrane tethered GSK3β inhibitory peptide (CAAX-GID)[69]. LRP5/6 depends on Fz receptor function, which itself depends on Dishevelled (Dvl). Since Dvl acts as a cytoplasmic scaffold, interacting with Axin, and is indispensable for Axin recruitment to the plasma membrane, GSK3β phosphorylation of LRP5/6 might be

mediated via Axin after initiation of the Axin translocation by a Fz-Dvl interaction[69]. Besides this, Dvl is an interaction partner of multiple other proteins, including CK1δ and ε, PP2A and phosphatidylinositol-4-phosphate 5-kinase I. Thereby Dvl is involved in several regulatory aspects of LRP5/6 phosphorylation and activation. An additional protein, facilitating recruitment of Axin-GSK3β to the plasma membrane, is the microtubule actin cross-linking factor 1 (MACF1). MACF1 was found to link F-actin to microtubules in the cytosol. It is involved in cellular polarization and the coordination of cellular movements[70]. In the absence of Wnt, MACF1 interacts with the degradation complex, including APC, in the cytosol and upon Wnt stimulation with the Axin-GSK3β complex at the membrane[71]. The cytosolic Axin-GSK3β complex gets rapidly disrupted upon Wnt stimulation, involving G protein activation by Fz receptor and Dvl recruitment, accompanied by inhibition of β-catenin phosphorylation[72]. In addition, it can be dissociated by PP1 dephosphorylation of Axin, but whether this is Wnt-induced or constitutive remains unknown[59]. Another model, which aims to explain the inhibition of β-catenin phosphorylation, is the inhibition of GSK3β by the intracellular domain of phosphorylated LRP. Axin degradation[73,74] and APC increase[64,75] are most likely downstream, but potentially a bilaterally regulated effect of β-catenin stabilization.
Stabilized β-catenin interacts with a multitude of proteins, both in the cytosol and in the nucleus. How β-catenin shuttles between these distinct locations is not well understood. While Axin and APC seem to bind β-catenin preferentially in the cytoplasm, interaction partners of the β-catenin C-terminal domain cause enrichment in the nucleus.
Once translocated to the nucleus via the interaction of armadillo-repeats with nucleoporins[76], β-catenin can bind to TCF/Lef family transcription factors. It functions as a transcription regulator leading to transcription of target genes. In competition with canonical Wnt signalling, there are also TCF/Lef-independent transcription factors as platforms for β-catenin/DNA binding e.g. during cell lineage determination[77]. How the decision towards the interaction with this transcription factors is regulated, remains unfortunately unclear. The signal termination is generally thought to be controlled by the export of β-catenin from the nucleus, e.g. via interaction with APC or RanBP3[78]. On a transcriptional level, the modulation of β-catenin signalling could be controlled by TCF1. TCF1 itself is

induced by β-catenin/TCF4 transcriptional activity. The most abundant isoforms of TCF1 lack a β-catenin interaction site but interact with Groucho, the transcriptional repressor of TCF/Lef family of transcription factors, thus repressing β-catenin/TCF4 transcriptional induction[79]. Additionally, there is a potential negative feedback on β-catenin stability via rapid expression of Conductin (also known as Axin2 or Axil), induced by β-catenin transcriptional activity after translocation. Besides its role in axis formation during embryonic development, Conductin is a scaffold protein homolog to Axin. Upon expression, Conductin can substitute Axin within the degradation complex, thus generating a more efficient degradation of β-catenin. This is described as one possible mechanism to modulate or shut down β-catenin signalling activity[80]. Downstream of the degradation complex, the E3 Ligase specific for β-catenin, β-Trcp targets β-catenin for ubiquitination and subsequent proteasomal degradation. As it is itself a target of β-catenin/TCF transcriptional induction, β-catenin/TCF activity facilitates β-catenin degradation[81]. The sum of β-catenin transport and retention by interaction partners determines the overall distribution of β-catenin throughout the cell.

3.3.4 Wnt/β-catenin signalling in cell cycle regulation and progression

Upon Wnt/β-catenin signalling, transcriptional regulation of different target genes is induced, including c-myc and CyclinD1. The effect of β-catenin on c-myc transcription is direct, whereas CyclinD1 expression is promoted by the Wnt induced GSK3β inhibition. Both, c-myc and CyclinD1 stimulate G1 cell cycle progression[82-85]. C-myc induces Cyclin D expression and represses p21 and p27, two proteins that inhibit Cyclin E and thereby G1/S transition[84,85]. GSK3β itself is destabilizing cell cycle effectors by phosphorylation and priming for proteasomal degradation. After Wnt stimulation, GSK3β inhibition leads to stabilization of its target proteins, among which are c-myc, CyclinD1 and CyclinE1, further promoting cell cycle progression.

During mitosis, multiple components of the Wnt/β-catenin pathway are involved in microtubule dynamics, spindle formation and centrosome segregation[86]. Stabilizing mutations in β-catenin, depletion of Conductin and long-term GSK3β

inhibition was shown to reduce microtubule growth, while acute GSK3β inhibition promoted microtubule reorganization[87].

Conductin and APC localize at the mitotic spindle, where APC connects microtubule plus ends to the kinetochores in order to induce chromosome segregation. In case of Conductin overexpression, its interaction with Plk1 induces chromosome instability[88]. Dvl though cooperates with Plk1 in order to establish spindle orientation, Fz/LRP6 coreceptors were reported to be involved but not necessarily Wnt ligands[89]. GSK3β- phosphorylated β-catenin, Conductin and GSK3β also localize to the centrosomes, which align the mitotic spindle[87]. They contribute to the centrosome division by regulation of microtubule growth.

Some components of the Wnt/β-catenin pathway are expressed in an oscillating fashion with the cell cyle, e.g β-catenin and its target genes Lgr5 and Conductin in G2/M[90]. This is explained by priming of LRP5/6 for Wnt signaling by phosphorylation of its PPPSP motif through cyclin-dependent kinase 14. Cyclin-dependent kinase 14 itself is associated with Cyclin Y, therefore expressed in the G2/M phase of the cell cycle[91]. C-myc on the other hand peaks in G1/S[92].

3.3.5 Wnt signalling in liver regeneration

Among the adult organs, the liver is unique in its high ability to regenerate. In resting adult mouse hepatocytes, β-catenin is predominantly localized at the plasma membrane, bound either to receptor tyrosine-kinases (RTKs) (30-40% to c-Met[93]) or to E-cadherin at the site of adherens junctions[94]. Throughout the liver lobule, the smallest structural unit in the liver, there is a gradient of Wnt vs. extracellular-signal regulated kinase activation in the resting liver, contributing to the liver lobule metabolic zonation, which expands and overlaps in the priming phase of liver regeneration[95] (Figure 8). In case of acute liver damage e.g. partial hepatectomy (PHx) or toxic liver failure, Wnt/β-catenin activation is one of the earliest events in order to start liver regeneration. Although Wnt is active in resting adult liver hepatocytes only in the pericentral region, Wnt/β-catenin activation during liver regeneration induces proliferation in a panlobular manner[96]. How this panlobular activation takes place and what pre-activation state the proliferating cells had, remains yet unclear due to the lack of tools and methods to directly observe it. A recent study provides evidence that Wnt ligands

are secreted not by hepatocytes, macrophages or cholangiocytes, but by Kupffer cells and indeed Wnt/β-catenin signalling is the major upstream effector of β-catenin activation during liver regeneration after PHx[97]. In the midlobular region, ERK activation and Wnt activation overlaps during liver regeneration, therefore the interplay between Ras and Wnt signalling would be interesting to investigate in order to unravel how hepatocyte proliferation is driven during regenerative processes.

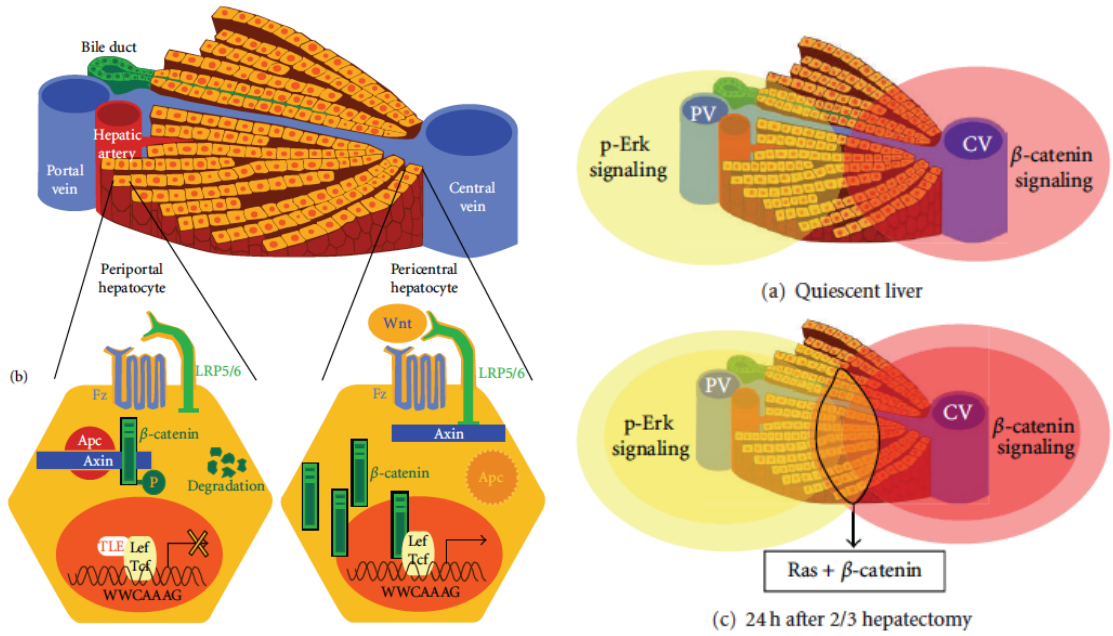

Figure 8: **Model of Wnt signalling activation in the adult liver lobule.** Due to high APC levels in the periportal region, β-catenin is constantly degraded. In the pericentral hepatocytes, Wnt signalling is present, even in the resting state. Upon liver damage (e.g. PHx), the region of activated Wnt signalling expands.[96]

3.4 Wnt reporter systems

A lot of studies were performed with the existing β-catenin transcriptional reporter system called "TOPflash", using a Luciferase or, more recently, a destabilized GFP sequence, controlled by a TCF/Lef binding site (CCTTTGATC) oligomer as the reporter for β-catenin transcriptional activity[98-100]. The destabilized fluorophore should speed up the reporter response and minimize the backgroung fluorescence. In TCF/Lef:H2B-GFP transgenic mice, this reporter expression was used to determine spatio-temporal transcriptional Wnt response on tissue level during embryonal development[101]. The derivatives of the

"TOPflash" system are powerful tools to investigate transcriptional activity of β-catenin interacting with transcription factors of the TCF/Lef family. However, the major disadvantage is the high background of transcriptional activity, which is not necessarily driven by Wnt/β-catenin dependent nuclear translocation of β-catenin. In addition, it neglects the probability of β-catenin binding to other transcription factors (e.g. forkhead box proteins (FOXO), sequestering β-catenin under oxidative stress conditions)[102], as well as the non-transcriptionally active β-catenin pools outside of the nucleus, e.g. at adherens junctions.

4 Objective

Multiple components of the Wnt/β-catenin signalling pathway undergo continuous feedback cycles in order to regulate signalling activity within the cell. Although the energy costs for continuous β-catenin protein expression is high, it seems to be beneficial for the cell to be able to respond much faster to Wnt ligand binding due to the continuous supply of β-catenin, than a transcriptionally induced system would allow for. In addition it also allows the system to adapt to chronic perturbations by a balance between β-catenin level and negative feedback loop induced higher degradation rates. This explains why Wnt/β-catenin signalling should be measured as a relative increase in stability rather than absolute levels of β-catenin protein within the cell. In order to address and directly observe β-catenin as the key molecule in Wnt/β-catenin signalling, a FRET-based biosensor that reports changes of β-catenin stability as an early indicator of the activation of canonical Wnt signalling pathway has to be developed. The challenge is to set up a sensor that only reports β-catenin stability induced by Wnt and that neither interferes with the degradation kinetics of the endogenous β-catenin nor the downstream effectors or the induction of feedback loops.

Aiming for a better understanding of spatio-temporal (Wnt/) β-catenin signalling in living cells, the sensor will be developed in cell culture. Later on, this approach should be transferred from cultured cell lines into primary hepatocytes. Live-cell imaging will reveal new insights into the β-catenin molecular activities in time and space.

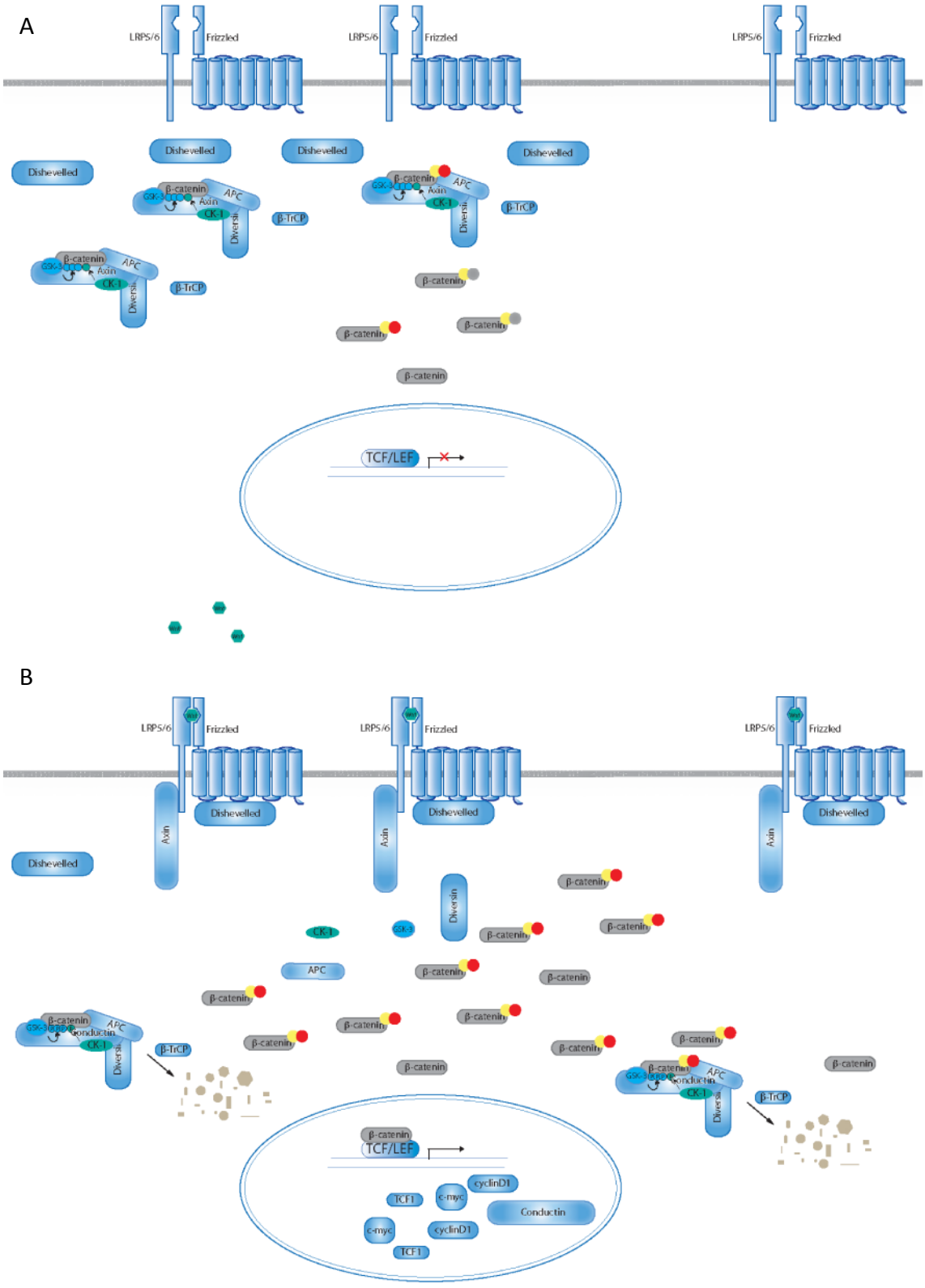

Figure 9: **Principle of the proposed β-catenin stability sensor.** In the absence of Wnt ligand, β-catenin is constantly targeted for degradation by the APC/Axin/GSK3-β complex. The aim of the β-catenin stability sensor is to report changes concerning the stability of β-catenin. A. When Wnt signalling is absent, β-catenin and the sensor molecules are constantly degraded and therefore the acceptor does not have enough time to mature. B. Upon Wnt stimulation, canonical Wnt signalling is activated thus leading to disassembly of the degradation complex and stabilization of β-catenin and the sensor molecules, thus providing time for the acceptor fluorophore to mature. Stabilized endogenous β-catenin translocates to the nucleus, inducing target gene expression. The temporal profile of β-catenin activation can be directly observed and correlated with the localization and environment of the cells.

5 Material and Methods

5.1 Material

5.1.1 Buffers, media and solutions

5.1.1.1 Molecular Biology

10x DNA loading buffer	50 % glycerol, 0.1 M EDTA, 0.1 % Orange G in H_2O
1x TAE buffer	40 mM Tris/Acetate (pH 7.5), 20 mM NaOAc, 1 mM EDTA
2-log DNA ladder	1 mg/ml 2-log DNA ladder (NEB) diluted in 1x DNA loading buffer (50 µg/ml)
LB agar plates	15 g/l agar in LB medium (ZE Biotechnologie, MPI Dortmund)
LB agar plates with antibiotics	15 g/l agar in LB medium, autoclaved, supplemented with respective antibiotics (ZE Biotechnologie, MPI Dortmund)
LB medium	10 g/l Bacto-Trypton, 5 g/l yeast extract, 10 g/l NaCl, pH7.4 (ZE Biotechnologie, MPI Dortmund)
SOC medium	20 g/l Bacto-Trypton, 5 g/l Bacto-yeast extract, 0.5 g/l NaCl, 2.5 mM KCl, 10 mM $MgCl_2$, 20 mM glucose (ZE Biotechnologie, MPI Dortmund)

5.1.1.2 Proteinbiochemistry

10 % APS	100 mg/ml APS in H_2O (freshly prepared)
10 % SDS	100 g/l SDS in H_2O
1x TBS	50 mM Tris-HCl (pH 7.4), 150 mM NaCl
1x TBS-T	50 mM Tris-HCl (pH 7.4), 150 mM NaCl, 0.1 % Tween-20
5x SDS sample buffer	60 mM Tris-HCl (pH 6.8), 25 % glycerol, 2 % SDS, 14.4 mM 2-mercapto-ethanol, 0.1 % bromo-phenolblue
SDS running buffer	25 mM Tris-base, 192 mM glycine, 0.1 % SDS
Separating gel buffer	1 M Tris-HCl (pH 8.8)
Stacking gel buffer	0.375 M Tris-HCl (pH 6.8)
Transfer buffer	25 mM Tris-base, 192 mM glycine, 20 % (v/v) methanol

5.1.1.3 Cell culture

1M NaOH	1M NaOH in H_2O
1x PBS	138 mM NaCl, 10 mM Na_2HPO_4, 2.7 mM KCl, 1.8 mM KH_2PO_4, pH 7.4
4% PFA	4 g para-formaldehyde, 1 x PBS (pH 7.4)
$CaCl_2$ solution	130 mM $CaCl_2$
Collagenase buffer	28 mM D(+)-glucose, 100 mM NaCl, 2.3 mM KCl, 1.2 mM KH_2PO_4, 25 mM HEPES pH 8.5, 0.15 vol. Amino acids, 500 µM L-Glutamine, 5 mM $CaCl_2$, 350 U/ml Collagenase
DMEM FGM	10 % FCS, 1 % NEAA and 2 mM L-Glutamine in DMEM high glucose
DMEM starvation	0.1 % FCS, 1 % NEAA and 2 mM L-Glutamine in DMEM high glucose
EGTA buffer	28 mM D(+)-glucose, 100 mM NaCl, 2.3 mM KCl, 1.2 mM KH_2PO_4, 25 mM HEPES pH 8.5, 0.15 vol. Amino acids, 500 µM L-Glutamine, 0.5 mM EGTA
EGTA solution	125 mM EGTA, NaOH for solvation, pH 7.6 with HCl
Glucose solution	45 mM D(+)glucose-monohydrate
Glutamine (perfusion)	48 mM l-Glutamine
HEPES pH 7.6	250 mM HEPES pH 7.6
HEPES pH 8.5	250 mM HEPES pH 8.5
KH buffer	1 M NaCl, 23.5 mM KCl, 12 mM KH_2PO_4, pH 7.4 with NaOH
$MgSO_4$ solution	100 mM $MgSO_4$
PBS (perfusion)	135 mM NaCl, 2.7 mM KCl, 10mM Na_2HPO_4, 2 mM KH_2PO_4, pH 7.4
Suspension buffer	28 mM D(+)-glucose, 100 mM NaCl, 2.3 mM KCl, 1.2 mM KH_2PO_4, 25 mM HEPES

	pH7.6, 0.15 vol. Amino acids, 500 µM L-Glutamine, 1 mM $CaCl_2$,, 0.4 mM MgSO4, 4g/l BSA
William's E FGM	10 % SeraPlus in William's E starvation Medium
William's E starvation Medium	William's E Medium, 1 % Penicillin/Streptomycin, 2 mM L-Glutamine, 10 µg/ml Gentamycine, 0.001 % ITS reagent, 100 nM Dexamethasone

5.1.2 Kits and Commercials

5.1.2.1 Oligonucleotides

All oligonucleotides were purchased from MWG Eurofins as unmodified DNA Oligos.

5.1.2.2 Plasmids

pcDNA™3.1+	Invitrogen™ Life Technologies
pmCherry	Clontech Laboratories Inc.
pmCitrine-N1	Clontech Laboratories Inc.
pmKate2	Evrogen Laboratories Inc.
pmPlum	Clontech Laboratories Inc.
pmRaspberry	Clontech Laboratories Inc.
pmTagBFP-N	Evrogen Laboratories Inc.
pTCF/Lef:H2B-GFP	Addgene # 32610, Depositor: Anna-Katerina Hadjantonakis

5.1.2.3 Cloning

100 mM dNTP set (#10297-117)	Invitrogen™ Life Technologies
10x Pfu amplification buffer (#600384)	Agilent Technologies
2-log DNA ladder (#N3200)	New England Biolabs Inc.
5x T4 DNA Ligation Buffer (#46300-018)	Invitrogen™ Life Technologies
BigDye® Terminator v 3.1 Cycle sequencing kit (#4337455)	Invitrogen™ Life Technologies
Bovine serum albumin (BSA) (20 mg/ml) (#B9000)	New England Biolabs Inc.
Calf intestinal phosphatase (CIP) (10,000 U/ml)(#M0290)	New England Biolabs Inc.
CutSmart™ Buffer (#B7204)	New England Biolabs Inc.
DNA clean and concentrator™ kit (#D4004)	Zymo Research Corporation
High-fidelity (HF®) restriction endonucleases	New England Biolabs Inc.
NucleoBond® finalizer (#740519)	Macherey-Nagel GmbH und Co. KG
NucleoBond® Xtra Midi/Maxi EF Kit (#740422)	Macherey-Nagel GmbH und Co. KG
NucleoSEQ (#740523)	Macherey-Nagel GmbH und Co. KG
OneShot® Stbl3™ chemically competent E.coli (#C7373-03)	Invitrogen™ Life Technologies
PfuUltra High-fidelity DNA Polymerase 2.5 U/µl (#600384)	Agilent Technologies
QuickLigation™ Kit (#M2200)	New England Biolabs
Restriction endonucleases	New England Biolabs Inc.
Roti®-Prep Plasmid Mini Kit (#HP29)	Carl Roth GmbH
T4 DNA Polymerase (#18005-025)	Invitrogen™ Life Technologies
TE-EF and H_2O-EF	Macherey-Nagel GmbH und Co. KG
UltraPure™Agarose (#16500-500)	Invitrogen™ Life Technologies
XL10-Gold® Ultracompetent cells (#200314)	Agilent Technologies (amplified and provided by J. Luig and L. Rossmannek)
Zymoclean™ Gel DNA Recovery Kit (#D4001)	Zymo Research Corporation

5.1.2.4 Biochemistry

10x Cell lysis Buffer (#9803)	Cell Signaling
Albumin bovine fraction V, pH 7.0 (BSA) (#11930)	Serva Electrophoresis GmbH
cOmplete, Mini, EDTA-free Protease Inhibitor Cocktail Tablets (#04693159001)	Roche Diagnostics
Immobilon-FL polyvinylidene fluoride (PVDF) membrane (#05317)	Merck-Millipore
Odyssey Infrared Imaging System blocking buffer (#927-40000)	LI-COR Biosciences GmbH
Phosphatase Inhibitor Cocktail 2 (#P5726)	Sigma-Aldrich®
Phosphatase Inhibitor Cocktail 3 (#P0044)	Sigma-Aldrich®
Precision Plus ProteinTM Dual Color Prestained standard (#161-0374)	Bio-Rad Laboratories, Inc.
Protease Inhibitor Cocktail Tablets (#04693132001)	Roche Diagnostics
Rotiphorese® NF-acrylamide/bis-solution 40 % (29:1) (#A121.1)	Carl Roth GmbH
Whatman filter paper	Fisher Scientific

5.1.2.5 Cell culture

Albumine bovine fraction V, ph 7.0 (#11930.02)	Serva Electrophoresis GmbH
Amino acid solution, special formulation (#SO-33100)	PAN Biotech Inc.
Collagen R solution 0.2 % (#47254)	Serva Electrophoresis GmbH
Collagen, cell culture grade, (#11179179001)	Roche Diagnostics
Dexamethasone 100 µM (#D8893)	Sigma-Aldrich®
DMEM 10x 100ml (# D2429)	Sigma-Aldrich®
DMEM high glucose (#P04-03600)	PAN Biotech Inc.
DMEM high glucose without phenolred (#P04-01163)	PAN Biotech Inc.
DPBS (#P04-36500)	PAN Biotech Inc.
Fetal calf serum (FCS)(#P30-0402)	PAN Biotech Inc.
Fugene HD (#E2312)	Promega Corporation
Gentamycine sulphate 10 mg/ml (#P06-03001)	PAN Biotech Inc.
ITS reagent (#I3146)	Sigma-Aldrich®
L-Glutamine 200 mM (#P04-80100)	PAN Biotech Inc.
MCF7 (ATCC® HTB-22™) HEK293 (ATCC® CRL-1573™) HEK293-T (ATCC® CRL-3216™) A431 (ATCC® CRL-1555™) Caco-2 (ATCC® HTB-37™)	ATCC American tissue culture collection
Non-essential amino acids 100x (MEM NEAA)(#P08-32100)	PAN Biotech Inc.
Penicillin (10,000 U/ml)/Streptomycin (10 mg/ml) (#P06-07100)	PAN Biotech Inc.
SeraPlus (#P30-3700)	PAN Biotech Inc.
Trypsin-EDTA solution (#P10-023100)	PAN Biotech Inc.
William's E Medium (#P04-29510)	PAN Biotech Inc.

5.1.2.6 Animal resources and hepatocyte preparation

C57/Bl6N, 8-12 weeks, male	Janvier Labs, France
Catherter IV Insyte-W 24Gx0.75 inch (#BDAM381312)	VWR International GmbH
Cell strainer 100 µm, yellow, sterile (#734-0004, BD)	VWR International GmbH
Cell Trics 10 µm (#04-004-2324)	Partec Inc.
Collagenase CLSII (#C2-22)	Biochrom AG
Discofix 3-way valves (#16494)	Ryma Pharm GmbH
ES-Kompressen 8-fach 7.5x7.5 cm (#HART401823/6)	VWR International GmbH
Glass bottom 6-well plates, 1.5H glass bottom (#P06-1.5H-N)	IBL Baustoff + Labor GmbH

High-Med silicone hose 1x3 mm 5 m (#339912)	Reichelt Chemietechnik GmbH
Hose coupling olive N7, PVDF (#F1179931)	Gilson International
Hose coupling olive N8, PVDF (#F1179941)	Gilson International
Insert for screw caps GL14 3.0 mm (#5209454)	Omnilab
Insert for screw caps GL14 3.2 mm (#5209455)	Omnilab
IR bulb 100 W PAR38 clear (#01244209)	Philips
Ketamin 10 % (Ketaminhydrochlorid 100 mg/ml)	
LS-2 Connector, LL (#4097122)	Ryma Pharm GmbH
Membrane filter PTFE GL14 (#5209459)	Omnilab
Minipuls 3 perfusion pump	Gilson International
Mucasol® (#60442)	Merz Hygiene GmbH
Neubauer improved, C-Chip (#PK36.1)	Carl Roth GmbH
Perfusor® lines PE, 1.5x2.7 mm, 150 cm (#8722960)	Ryma Pharm GmbH
Perfusor® lines PE, 1x2 mm, 100 cm (#8255067)	Ryma Pharm GmbH
Pressure compensation set for 2 and 3 port caps (#5209457)	Omnilab
Rompun® 2% (Xylazinhydrochlorid 20 mg/ml)	Bayer AG
Rotilabo cotton buds, wood, sterile (#EH12.1)	Carl Roth GmbH
Screw cap GL14 (#BUCH032884)	VWR international GmbH
Screw cap GL45 PP 2 ports GL14 (#5209450)	Omnilab
Screw caps GL14 for hose connection (#5209452)	Omnilab
Sterican injection needle 0.55x25 mm, G24 (#612-0146)	VWR International GmbH
Sterican Insulin injection needle 0.4x12 mm, G27 (#5427806)	Omnilab
Surgical instruments	Gebrüder Martin GmbH & Co. KG
Syringe 1 ml Luer lock, Omnifix, (#612-2899)	VWR International GmbH
Syringe 20 ml Luer lock, Omnifix (#612-2898)	Braun Melsungen
Thomafluid®-High-Med-TPE-S hose 3 mm x 6 mm, 5m (#351086)	Reichelt Chemietechnik GmbH
Thomafluid®-High-Med-TPE-S hose 5 mm x 6 mm, 5m (#351098)	Reichelt Chemietechnik GmbH

5.1.2.7 Antibodies

Primary antibodies	Dilution WB	Company
anti-active β-catenin (mouse)(#05-665)	1:500	Merck-Millipore
anti-cmyc (rabbit)	1:1000	Cell signaling
anti-GAPDH (mouse)(6C5)(#CB1001)	1:5000	Calbiochem, Merck Biosciences
anti-GSK3β (rabbit)	1:1000	Cell signaling
anti-H2B (rabbit)	1:1000	Cell signaling
anti-TCF1 (rabbit)	1:1000	Cell signaling
anti-tRFP (rabbit)(#AB234)	1:1000	Evrogen
anti-β-catenin (goat)(#AF1329)	1:1000	R&D Systems
anti-β-catenin (rabbit)(#sc-7199)	1:1000	Santa Cruz Bioscience
anti-β-catenin NTD (rabbit) clone E247 (#04-1002)	1:1000	EMD Millipore

Secondary antibodies	Dilution	Company
Alexa Fluor® 546 donkey anti-rabbit IgG(#A10040)	1:1000	Invitrogen™ Life Technologies
Alexa Fluor® 647 Goat Anti-Mouse IgG (#A21236)	1:1000	Invitrogen™ Life Technologies
IRDye® 680 donkey anti-rabbit IgG	1:10000	LI-COR® Biosciences
IRDye® 800CW donkey anti-goat IgG (926-32214)	1:10000	LI-COR® Biosciences
IRDye® 800 donkey anti-mouse IgG	1:10000	LI-COR® Biosciences

5.1.2.8 Ligands and inhibitors

Substance	reconstitution	company
GSK3β inhibitor SB216763 (#10010246)	50 mM in DMSO	Cayman Chemical Company
Porcupine inhibitor LDK974 (#M60106-2)	10 mM in DMSO	Xcess Bioscience Inc.
Recombinant murine Wnt3a, purified (#315-20)	10 µg/ml in 0.1 % BSA in PBS	PeproTech GmbH
Tankyrase inhibitor IWR-1 endo (#13659)	100 mM in DMSO	Cayman Chemical Company
Wnt inhibitory factor (WIF-1)(#1341-WF-050)	200 µg/ml in 0.1 % BSA in PBS	R&D Systems

5.1.3 Microscopes

Cell^R	Olympus
Leica TCS SP5	Leica Microsystems
Motic	Motic
FluoView1000	Olympus
Fiber coupling Uni	Picoquant GmbH
Sepia II controller	Picoquant GmbH

5.1.4 Software

Adobe Illustrator	Adobe Systems Inc.
FV10-ASW Fluoview Software	Olympus
Fiji	Schindelin et al. Nat. Meth. (2012)
Microsoft Office 2011	Microsoft Corporation
Leica Application Suite	Leica
NanoDrop ND-1000	Coleman Technology Inc.
Quantity One 4.6.9	Bio-Rad Laboratories, Inc.
ImageJ64 v1.44	http://rsbweb.nih.gov/
SymPhoTime v5.12	Picoquant GmbH
Odyssey® Infrared Imaging System Application software Version 2.1	LI-COR Biosciences GmbH
Multiscan Ascent Software Version 2.6	ThermoElectron Coorperation
Image Studio Lite Version 4.0.21	LI-COR Biosciences GmbH
IgorPro v6.12	WaveMetrics
DNASTAR Navigator Version 11.0.0.164	DNASTAR Inc.

5.1.5 General material and equipment

2-Mercapto-ethanol	SERVA Electrophoresis GmbH
Acetic acid conc.	
Acetone	Fluka
Ammonium persulfate (APS)	SERVA Electrophoresis GmbH
Ampicillin sodium salt	SERVA Electrophoresis GmbH
Bromophenolblue	Sigma-Aldrich®
Dimethyl sulfoxide (DMSO)	SERVA Electrophoresis GmbH
Dithiothreitol (DTT)	Fluka® Analytical
Ethanol (EtOH)	J.T.Baker
Ethylenediaminetetracetic acid (EDTA)	Fluka® Analytical
Glycerol	GERBU Biotechnik GmbH
Isopropanol	J.T.Baker
Kanamycin sulfate	GERBU Biotechnik GmbH
Magnesium chloride ($MgCl_2$)	Merck KG/J.T.Baker
Methanol (MeOH)	AppliChem GmbH
N,N,N',N'-Tetramethylene-diamine (TEMED)	Sigma-Aldrich®
Para-formaldehyde (PFA)	Serva

Sodium chloride (NaCl)	Fluka® Analytical
Sodium dodecyl sulfate (SDS)	SERVA Electrophoresis GmbH
Sodiumhydroxide (NaOH)	
Tris-base	Carl Roth GmbH
Tris-HCl	J.T.Baker
Triton X-100	SERVA Electrophoresis GmbH
Tween 20	SERVA Electrophoresis GmbH

"Vortex Genie 1" touch mixer	Scientific Industries
1.5 mm 10-well combs	InvitrogenTM Life Technologies
1.5 mm cassettes for western blots	InvitrogenTM Life Technologies
35-mm MatTek petri dishes No. 1.5	MatTek Corporation
4-well LabTek® chambers No. 1.0	Nalge Nunc International
AutoFlow NU-4750 Water Jacket CO_2 Incubator	Integra Biosciences
BioRad Power Pac HC	Bio-Rad Laboratories, Inc.
Cell scraper 16 cm 2-Pos.-blade (#83.1832)	Sarstedt AG und Co.
Centrifuge 5415R	Eppendorf
Centrifuge 5810R	Eppendorf
Eppendorf safe lock tubes (0.5/1.5/2 ml)	Eppendorf
Falcon tubes (15/50 ml)	BD Falcon™
Heatable magnetic stirrer "IKMAG®RCT"	IKA®Labortechnik
Heating block "QBD4"	Grant Instruments
Incubation box for western blots	Li-Cor® Biosciences
Incubator Shaker Series I26	New Brunswick Scientific
MilliQ water, Millipore Advantage A	Millipore
Mini and Midi agarose gel chamber	Carl Roth GmbH
Molecular Imager Gel Doc XR	Bio-Rad Laboratories, Inc.
Nanodrop® ND-1000 spectrophotometer	Peqlab Biotechnologie GmbH
NUAIRE™ Cellgard class II biological safety cabinet	Integra Biosciences
Odyssey Infrared Imager	Li-Cor® Biosciences
Parafilm®	Pechiney Plastic Packaging
PFE powder-free latex exam gloves (S)	Kimberly-Clark
Pipetboy acu	Integra Biosciences
Research, Research Plus and Reference pipettes	Eppendorf
Safe Imager™	Invitrogen™
Safegrip® nitril gloves	Süd-Laborbedarf GmbH
Sarstedt serological pipettes (5/10/25 ml)	Sarstedt Aktiengesellschaft & Co.
Surgical disposable scalpel (No. 11, No.21)	Braun Melsungen AG
Thermomixer comfort	Eppendorf
Tissue culture plates	BD FalconTM
Vacusafe comfort	Integra Biosciences
XCell II™ Blot Module	InvitrogenTM Life Technologies
XCell SureLock™ Mini-Cell Electrophoresis System	InvitrogenTM Life Technologies

5.2 Methods

5.2.1 Molecular biology

5.2.1.1 Cultivation of E.coli

Single colonies grown on agar plates with antibiotics (37 °C, o.n.) were transferred into 2-4 ml LB medium containing the appropriate antibiotics. This pre-cultures, grown for 6-10 h at 37 °C and 200 rpm shaking, were directly used for plasmid preparation or to inoculate the desired volume for large-scale plasmid preparations (5.2.1.4).

5.2.1.2 Transformation of chemically competent cells

100 µl chemically competent *E.coli XL10 Gold* cells were gently mixed with 10 ng pDNA for retransformation or 2-7 µl ligation reaction or DpnI digested Mutagenesis-PCR mix and incubated on ice for 20-30 min. Afterwards the transformation reaction mix was heat-shocked at 42 °C for 45 s and cooled for 2 min on ice. 600 µl SOC medium was added and transformation reactions were incubated at 37 °C, 200 rpm shaking for 1 h. Successfully transformed bacterial cells developed the plasmid-encoded antibiotic resistance during this time. Re-transformations are diluted 1:500 before plating, while ligation reactions and Mutagenesis-PCRs were plated on two plates in a 1:10 dilution and the rest of the transformation reaction. LB-agar plates containing the appropriate antibiotics were incubated o.n. at 37 °C or at RT for 72 h to obtain single colonies.

5.2.1.3 DNA preparation using Roti®-Prep Plasmid Mini Kit

According to the manufacturers standard protocol, 2-4 ml bacterial culture transformed with the desired plasmid were harvested at 8000 x g in a conventional table top microcentrifuge. Acidic lysis and neutralization according to the users manual was performed in order to obtain purified plasmid DNA in 30 µl elution buffer or MilliQ water.

5.2.1.4 Endotoxin-free plasmid DNA preparation with NucleoBond® Xtra Midi/Maxi EF Kit

Endotoxin-free plasmid purification was carried out according to the users manual. Usually plasmids were treated as low-copy plasmids in order to obtain high plasmid yield. 150-300 ml LB medium in an Erlenmeyer flask were inoculated with

1-4 ml pre-culture prepared as described before (1.1.1.1). Bacterial wet pellet was obtained by centrifugation for 20 min at 4000 x g, 4 °C in a standard tabletop centrifuge with a swinging bucket rotor. Precipitation of plasmid DNA was followed by loading to the NucleoBond® finalizer according to the users manual. Ultra-pure plasmid DNA was eluted twice with 300 µl TE-EF or H_2O-EF, before a second elution took place using 200 µl.

5.2.1.5 UV/VIS spectrophotometric determination of DNA concentration

The quality and concentration of isolated pDNA was determined using a NanoDrop spectrophotometer. 1 µl elution buffer or MilliQ water was used as a reference "blank". The DNA concentration was determined by measurement of 1 µl of the sample in elution buffer or MilliQ water at 260 nm. The quality of the sample was determined by measurements of the 260/280 nm as well as 260/230 nm ratio.

5.2.1.6 Agarose gel electrophoresis of DNA

To obtain agarose gels, 0.6-2 % low-melting point UltraPure agarose was melted in 1x TAE buffer, supplemented with RedSafe nucleic acid staining solution (20.000x) and poured into Mini or Midi gel chambers. RedSafe is a chemical that intercalates into dsDNA and can be visualized using a conventional UV-table, excited by UV light (309 nm), but as well by 419 nm and emission can be detected at 537 nm (orange/red). DNA fragments to be separated determined the agarose concentration used: 2 % for 0.1-3 kb, 1 % for 0.5-8 kb and 0.6 % for 1-12 kb. For electrophoresis gels were transferred to electrophoresis chambers, filled up with 1x TAE buffer, loaded with samples and 2-log DNA ladder (1 µg). Constant voltage of 60-80 V for Mini or 100-120 V for Midi gels was applied for 20-40 min. After gel electrophoresis images of the DNA separation were taken using the molecular imager Gel Doc XR (Bio-Rad).

5.2.1.7 Isolation of DNA fragments from agarose gels

The Zymo Gel Extraction Kit was used for DNA gel extraction up to 10 µg DNA (70 bp to 10 kb). The DNA fragment of interest was excised from the agarose gel, weighted and dissolved in 2 volumes ADB buffer at 50 °C for 5-10 min. In a column-based procedure DNA was bound to a silica-membrane in a column under high salt conditions according to the users manual. Contaminating small DNA

fragments (<50 bp), proteins and agarose were washed off in two washing steps, before DNA was eluted in 6-10 µl H_2O or EB.

5.2.1.8 Purification of DNA fragments from PCR reactions

The Zymo DNA clean and concentrator kit follows the same approach like the gel extraction kit for DNA fragment purification. DNA of any origin can be dissolved in high salt buffer and bound to a silica-membrane in a column. According to the manufacturers protocol contaminating small DNA fragments (<50 bp), proteins and salt are washed off in two washing steps, before DNA elution in 6-10 µl H_2O or EB.

5.2.1.9 Restriction digest

Up to 3 µg dsDNA were digested in a 50 µl reaction mix containing 5 µl reaction buffer (10x), 0.5 µl BSA (100x) if indicated, 5 U/µg DNA of each restriction enzyme (NEB) and MilliQ H_2O (ad 50 µl). The restriction mix was incubated at 37°C for 1 h up to 16 h to completely digest dsDNA. Reactions were set up according to the "double digest finder" online tool on NEB website.

5.2.1.10 Dephosphorylation of 5´-DNA ends

To inhibit religation, the digested vector DNA 5´-end can be dephosphorylated by alkaline phosphatase after restriction digest of the vector.

For 5´-dephosphorylation 1 U CIP was added to a restriction digest reaction mix and incubated for at least 5 min at 37 °C.

5.2.1.11 Ligation pDNA with Inserts

50-100 ng cut and dephosphorylated vector was mixed with a 3-5x molar excess of cut insert DNA, calculated according to:

$$insert[ng] = \frac{molar\ excess \times vector[ng] \times insert\ size[kb]}{vector\ size[kb]}$$

The vector/insert DNA mix was adjusted to 10 µl with MilliQ H_2O and then mixed with 10 µl 2x QuickLigase buffer before 1 µl QuickLigase was added. Ligation reaction incubated 5 min at RT before transformation into chemically competent bacterial cells.

5.2.1.12 Amplification of DNA fragments

The PCR primers (forward and reverse) are designed to hybridize with the template DNA on sense and anti sense strand using DNAStar Software. For calculation of the approximate primer melting temperature T_m see:

$$T_m = \left[\left(2 \cdot nA + nT\right) + 4 \cdot \left(nG + nC\right)\right]°C - 5°C$$

The number of PCR cycles varied between 20 (Mutagenesis PCR) and 35 (very short sequence amplification e.g. for colony PCR). PfuUltra high fidelity DNA polymerase was used for standard cloning procedures according to manufacturers standard protocol, unless otherwise described. With an error rate of 1 per 2.5×10^6 bases, even plasmids can be amplified without mismatching.

Table 1: **50 µl standard PCR reaction mixture using PfuUltra HF polymerase**

DNA template	100 ng
dNTPs (10mM each)	1 µl
Forward primer	100 ng
Reverse primer	100 ng
10x PfuUltra reaction buffer	5 µl
PfuUltra HF polymerase (2.5 U/µl)	1 µl
H_2O	ad 50 µl

Table 2: **Standard PfuUltra PCR protocol**

1x	dsDNA denaturation	95 °C	2 min
30x	dsDNA denaturation	95 °C	30 s
	Annealing	T_M-4 °C	30 s
	Extension	72 °C	1 min/kb
1x	Final extension	72 °C	10 min

Table 3: **Primer sequences for cloning**

Gene	Short description	Sequence	T_M (° C)
β-catenin	fwd BamHI	G CGC GGA TCC ATG GCT ACT CAA GCT GAT TTG ATG G	66.9 (57.3)
β-catenin	rev SacII XbaI with stop	GCA TCT AGA AAA AGA CCG CGG TTA CAG GTC AGT ATC AAA CCA GGC	68.1 (56.7)
β-catenin	Δ664 rev SacII XbaI with stop	GCA TCT AGA AAA AGA CCG CGG TTA CTC AGA CAT TCG GAA CAA AAC AGC	67.0 (57.5)
β-catenin	Δ695 rev SacII XbaI with stop	GCA TCT AGA AAA AGA CCG CGG TTA ATC AGC AGT CTC ATT CCA AGC C	67.3 (57.2)
β-catenin	Δ733 rev SacII XbaI with stop	GCA TCT AGA AAA AGA CCG CGG TTA GGG GTC CAT ACC CAA GGC	68.9 (58.8)
mCherry	fwd SalI	GC ATG GAC GAG CTG TAC AAG GTC GAC ATG GTG AGC AAG GGC GAG	71.2 (57.9)
mCherry	rev BamHI with Stop	CGC GGA TCC CTA CTT GTA CAG CTC GTC CAT GC	67.1 (57.5)
mCherry	rev BamHI w/o Stop	CGC GGA TCC CTT GTA CAG CTC GTC CAT GCC	68.3 (58.2)
mCitrine	fwd KpnI	CGC GGT ACC ATG GTG AGC AAG GGC GA	68.3 (57.1)
mCitrine	rev SalI w/o Stop	CTC GCC CTT GCT CAC CAT GTC GAC CTT GTA CAG CTC GTC CAT GC	71.2 (56.0)
mKate	fwd SalI	C ATG GAC GAG CTG TAC AAG GTC GAC ATG GTG AGC GAG CTG ATT AAG G	69.1 (57.1)
mKate	rev BamHI with Stop	CGC GGA TCC TCA TCT GTG CCC CAG TTT GCT AG	67.7 (58.2)
mKate	rev BamHI w/o Stop	CGC GGA TCC TCT GTG CCC CAG TTT GCT AG	66.8 (57.4)
mRaspberry	rev BamHI with Stop	CGC GGA TCC CTA GGC GCC GGT GGA GTG	74.3 (67.4)
mRaspberry	rev BamHI w/o Stop	CGC GGA TCC GGC GCC GGT GGA GTG GCG	75.4 (67.8)
PEST	PEST sequence fwd LIC	CAAACTGGGGCACAAGCTTAATAGCCATGGCTTCCCGCCGGCGGTGGCGGCGCA GGATGATGGCACGCTGCCCATGTCTTGTGCCCAGGAG	
PEST	PEST sequence rev LIC	GATCTAGAGTCGCGGCCGCTCTACACATTGATCCTAGCAGAAGCACAGGCTGCA GGGTGACGGTCCATCCCGCTCTCCTGGGCACAAGACATGGG	

5.2.1.13 Two-step fusion PCR

Two-step fusion PCR was used to fuse single PCR products to omit cloning steps when introducing the SalI restriction site in the MCS of pcDNA3.1S+. 4 primers

have to be designed: a starting forward primer A, an internal reverse B, an internal forward C and a terminal reverse primer D, with a 20 bp sequence overlap between B and C. In two separate PCR reactions the template DNA is amplified using A and B as well as C and D. Both PCR products were then fused in a second PCR using an equimolar mixture of this products as template DNA and A and D primers. The final fusion PCR product was cloned into a vector of choice (5.2.1.8-5.2.1.11).

Table 4: **Fusion PCR protocol**

1x	dsDNA denaturation	95 °C	2 min
30x	dsDNA denaturation	95 °C	30 s
	Annealing	T_M-4 °C	30 s
	Extension	72 °C	1 min/kb
1x	Final extension	72 °C	10 min

5.2.1.14 Site-Directed Mutagenesis

Point mutations, small insertions and silencing of restriction sites were done using Q5 mutagenesis kit from NEB according to the manufacturers standard procedure or QuickChange mutagenesis PCR as described below. A gene of interest was modified at a specific site using long mutagenesis primer pairs (sense and antisense) covering the mutation for PCR amplification. The mutation was introduced flanked by 15-25 bp on either side, if possible with GC-rich sequences at the end and a T_m of approx. 72 °C.

Table 5: **Standard QuickChange mutagenesis PCR reaction using PfuUltra HF polymerase**

DNA template	50 ng
dNTPs (10 µM each)	1 µl
Forward primer	125 ng
Reverse primer	125 ng
10x PfuUltra reaction buffer	5 µl
PfuUltra HF polymerase (2.5 U/µl)	1 µl
H_2O	ad 50 µl

Table 6: **QuickChange Mutagenesis PCR protocol**

1x	dsDNA denaturation	95 °C	2 min
18x	dsDNA denaturation	95 °C	30 s
	Annealing	T_M-4 °C	30 s
	Extension	72 °C	1 min/kb
1x	Final extension	72 °C	10 min

Table 7: **QuickChange mutagenesis primer sequences**

Gene	Short description	Sequence	T_M (° C)
β-catenin	Y33S fwd	GTC TTA CCT GGA CTC TGG AAT CCA TTC TGG	61.2
β-catenin	Y33S rev	CCA GAA TGG ATT CCA GAG TCC AGG TAA GAC	61.2
β-catenin	H470A fwd	CTG CCA TCT GTG CTC TTC GTG CTC TGA CCA GCC GAC ACC AAG	69.9
β-catenin	H470A rev	CTT GGT GTC GGC TGG TCA GAG CAC GAA GAG CAC AGA TGG CAG	69.9
β-catenin	Y333F fwd	GTA AAT ATA ATG AGG ACC TAT ACT TTC GAA AAA CTA CTG TGG ACC ACA AG	66.2
β-catenin	Y333F rev	CTT GTG GTC CAC AGT AGT TTT TCG AAA GTA TAG GTC CTC ATT ATA TTT AC	66.2
β-catenin	S552A fwd	AGG ATA CCC AGC GCC GTA CGG CCA TGG GT	68.6
β-catenin	S552A rev	GTA CGG CCA TGG GTG GGA CAC AGC AGC AA	68.6
β-catenin	Y654E fwd	CTA GGA ATG AAG GTG TGG CGA CAG AAG CAG CTG C	68.0
β-catenin	Y654E rev	ATT CGG AAC AAA ACA GCA GCT GCT TCT GTC GCC A	68.0
β-catenin	S675A fwd	GCC ACA AGA TTA CAA GAA ACG GCT TGC AGT TGA GCT G	66.7
β-catenin	S675A rev	AAG AGA GAG CTG GTC AGC TCA ACT GCA AGC CGT TTC T	66.7
pcDNA3.1+	rev 3242T/A	CAT GTC TGT ATA CCG ACG ACC TCT AGC TAG	60.3
pcDNA3.1+	fwd 3242T/A	CTA GCT AGA GGT CGT CGG TAT ACA GAC ATG	60.3
pcDNA3.1+	fwd 3C/T	GCC ACC TGA CGT CGA TGG ATC GGG AGA TCT C	66.9
pcDNA3.1+	rev 3G/A	GAG ATC TCC CGA TCC ATC GAC GTC AGG TGG C	66.9

Following PCR the template DNA was digested 1 h at 37 °C with 1 µl DpnI (10 U/µl) directly in the PCR reaction mixture before transformation of 2 µl into 100 µl competent bacteria. The bacteria ligate single strand breaks left by the PCR reaction without the need of an *in vitro* ligation step.

5.2.1.15 DNA sequencing

Sanger sequencing was performed using BigDye Terminator v 3.1 Cycle sequencing kit and analysed in our in-house facility „Zentrale Einrichtung Biotechnologie".

Sequencing reactions were prepared according to table 3, run in a standard sequencing PCR protocol, cleaned from unbound dNTPs and ddNTPs by a NucleoSeq column, dried at 60 °C in a vacuum centrifuge and send for in-house sequencing.

Table 8: **BigDye Terminator sequencing PCR reaction**

DNA template	125-250 ng
BigDye Terminator Premix	1 µl
5x sample buffer	1.5 µl
Sequencing primer	0.25 µl (2.5pmol)
H_2O	ad 10 µl

Table 9: **BigDye Terminator sequencing PCR protocol**

1x	dsDNA denaturation	96 °C	60 s
25x	dsDNA denaturation	96 °C	10 s
	Annealing	50 °C	5 s
	Extension	60 °C	4 min

Table 10: **Sequencing primer for β-catenin constructs**

Gene	Short description	Sequence	T_M
β-catenin	493-515 fwd	CAG GTG GTG GTT AAT AAG GCT GC	**58.2**
β-catenin	1714-34 rev	GTG AAG GGC TCC GGT ACA ACC	**60.2**
β-catenin	1080-1103 rev	AGT CCT AAA GCT TGC ATT CCA CCA	**58.0**
β-catenin	114-137 rev	AGA GAA GGA GCT GTG GTA GTG GCA	**58.2**
β-catenin	1173-1196 fwd	TGC AAC TAA ACA GGA AGG GAT GGA	**58.6**
β-catenin	1968-1991 fwd	TGC TGT TTT GTT CCG AAT GTC TGA	**58.3**
pcDNA3.1	292-313 rev	CGC GGA ACT CCA TAT ATG GGC	**58.0**
pcDNA3.1	1615-1639 fwd	GGA ACA ACA CTC AAC CCT ATC TCG G	**59.0**
pcDNA3.1	2297-2316 fwd	CGG TGC CCT GAA TGA ACT GC	**59.2**
pcDNA3.1	3004-3025 fwd	CGC CTT CTA TGA AAG GTT GGG C	**58.5**
pcDNA3.1	3698-3721 fwd	GAC GAG CAT CAC AAA AAT CGA CGC	**58.9**
pcDNA3.1	4281-4300 fwd	CTA CGG GGT CTG ACG CTC AG	**59.5**

5.2.2 Proteinbiochemistry

5.2.2.1 Whole cell lysate

Whole cell lysates (WCL) for immunoblots were obtained from cell culture dishes of various size. For cell lines in 6-well plates 50 µl lysis buffer were used per well, in 12-well plates 30 µl per well. For collagen-sandwich cultures 100 µl of 7 x lysis buffer were used per well, due to the 600 µl collagen matrix per well.

After removal of media, cells were lysed directly by application of ice-cold lysis buffer supplemented with Complete Mini EDTA-free protease inhibitor cocktail as well as phosphatase inhibitor cocktail 2 and 3. After 5 min incubation on ice, cells were scraped and lysates transferred to cold 1.5 ml reaction tubes on ice. Cell debris was removed in a conventional table top centrifuge at 20000 x g for 15 min at 4 °C. After transfer of supernatant to a cold 1.5 ml reaction tube, samples were either directly used or frozen and stored at -80 °C.

5.2.2.2 Bradford Assay

Protein concentration in WCL was determined using the Bradford Assay according to the manufacturers protocol. Standard plastic cuvettes have been used with a total volume of 1 ml, according to Table 11.

Table 11: **Bradford assay sample praparation for determination of the protein concentration**

Sample/BSA standard volume	1 µl
H_2O	500 µl
Bradford reagent	500 µl

5.2.2.3 Sample preparation for SDS-PAGE

After protein concentration was determined using Bradford assay, samples were prepared for SDS-PAGE. 10-40 µg of total protein (BSA-equivalent) were mixed with 5 x Lämmli sample buffer to a final concentration of 1 x and a total volume of 20 µl for 15 well and max. 40 µl for 10 well 1.5 mm gels. After short centrifugation, samples were boiled to 95 °C 5-10 min and cooled on ice for additional 2 min in order to break up tertiary structures like disulfide bonds.

5.2.2.4 SDS-PAGE

A denaturing sodiumdodecylsulfate-polyacrylamide gel electrophoresis (SDS-PAGE) was performed in order to separate proteins in WCL samples. Semi-discontinuous 1.5 mm SDS-PAGE gels were cast with 12 % acrylamide in the lower and 8 % acrylamide in the upper half of the gel, allowing a wide range of proteins to be separated and analysed on the same gel. Each separating gel was covered with isopropanol for polymerization. Combs with different well format were directly introduced, when the stacking gel containing 4 % acrylamide was cast.

Table 12: **Recipe for stacking and separating gels (semi-discontinuous SDS-PAGE), for 4 gels**

reagents	4 %	reagents	7.5 %	12 %
ddH2O	6.1 ml	ddH2O	7.28 ml	5.03 ml
0.5 M Tris pH 6.8	2.5 ml	1.5 M Tris pH 8.8	3.75 ml	3.75 ml
10 % SDS	100 µl	10 % SDS	150 µl	150 µl
Acrylamide/Bis (30%)	1.33 ml	Acrylamide/Bis (30%)	3.75 ml	6.0 ml
10 %APS	50 µl	10 %APS	75 µl	75 µl
TEMED	10 µl	TEMED	7.5 µl	7.5 µl

The polymerized ready-to-use gel was transferred to a gel electrophoresis chamber filled with running buffer. Protein standard (BioRad Precision Plus Protein Dual Color Prestained standard) and samples were pipetted into separate wells, after flushing them with running buffer to remove non-polymerized acrylamide.

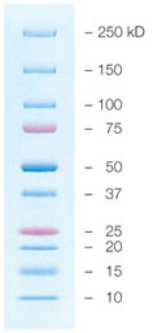

Figure 10: **Precision Plus Dual Color protein standard.** A prestained mix of 10 recombinant proteins (10-250 kD) with two pink reference bands at 25 and 75 kD in loading buffer (30% (w/v) glycerol, 2 % SDS, 62.5 mM Tris, pH 6.8, 50 mM DTT, 5 mM EDTA, 0.02 % NaN_3, 0.01 % bromophenol blue).

Electrophoresis was performed for 90-120 min with constant voltage of 120 V until the bromophenol blue reached the end of the gel. SDS-PAGE gels were taken for Western blot subsequently.

Commercial 1.5 mm 4-12 % BisTris gels (Novex) were used for the maximal separation of proteins in the range of 20-60 kD with MOPS buffer. All steps were performed according to the user manual, including a electrophoresis at 200 V for 50 min.

5.2.2.5 Western Blot

The SDS-PAGE stacking gel was removed from the separating gel before equilibration in transfer buffer. PVDF membranes were first activated in MeOH for 2 min and then equilibrated in transfer buffer. The blotting sandwich was assembled due to manufacturers standard protocol (Invitrogen Novex Blotting system), transfer took place at 45 V for 75 min. The membranes were marked at the upper right edge to fix orientation and blocked for unspecific binding in Licor blocking reagent containing herring sperm for 1 h at RT shaking before incubation with primary Ab o.n at 4 °C shaking. After washing three times 10 min with 1 x TBS-T in black boxes, membranes were incubated 1 h at RT shaking with 1:10000 dilution of secondary IR-dye labelled Ab. Before detection with Licor Odyssey Scanner, blots were washed again 3 x 10 min with 1 x TBS-T. Since secondary antibodies are available with two different IR dyes, simultaneous detection of two different probes even with the same band position was performed. As an internal reference and loading control GAPDH was detected on all membranes.

5.2.3 Cell culture

5.2.3.1 Cultivation of immortalized mammalian cells

Cells were cultivated in T75 culture flasks in DMEM high glucose supplemented with NEAA, L-Glutamine and 10 % FCS (PAA Bioscience) in 5 % CO_2 at 37 °C. At 80-90 % confluence cells were split. In order to weaken cell-cell and cell-surface interaction, DPBS without Ca^{2+} and Mg^{2+} was used for washing and then Trypsin-EDTA (0.05 %/ 1 mM) was applied to digest cell surface proteins with Trypsin and reduce interactions by withdrawal of bivalent cation complexed by EDTA. Trypsin digest was stopped by addition of FCS supplemented full growth medium (FGM) when cells were floating. After collection of cell suspension in conical tubes cell debris was removed in a centrifugation step for 3 min at RT and 200 x g. The cell pellet was resuspended, cell number was determined using a Coulter counter and cells were seeded in new flasks or dishes in FGM.

5.2.3.2 Cryo-preservation of mammalian cells

To store and recover cells later, cryo-stocks were frozen in liquid nitrogen. 1 x 10^6 cells were resuspended in 1 ml cryo-medium containing 10 % DMSO in FGM,

cooled slowly in isopropanol in -80 °C freezer over night and transferred to the liquid nitrogen.

In order to thaw cells and cultivate them, frozen stocks were heated in a 37 °C water bath, transferred to warm FGM and seeded in T75 flask in 20 ml FGM. Media exchange on the following day removed cell debris as well as residual DMSO.

5.2.3.3 Transfection with plasmid DNA

For expression of exogenous DNA, cells were transiently transfected with plasmid DNA containing the gene of interest using FugeneHD (Promega) transfection reagent according to the standard protocol. A ratio of 1 µg DNA per 3 µl Fugene pre incubated for 5 min in 100 µl OPTI-MEM was used for transfection after incubation of the transfection mix for 15 min at RT. 6-well plates were transfected with 100 µl of transfection mix per well, 8-well labteks with 12.5 µl per well.

5.2.3.4 Isolation of primary mouse hepatocytes (pmHep)

Primary mouse hepatocytes (pmHep) were obtained from 8-12 weeks old male C57/Bl6N mice by retrograde liver perfusion via the vena cava, as taught by the Hengstler lab, IfADo Dortmund[103].

Animals were anaesthetized with intraperitoneal injection of 100 mg per kg bodyweight ketamine and 10 mg per kg bodyweight xylazine in 100-200 µl sterile NaCl solution. Chirurgical tolerance was tested by pedal reflex, pinching the tip of the hind legs. If necessary, up to 50 % of initial anaesthetics were injected to obtain chirurgical tolerance. Under semi-sterile conditions, mice were fixed on a tray by taping their limbs. An IR-bulb was used to keep operation field temperature at 35-40°C. The abdominal fur was sterilized with a small amount of 70 % ethanol before dissection of the skin to expose the abdominal cave. Intestines were moved to the right to reveal the vena cava for retrograde perfusion of the liver. Two ligatures were performed around the vena cava using blunt hooked forceps, one directly anterior to the renal vein, the second at the posterior end of the vena cava in order to fix the catheter during perfusion. A 24G catheter was introduced into the vena cava after incision with iris scissors approximately 3 mm distal to the upper ligature and advanced until the tip of the catheter is anterior to the upper ligature. Ligatures were carefully tightened and pressure was immediately released by disruption of the portal vein. Liver colour changed from dark red to an uniform

light tan colour during perfusion with KH buffer due to removal of blood cells from the organ. While the retrograde perfusion led to a high initial pressure in the liver mechanically disrupting blood vessels, EGTA in the KH buffer complexes magnesium and calcium cation, leading to disruption of cell-cell contacts like adherens junctions. After 3 min KH buffer was replaced with collagenase buffer. Collagenase digested the extracellular matrix, predominantly consistent of collagen, in the liver for another 8-11 min. Exact time of digest was determined by the lot dependent efficiency of the collagenase used. The perfused liver became soft and beige. It was removed by careful dissection of the diaphragm and the oesophagus, transferred to a cell culture dish with ice-cold suspension buffer and further processed under a sterile cabinet using sterile equipment on ice.

The perfused liver was washed 2 x with ice cold suspension buffer. Hepatocytes were obtained by opening the liver capsule using two forceps, one to hold the capsule at the gall bladder, one to disrupt the capsule and with low force gently squeeze the hepatocytes out. The capsule was not supposed to become dry, nor the hepatocytes to be mechanically stressed by dripping or shearing. The cells passed through a 100 µm pre-wet cell strainer into a 50 ml conical tube on ice and suspension buffer was added to 35 ml. To harvest intact hepatocytes the cell suspension was centrifuged 5 min at 50 x g and 4 °C. Most of the NPCs were removed with the supernatant using a serological pipette already, while the hepatocytes were gently resuspended in 10 ml suspension buffer by rolling the tube carefully on ice. For counting the number of hepatocytes in a Neubauer chamber 100 µl of the cell suspension was diluted in 400 µl suspension buffer using cut tips. 100 µl of the diluted cells were mixed with 100 µl trypan blue solution and 10 µl of this transferred to the Neubauer chamber to count viable and dead cells (blue nuclei).

pmHep were maintained under non-proliferative conditions in collagen sandwich culture (CS) or under proliferative conditions on collagen monolayer (CM).

5.2.3.5 Rigid collagen monolayer cultures of pmHep (CM)

For standard 2 D cultures, pmHep were spread on culture dishes coated with a rigid monolayer of rat-tail collagen I as collagen monolayer (CM). Cell culture dishes were evenly covered with 2 mg/ml collagen I in 0.1 % acetic acid

neutralized with 1M NaOH. Excess of collagen I solution was removed and dishes were left to dry at RT under UV-light. To remove remaining acid, dishes were washed twice with PBS or plain medium before use. Prepared dishes were stored at 4 °C sealed with parafilm. For microscopy collagen pre-coated commercially available MatTek dishes with 1.5 mm glass bottom were used. pmHeps were seeded in Williams E medium containing 10 % SeraPlus. After 3 h healthy, attached pmHeps were washed 3 x with Williams E medium, in order to remove cell debris as well as NPCs or remaining blood cells. Medium was exchanged daily. For cell number and appropriate media volume see Table 13.

Table 13: **Culture dish size, cell number and media volume for collagen monolayer.**

Cell culture dish	Media volume/well	Cell number/well
MatTek dish 3 cm	**2 ml**	4×10^5
6-well plate	**2 ml**	4×10^5
12-well plate	**1 ml**	1.5×10^5

5.2.3.6 Collagen sandwich cultures of pmHep (CS)

pmHeps were cultured in collagen sandwich cultures (CS) in order to keep the post-mitotic state of pmHeps for an extended period of time as compared to CM, because pmHeps get comforted by a surrounding rat tail collagen matrix, providing a environment more close to tissue culture. Lyophilized rat tail collagen was dissolved in 0.2 % acetic acid on ice o.n. or at least for 3 h to 1.1 mg/ml. Addition of 10 x DMEM finally reduced concentration to 1 mg/ml. Titration with 1 M NaOH on ice, until the equivalent point of the pH indicator phenol red was observed by a change from yellow to fuchsia, neutralized the acetic acid. Appropriate amounts of soft collagen were evenly spread on ice-cold culture dishes using a cell scraper and polymerized for 45 min at 37 °C. pmHeps were seeded on soft collagen according toTable 14.

Table 14: **Culture dish size, cell number and media volume for collagen sandwich culture.**

Cell culture dish	collagen volume/well	Media volume/well	Media volume/well	Cell number/well
MatTek dish 3 cm	**2 ml**	**2 ml**	**2 ml**	8 x 10^5
6-well plate	**2 ml**	**2 ml**	**2 ml**	8 x 10^5
12-well plate	**1 ml**	**1 ml**	**1 ml**	3 x 10^5

After 3 h viable pmHeps were attached. The supernatant containing cell debris was removed carefully, in order not to disturb the cell layer or destroy the collagen layer, using a serological pipet. 3 washing steps were performed with plain Williams E. During the last washing step, the upper collagen layer was prepared. 1.1 mg/ml collagen in 0.2 % acetic acid was further diluted 1:1 with 0.2 % acetic acid to a final concentration of 0.55 mg/ml. 10 x DMEM was added and the pH again adjusted with 1 M NaOH on ice. The last washing step with plain Williams E was replaced by slow and careful addition of the liquid collagen to the center of the dish. The collagen upper layer was distributed by tilting the plate north/south and east/west. Within 45 min in the incubator the upper layer became a gel. Williams E FGM was added to the centre of each well, carefully dripping in order not to destroy the collagen sandwich or lift the collagen sandwich by circling the dish.

5.2.3.7 Total RNA isolation from pmHep

Total RNA was isolated from a wet cell pellet of freshly isolated pmHep in order to obtain cDNA from non-transformed mouse hepatocytes. Following the user manual instructions of the innuPREP DNA/RNA Mini Kit from Analytik Jena AG for isolation of DNA/RNA from eukaryotic cells, 1 x 10^5 pmHeps were pelleted in a 1.5 ml reaction tube, resuspended in 400 µl lysis buffer by trituration after 2 min incubation at RT. After additional 3 min at RT and centrifugation at 13000 x g genomic DNA was bound to a spin filter membrane upon centrifugation at 10000 x g for 2 min. The flow trough was mixed 1:1 with 70 % EtOH and transferred to another spin filter column in order to bind total RNA upon centrifugation at 10000 x g for 2 min. After 2 washing steps with high- and low-salt buffer, genomic DNA as well as total RNA was eluted in 50 µl RNase free water.

5.2.3.8 Reverse transcriptase reaction of pmHep total RNA

ProtoScript II first strand cDNA synthesis kit (NEB, #E6560S, Lot. 0041212) was used to transcribe mRNA to cDNA according to the standard protocol in the users manual. Denaturation of 1 µg total RNA (approx. 100 ng mRNA) took place for 5 min at 65 °C with $d(T)_{23}$ VN primer 12.5 µM in a total volume of 8 µl nuclease-free water, followed by immediate incubation on ice. After addition of 10 µl ProtoScript Reaction Mix and 2 µl ProtoScript Enzyme Mix, cDNA synthesis proceeded for 30 min at 42 °C, cooling down to RT within 30 min and another 30 min incubation at 42 °C. ProtoScript reverse transcriptase was inactivated at 80 °C for 5 min. cDNA was stored at -20 °C and used as PCR Template 1 µl per reaction volume.

5.2.3.9 Wnt3a stimulation of mammalian cells

Cells were stimulated with recombinant mouse Wnt3a for WB or imaging using a stock of Wnt3a 10 µg/ml dissolved in PBS with 0.1 % BSA diluted to 100 ng/ml final concentration. Stocks were stored at -20 °C for up to 6 month or 4 °C for up to 1 week.

5.2.4 Immunohistochemistry

Transfected cells were fixed after treatment for antibody staining and microscopic analysis with a 1:1 mixture of ice-cold MeOH and acetone for 10 min on ice. Removal of organic solvents was followed by a 10 min drying step before cells were washed 2 x with 1 x PBS-T and blocked 1 h with Licor blocking buffer at RT. Primary antibodies were incubated o.n. in Licor buffer at 4 °C shaking. 3 x washing with PBS-T removed unspecific antibody binding, followed by 1 h incubation with respective secondary antibody labelled with fluorescent dye at a 1:1000 dilution in PBS-T in a dark box shaking. For nuclear staining Hoechst33342 in a final concentration of 0.1 µg/ml was incubated for 5 min, before cells were washed again 3 x with PBS-T. If not imaged immediately cells were stored in 1x PBS with 0.01 % NaN_3 at 4 °C.

5.2.5 Microscopy

5.2.5.1 Fluorescence microscopy

Fluorescence images of live and fixed cells were obtained with an Olympus Cell^R IX81 inverted microscope after excitation with a MT-20 150 W mercury arc burner.

The following excitation lines/filters and emission filters were used for the detection of mTagBFP, mCitrine and mPlum (Table 15).

Table 15: **Excitation/Emission filters used at the Cell^R**

Fluorophore	excitation	Dichroic mirror	emission
mTagBFP	BP425-445	U-M3DAFITR	BA460-510
d1mTagBFP	BP425-445	U-M3DAFITR	BA460-510
mCitrine	BP490-500HQ	DM505	BA515-560HQ
mPlum	BP545-580	DM600	BA610IF

Images were sequentially collected using a 40x air objective and an Orca CCD camera (Hamamatsu Photonics). The Cell^R software was used for instrumental control and data acquisition. For fixed cells, fields of view were sequentially imaged in triplicates. In live cell experiments, up to 128 positions were marked using the Cell^R position control and the motorized stage controller. Every field of view was imaged 1 h pre- to 8 h post-stimulation in intervals of at least 1/h. Live cell experiments were performed at 37 °C, 5 % CO_2.

5.2.5.2 Confocal laser-scanning microscopy (LSM)

Confocal images of live cell were obtained with the Olympus FluoView 1000 confocal laser-scanning microscope. The excitation source, wavelength and the respective emission filter is presented in Table 16.

Table 16: **Excitation source, wavelength and emission filters used for confocal imaging.**

Fluorophore	laser	wavelength (nm)	emission band width
mTagBFP	UV	405	420-468
d1mTagBFP	UV	405	420-468
mCitrine	argon	488	500-551
mCherry	DPSS	561	580-680
mRaspberry	DPSS	561	580-680
mPlum	DPSS	561	580-680

The excitation light was focused on the sample using a 60x/1.35 NA oil objective or a 40x/0.9 NA air objective and channels were sequentially excited with a DM405/488/561/633 dichroic mirror. The sequential collection of intensity images was separated using a SDM510 beam splitter to spectrally separate blue and yellow and a SDM 560 beam splitter to separate yellow and red fluorescence. Live cell experiments were done at 37 °C with 5 % CO_2 in a humidified chamber.

5.2.5.3 Fluorescence lifetime imaging microscopy (FLIM)

Fluorescence lifetime imaging microscopy (FLIM) is a quantitative imaging approach to determine Förster resonance energy transfer (FRET) fractions between two fluorescent species[104]. Fluorescence describes the emission of photons by electrons relaxing from an (spin-allowed) excited singlet state to the ground state, as represented in the Jablonski diagram:

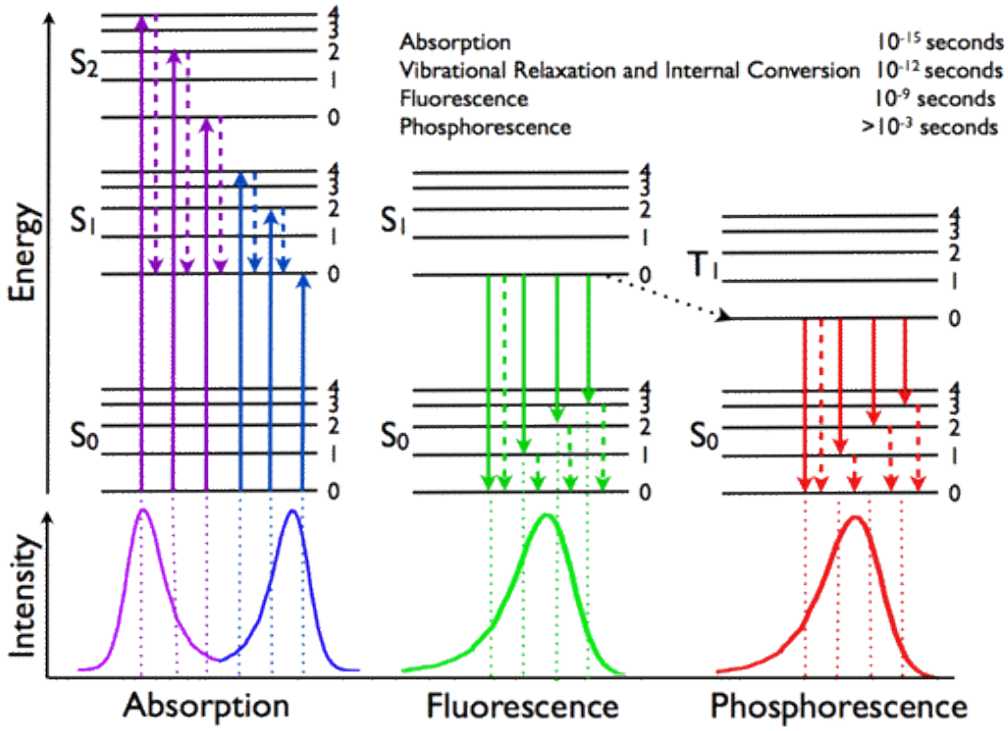

Figure 11: **Jablonski diagramm.** Solid arrows represent transitions by absorption or emission (fluorescence or phosphorescence. Dashed arrows represent non-radiative transitions. The black dotted arrow indicates intersystem transition to a triplet state, since spin multiplicity of S1 and T1 is different. (http://www.photobiology.info/Visser-Rolinski.html, 8.11.2014)

Upon excitation with light, valence electrons of the molecule absorb photons in the $S_{0,0}$ (ground) state and are elevated into higher order singlet states (S_1, S_2…), depending on the energy of the absorbed photon. Relaxation through different vibrational and rotational states to the lowest vibrational level of the first excited state S_1 causes an emission shift to lower energies, also known as Stokes shift. This effect is even stronger, because the most favored emission transition is not from $S_{1,0}$ to the energetic ground state $S_{0,0}$ but to the corresponding vertical vibrational level in S_0 following the Franck-Condon principle. The same is true for the excitation from $S_{0,0}$ to $S_{1,X}$.

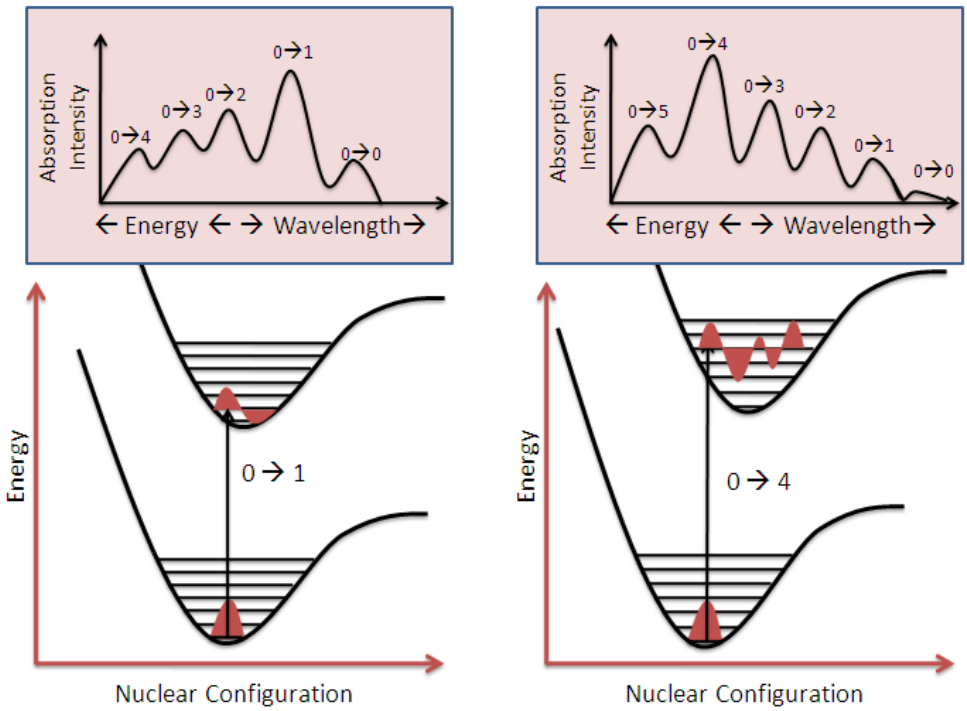

Figure 12: **Franck-Condon principle.** Occurrence of energy transfer from $S_{0,0}$ to elevated singlet states depends on the overlap of integrals indicating distribution of electrons in the given energy level. This leads to a "mirrored" excitation/emission profile of a molecule. (Image from: photochemistry.wordpress.com/2009/08/).

The fluorescence lifetime τ_D describes the decay time of a fluorophore in the excited state after a infinitesimally short excitation pulse (∂-excitation) and is described by

$$\tau_D = \frac{1}{k_F + k_{IC} + k_{IS}}$$

where lifetime τ_D exponentially decreases with the sum of fluorescent transition k_F and non-radiative transitions k_{IC} (interconversion) and k_{IS} (intersystem crossing) rate constants. τ_D is defined as the lifetime corresponding to an amplitude of $1/e$ $I(t_0)$.

$$I(t) = I_0 \, e^{-t/\tau_0}$$

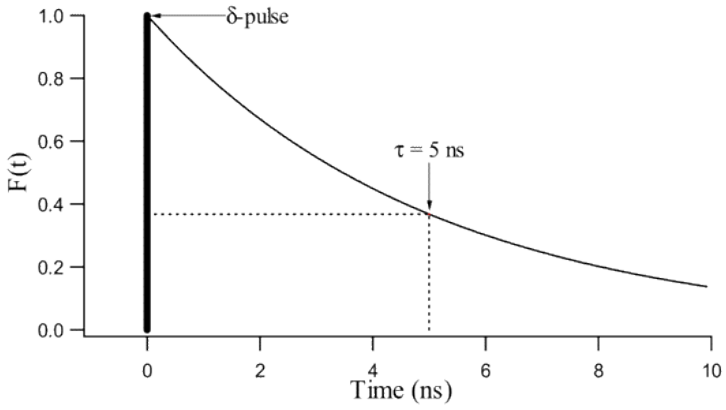

Figure 13: **Fluorescence decay $F(t)= F_0 e^{(-t/\tau 0)}$ with t (ns).**

FRET is a non-radiative energy transfer from an excited donor to an acceptor fluorophore in close proximity. The rate of the energy transfer k_{FRET} depends on the donor fluorescence lifetime τ_D, the Förster radius of the FRET pair molecules R_0 and the distance r:

$$k_{FRET} = \frac{1}{\tau_D}\left(\frac{R_0}{r}\right)^6$$

The Förster radius R_0 is defined as

$$R_0 = 0.211\left(\kappa^2 n^{-4} Q_D J(\lambda)\right)^{1/6}$$

where κ^2 is the dipole-dipole orientation factor, n is the medium refractive index, Q_D is the quantum yield of the donor alone and $J(\lambda)$ is the spectral overlap integral of the donor emission and acceptor absorption.

For free rotating donor and acceptor molecules κ^2 is 2/3. Parallel dipole orientation would allow for maximal FRET, while perpendicular orientation allows no FRET. The maximum dynamic range in FLIM measurements is achieved for a distance between the molecules close to R_0 (for FPs $\approx$ 5 nm), because the FRET efficiency is defined as :

$$E = \frac{{R_0}^6}{{R_0}^6 + r^6}$$

As one additional non-radiative process, the rate of FRET k_{FRET} is added to the sum of transition rates and therefore decreases the lifetime of the donor molecule.

$$\tau_{DA} = \frac{1}{k_{FRET} + k_F + k_{IC} + k_{IS}}$$

This decrease in the donor lifetime is measured by FLIM, the fraction of interacting molecules (α) or the FRET efficiency E can be derived from the lifetime of the donor alone and the lifetime of donor and acceptor in complex[104].

$$E = 1 - \frac{\tau_{DA}}{\tau_D}$$

FLIM data was acquired using the Olympus FluoView 1000 laser scanning confocal microscope equipped with an external PicoQuant's compact FLIM and FCS upgrade kit for laser scanning microscopes. The 507 nm pulsed laser is coupled to the Olympus FluoView 1000 through an independent port and controlled by a driver that can be digitally modulated (PicoHarp 300). Photons were detected by a single photon avalanche diode, and arrival time was transferred to the PicoHarp 300 data acquisition unit. The 40 MHz pulsed laser (507 nm) was controlled with the Sepia II software (PicoQuant GmbH) and detected via the an APD. Image integration time was around 3 min, approximately until an minimal photon count of 50/pixel was acquired. For lifetime measurements of mCitrine the 507 nm pulsed laser was set to 67 % intensity and the DM458/515 dichroic mirror were used to excite the sample mCitrine fluorescence was detected by APDs equipped with a 537/26 bandpass filter.

5.2.5.4 Image processing

Images where processed using Fiji image processing software. 32-bit images were background corrected and a minimal threshold of 0 was set before quantification of area, mean, min, max and integrated signal intensities in single cell region of interest (ROI). ROIs containing overexposed pixels were discarded from analysis.

5.2.5.5 FLIM analysis

Time-domain FLIM data was analysed by "precision FLIM 3 (pFLIM3)" by Kirstin Walther and Ali Kinkhabwala. Precision FLIM uses an parameterized model to correct for the instrument response function (IRF) of the Olympus FV1000 setup. Therefore it is an precise way to determine fluorescent lifetimes of the donor fluorophore without instrument artefacts. The pFLIM3 analysis was performed according to the manual supplied on the Igor webpage. Since mCitrine is a

monomeric fluorophore with a single exponential decay in lifetime, the decay curve was fitted with a mono-exponential model. In presence of an acceptor, more than one lifetime was expected within the sample and therefore a double-exponential decay model was used to fit the data. The fit was optimized by X^2 minimization.

$$I(t) = A_1\, e^{-t/\tau_1} + A_2\, e^{-t/\tau_2} + B$$

The actual lifetime images were represented as false colour images ranging from minimal 2 to maximal 3.2 ns, adjusted for each experiment.

5.2.5.6 Ratiometric imaging analysis

For the analysis of intensity ratios between two fluorophores, images of different fluorescent channels but the same field of view were background corrected using the same ROI as a measure of background intensity. Following the subtraction of the mean intensity in the background ROI, images threshold was set to 0, all pixels below were set to NaN. For each timepoint and position ROIs for single cells were applied manually to track single cells over time. The mean intensity ratio of the donor and acceptor channel were plotted against the stimulation time. For the analysis of the nuclear reporter intensity, integrated intensity of the nucleus was extracted. Results are represented as the mean $\pm$ standard deviation, unless otherwise described. Statistical significance was tested by the Mann-Whitney non-parametric t-test for the temporal profiles of the sensor response.

5.2.6 Affinity propagation test

The A/D intensity ratio was highly diverse for single cell analysis. Since a lot of parameters influence the stability of β-catenin, this is not very surprising. Hence, amplitude-based clustering to classify responders and non-responders was performed using an affinity propagation test provided and computed by Dr. habil. A. Koseska. The affinity propagation algorithm[105] takes the set of real-valued similarities (s(i,k)) calculated between all pairs of β-catenin sensor stability profiles after Wnt3a stimulation as an input. These similarities indicate how well a temporal profile is suited to be centre of a given cluster (exemplar). Considering that the goal is to minimize the squared error, each similarity is set to a negative Euclidean distance, where x_i and x_k are vector representations of the temporal stability profiles upon 2 different cellular response mechanisms after stimulation.

The number of clusters do not have to be pre-determined, since the algorithm takes a real number s(k,k) for each data vector k as input. Vectors with larger values of s(k,k) are more likely chosen as exemplars in the affinity propagation test. After a given data vector is chosen as an exemplar, the max-sum algorithm is derived, by sending messages from variables to functions and from functions to variables in a recursive manner. This allows to estimate weather a given vector is a good exemplar for the chosen members of the cluster, and vice versa, weather a given member of a specific cluster belongs to the corresponding exemplar. The procedure is repeated for a fixed number of iterations until changes in the number of exemplars and members in specific clusters fall below a threshold or until the local changes remain constant for certain number of iterations.

6 Results

6.1 An intramolecular biosensor for β-catenin stability

Starting from Wnt ligand binding up to β-catenin regulated target gene transcription several stages can be addressed as a read-out for Wnt/β-catenin signalling activation. Current transcriptional reporter based systems such as TOPflash are not ideal due to the time delay between ligand binding and β-catenin induced transcription. With these reporters single cell analysis of their Wnt response is essentially impossible. In order to overcome the time delay and be able to study Wnt/β-catenin induction on single cell level, a novel sensor was designed and described here. This sensor is based on the phenomena of β-catenin accumulation, which is an earlier and very well described read-out for Wnt/β-catenin signalling pathway activation. Since β-catenin interacts with multiple proteins in the degradation complex via its arm repeats, the protein structure itself needs to be kept. This allows degradation as well as stabilization of the sensor molecule similar to endogenous β-catenin. Both terminal ends of β-catenin are flexible. N-terminal fusion of a FRET-pair of two fluorophores with different maturation times as a measure of stability should therefore not interfere with the binding to the degradation complex. The new β-catenin stability sensor will make use of fluorophores as intracellular protein half-lifetime clocks, as shown before, for example by using fluorescent timer proteins with a change of spectral properties over the lifespan of fluorescent proteins[106]. In order to monitor β-catenin stability upon stimuli, the half-lifetime of β-catenin within the cell and the maturation time of the respective acceptor fluorophore needs to be matched. Previous studies estimated the half-lifetime of β-catenin in different tissues and cell culture systems to be less than 60 minutes in the absence and over 100 min in the presence of Wnt[107-109] (Table 18). Thus, a donor fluorophore with maturation time shorter than 60 min was chosen. The acceptor fluorophore must have a maturation time between 60 and 100 min. In the absence of Wnt, donor fluorophore, but not the acceptor fluorophore is able to mature before the whole sensor molecule is degraded. Therefore preferably donor fluorophore will be

detected (Figure 14, left). Upon Wnt stimulation, the half-lifetime of β-catenin is prolonged and the acceptor fluorophore can maturate, which can be quantified by a drop in the donor fluorescence lifetime in FLIM measurements (Figure 14, right). The aim was to maximize the dynamic range of the FRET signal in the absence and presence of β-catenin stabilization.

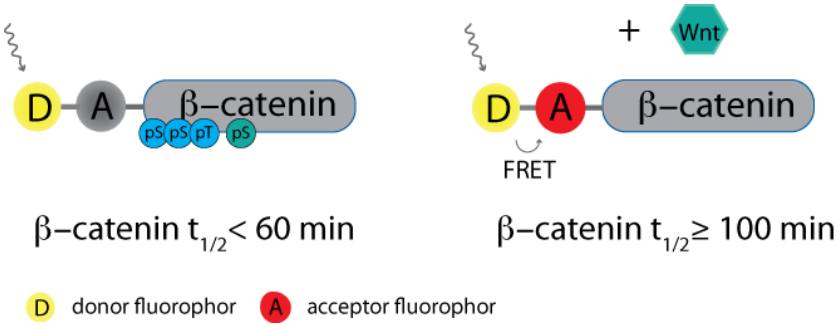

Figure 14: **Principle of the β-catenin stability sensor.** The donor fluorophore maturation time is much shorter than the half-lifetime ($t_{1/2}$) of β-catenin in the absence of Wnt signalling. The donor intensity is therefore a measure of sensor concentration within the cell. The acceptor fluorophore maturation time is higher than the half-lifetime of the β-catenin in the absence of Wnt, but lower than the half-lifetime in presence of Wnt. The constant degradation of β-catenin in absence of Wnt assures a low probability of acceptor maturation. Upon Wnt stimulation, the half-lifetime of β-catenin is prolonged and the acceptor fluorophore can maturate, which can be quantified by a drop in the donor fluorescence lifetime in FLIM measurements.

The reported maturation time of EYFP and its derivatives is very short, approximately 20-40 min[110-112]. In contrast, most red fluorophores that can be used as acceptor fluorophores in a FRET pair with the EYFP derivative mCitrine, exhibit maturation times of 15 min to hours[113-117].

Table 17: **Fluorophore maturation half-times.**

fluorophore	**maturation half-time (min)**	**species**	**reference**
EYFP	23	in vitro	Iizuka et el 2011
EYFP	40	S. cerevisiae	Gordon et al 2007
mVenus	40	in vitro	Iizuka et el 2011
mPlum	100	Human B lymphocytes	Wang et al 2004
mRaspberry	55	Human B lymphocytes	Wang et al 2004
mCherry	15	E. coli	Shaner et al 2004
	40		Merzlyak et al 2007
	16 + 30	S. cerevisiae	Khmelinskii et al 2012

The actual half-lifetime of β-catenin is highly context–dependent[12,107-109,118], ectopically expressed β-catenin has usually a longer protein half-life time, than endogenous β-catenin. This higher stability does not generally lead to an activation of Wnt signalling, because fold-change and not absolute β-catenin level dictate the β-catenin/Wnt activation and cells can adapt to higher β-catenin protein level.

Table 18: **β-catenin half-life times in different cellular context.**

Cell type	Protein half-life time (min)	condition	reference
AtT20	50	endogenous	Munemitsu et al 1996
RKO	16	endogenous	Hernandez et al 2012
RKO	104	endogenous+ 3 h Wnt-3a	Hernandez et al 2012
HEK293T	100	endogenous + 48 h Wnt-1	Mak et al 2003
HEK293T	300	ectopic	Mo et al 2009
HEK293T	120	ectopic ∂CTD	Mo et al 2009
Cos	120/240	ectopic +/- Axin1	Kishida et al 1998

The timeframe for the acceptor fluorophore maturation should therefore be between 60-100 min. After comparison of the published photophysical and biological characteristics and trials with different acceptor fluorophores, mKate2 and the red "fruit" fluorophores, mCherry, mRaspberry and mPlum were identified as promising candidates.

6.1.1 β-catenin biosensor cloning strategy and variants

β-catenin constructs were cloned into pcDNA3.1+ vector (Invitrogen). All SalI restriction sites in the backbone were removed by mutagenesis, thereby creating a plasmid backbone, which is further referred to as pcDNA3.1S+. A new SalI restriction site was introduced into the MCS in order to easily swap the fluorophores in order to fit the acceptor maturation to the β-catenin half-lifetime. In Figure 15, the sensor cloning strategy is shown.

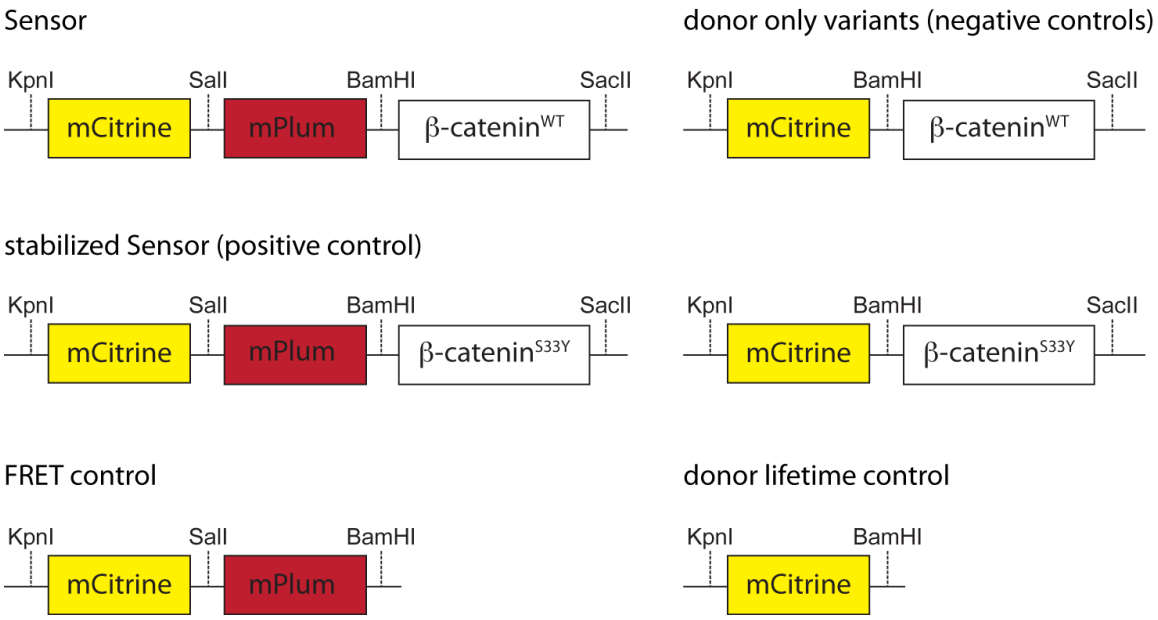

Figure 15: **Sensor constructs and controls cloned into pcDNA3.1S+ via the indicated restriction sites.** In order to exchange acceptor fluorophores while optimizing the sensor, SalI restriction site was introduced between the donor and acceptor fluorophore. The stabilized β-catenin mutant S33Y is used as control. mCitrine and mCitrine-mKate2 serve as controls for the dynamic range of FLIM measurements. mCitrine-β-catenin constructs were needed as the donor-only references required for the FLIM measurements. Constructs with mCherry, mPlum and mRaspberry as acceptor fluorophore were cloned accordingly.

As a positive control, β-catenin^{S33Y}, the stabilized mutant which mimics GSK3β inhibition upon Wnt stimulation was used. The exchange of serine 33 to tyrosine leads to a higher β-catenin half-lifetime due to blocked GSK3-β phosphorylation of β-catenin at residues S33, 37 and T41 and an inefficient degradation through the degradation complex[119,120]. In order to create a negative control, a donor-only tagged sensor was cloned. In absence of any acceptor, the fluorescence lifetime of the donor fluorophore should not be affected.

6.1.2 Comparison of the FRET acceptor candidates

The maximal dynamic range of the fluorescence lifetime change of the sensor is represented by the difference between the donor lifetime without acceptor and the donor lifetime of a construct with donor and acceptor directly fused (Figure 16). Accordingly, mCherry was found to be the best FRET acceptor, causing a reduction in mCitrine lifetime from 2.95 ns to 2.4 ns. However, because of its fast maturation time (<60 min), the average lifetime in the mCitrine-mCherry-β-catenin constructs was always low independent of Wnt signalling (data not shown). mPlum and mRaspberry were equally suitable as FRET-acceptors, however, with a smaller

dynamic range, mediating a reduction in the mCitrine lifetime from 2.95 ns to 2.7 ns. Since mPlum exhibits a slower fluorophore maturation time and less variation in the lifetime drop, it fit better to the sensor requirements.

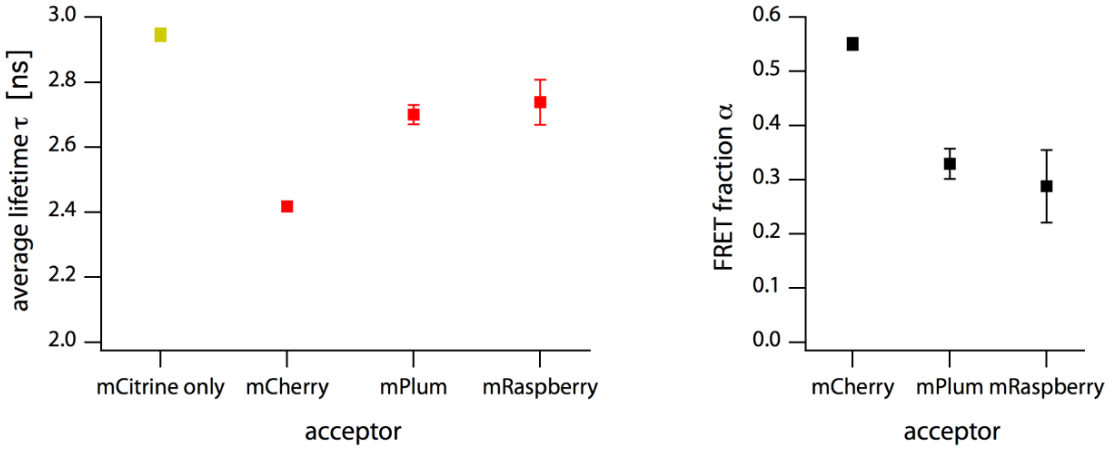

Figure 16: **Average lifetime of mCitrine and fraction of molecules exhibiting FRET of mCitrine in fusion constructs with different acceptor fluorophores.** mCitrine only or mCitrine in direct fusion to the indicated acceptor transfected into HEK293 cells. The lifetime and FRET fraction inversely correlate to each other. The higher the FRET efficiency, the lower is the lifetime of the donor molecule mCitrine. Average α and τ values per cell, represented are mean±SEM of N=5.

The sensor design and optimization was then performed using immortalized cell lines. To investigate β-catenin stabilization during liver regeneration, the acceptor fluorophore might be exchanged, in order to adapt the maturation time of the acceptor fluorophore to a different protein half-lifetime of β-catenin in this system.

6.1.3 Proof-of-principle of the β-catenin stability sensor

Fusion of proteins can alter the folding, structure and interactions of both proteins. Therefore, the influence of mCitrine on β-catenin and vice versa had to be tested. Initial FLIM measurements with fluorescently tagged β-catenin sensor (donor-only) in MCF7 cells revealed that fusing mCitrine to β-catenin did not alter mCitrine lifetime (2.95 ns) as compared to the documented lifetime of free mCitrine[121](Figure 17). The localization of β-catenin was in turn unaffected by mCitrine fusion.

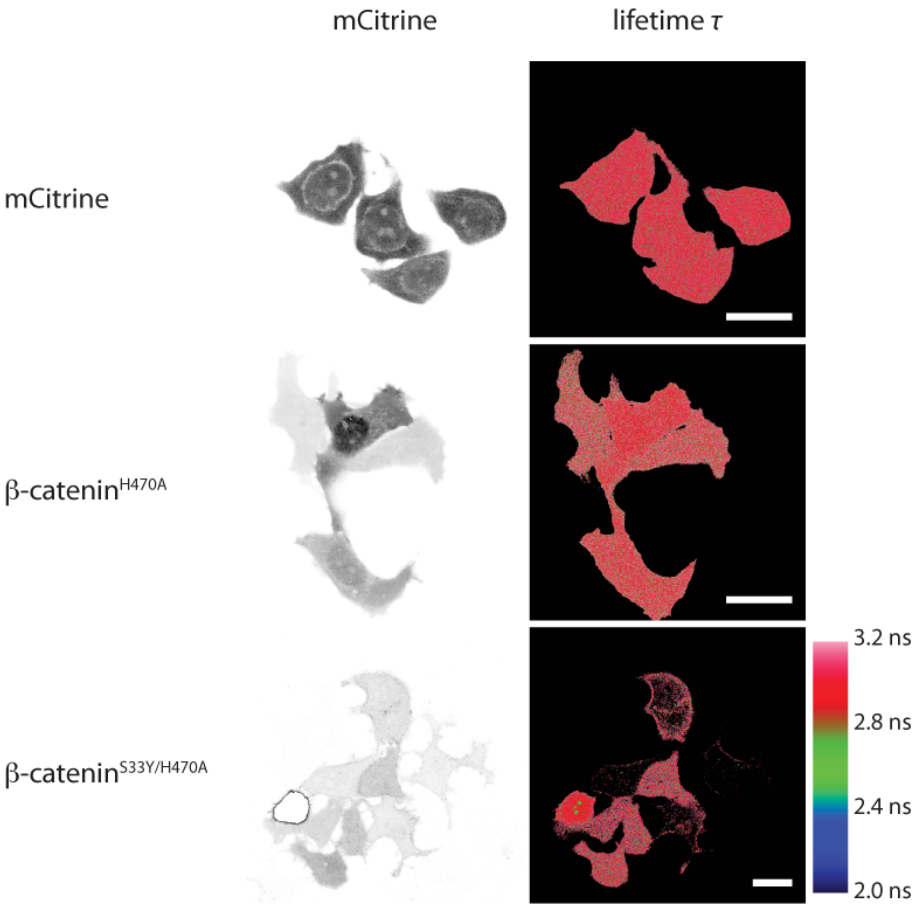

Figure 17: **mCitrine fluorescence lifetime τ was not altered in fusion constructs with β-catenin.** MCF7 cells transfected with mCitrine or mCitrine-β-catenin constructs. β-catenin is localized to the nuclei and plasma membrane of MCF7 cells 48 h post-transfection. mCitrine is solubilized. The average lifetime of mCitrine is 3 ns and not affected by fusion to β-catenin. β-catenin accumulation in the nuclei of cells rises with expression level. Scale bar 20 µm.

In initial transfections with wildtype β-catenin fusion constructs, poor cell survival was observed. Therefore β-catenin constructs were modified to prevent hyper activation of the Wnt pathway due to the elevated β-catenin level after transfection. It has been shown, that the H470A mutation reduces the interaction with transcription factors to a minimum ($< 3\,\%$)[122]. β-catenin^{H470A}, the transcriptionally inactive mutant, was distributed mainly at the plasma membrane and in the cytosol of MCF7 cells, but in high expressing cells translocated to the nucleus. High expression of the stabilized and transcriptionally inactive mutant, β-catenin$^{S33Y/H470A}$, was lethal to the cells within 24 h post-transfection. In cells with low expression levels, it was mainly localizing to the plasma membrane.

FLIM measurements of mCitrine-mPlum-β-catenin$^{WT/S33Y/H470A}$ as well as mCitrine-mCherry-β-catenin$^{WT/S33Y/H470A}$ single and double mutants in MCF7 cells

revealed a low lifetime in absence of Wnt3a stimulation, likely due to a high initial stimulation with autocrine Wnt signalling in cultured MCF7 cells (Figure 18)[123].

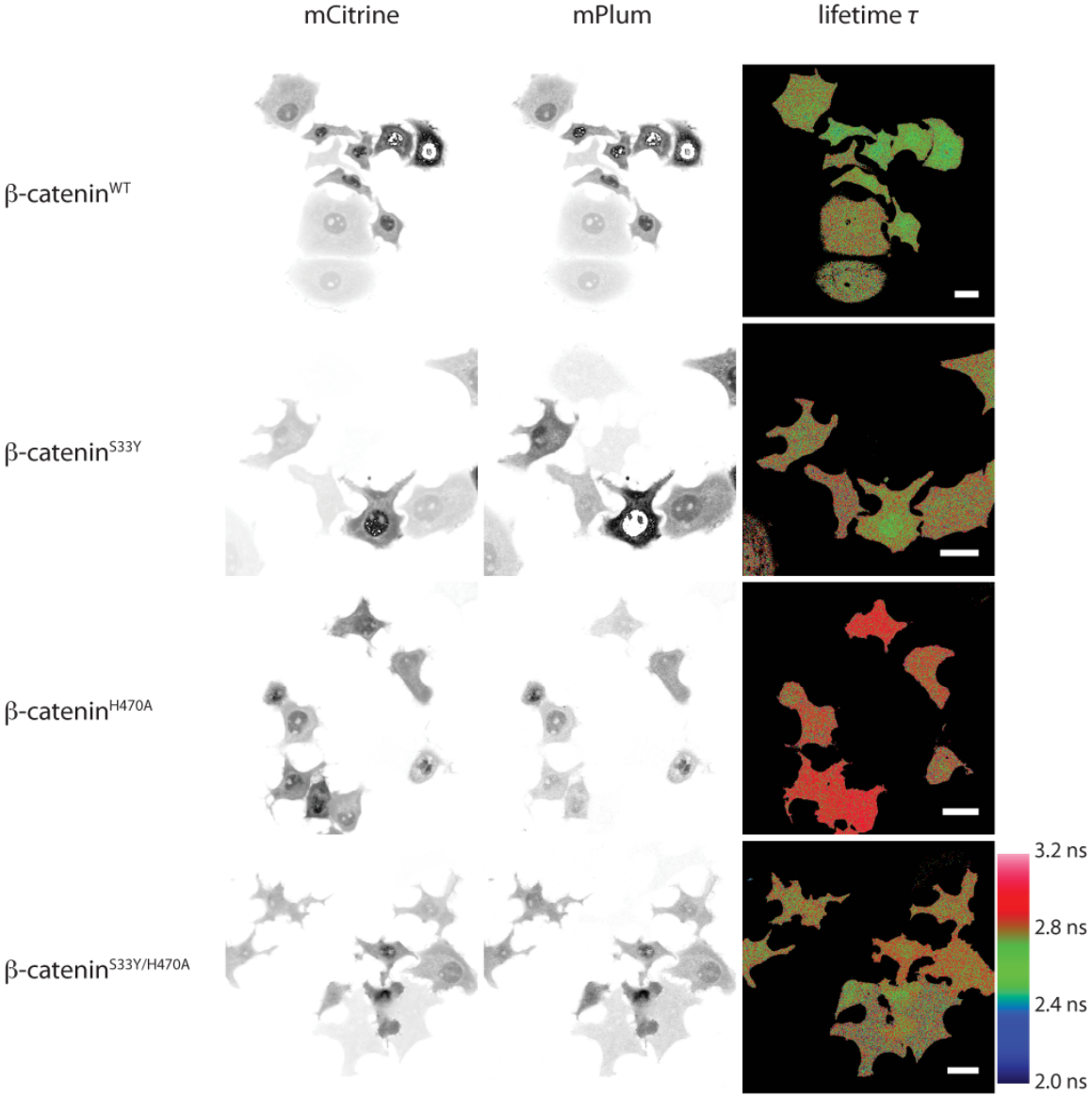

Figure 18: **Basal FRET of mCitrine-mPlum-β-catenin constructs.** β-catenin was predominantly localized to the cytosol and nuclei of MCF7 cells. The average lifetime of mCitrine was reduced in presence of acceptor in absence of Wnt ligand stimulation. The average lifetime in absence of ligand was 2.8 ns. Scale bar 20 µm.

In absence of Wnt stimulation, the average lifetime of mCitrine in the sensor variant transfected MCF7 cells was reduced. Especially in the nucleus of MCF7 cells, the donor lifetime was close to the maximally expected drop tested with mCitrine-mPlum constructs (Figure 16). These experiments point to a sensor half-lifetime longer than the maturation time of the acceptor mPlum. One possible reason might be that the β-catenin half-lifetime is longer than the mPlum maturation time. Since mPlum is the acceptor with the longest maturation time,

the current sensor design would not be applicable in such a case. Another possible reason is, that the β-catenin half-lifetime in MCF7 cells is influenced by an autocrine Wnt signalling within the cell culture. Thus, the inhibition of autocrine Wnt signalling or a change of the model system should be considered. Last, the ectopic overexpression of the sensor might overload the degradation machinery of the cells, leading to an artificial stabilization of β-catenin.

MCF7 cells transfected with the donor only construct mCitrine-β-catenin^{WT} were stimulated with Wnt3a for 2 h in order to verify that ligand stimulation does not influence the donor lifetime (Figure 19).

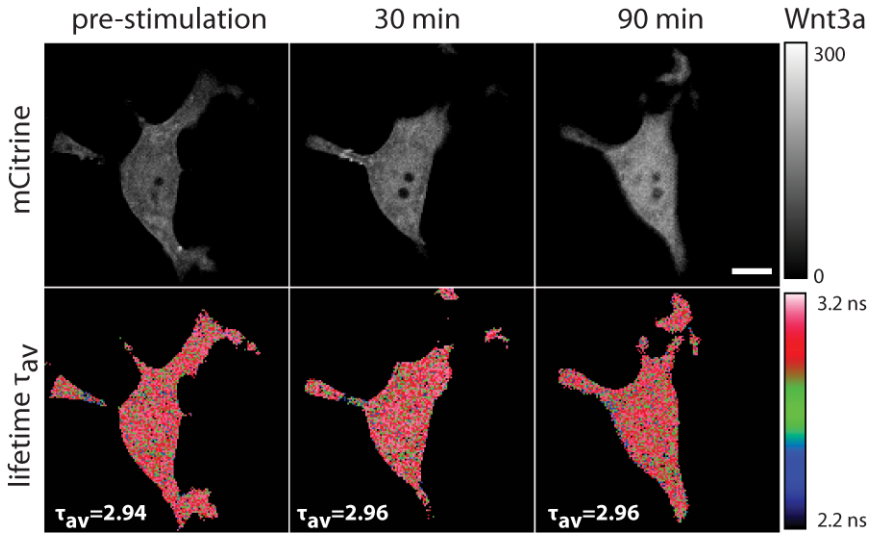

Figure 19: **FLIM Measurement of a donor only variant mCitrine-β-catenin^{WT}.** Time-domain FLIM of MCF7 cells transfected with mCitrine-β-catenin^{WT} stimulated with 150 ng/ml Wnt3a. The lifetime (τ_{AV}) of mCitrine was not reduced upon Wnt3a stimulation, although the sensor protein accumulated within the cells. Scale bar 10µm.

In mCitrine-mPlum-β-catenin^{WT} transfected MCF7 cells, Wnt3a stimulation for 3 h led to an increase in acceptor intensity compared to donor intensity, but very little changes in lifetime. In consistence with the WB analysis for MCF7 cells (Figure 22 and Figure 23), the initial lifetime of mCitrine-mPlum-β-catenin^{WT} was in most cells already close to the expected lifetime for maximal FRET with mature acceptor (2.7 ns). Autocrine Wnt signalling would cause a permanent inhibition of efficient β-catenin degradation and therefore stabilize the sensor long enough to allow for acceptor maturation and as a consequence enable FRET between the donor and the acceptor. However, some cells started with an initially high average lifetime of mCitrine (2.8s ns) and upon Wnt3a stimulation mCitrine-mPlum-β-catenin^{WT} translocated to the nucleus, was stabilized and the lifetime decreased within

90 min to 2.72 ns as expected (Figure 20). This indicates, that the β-catenin stability sensor correctly reports changes in β-catenin stabilization within very short time periods after Wnt induction in some cells.

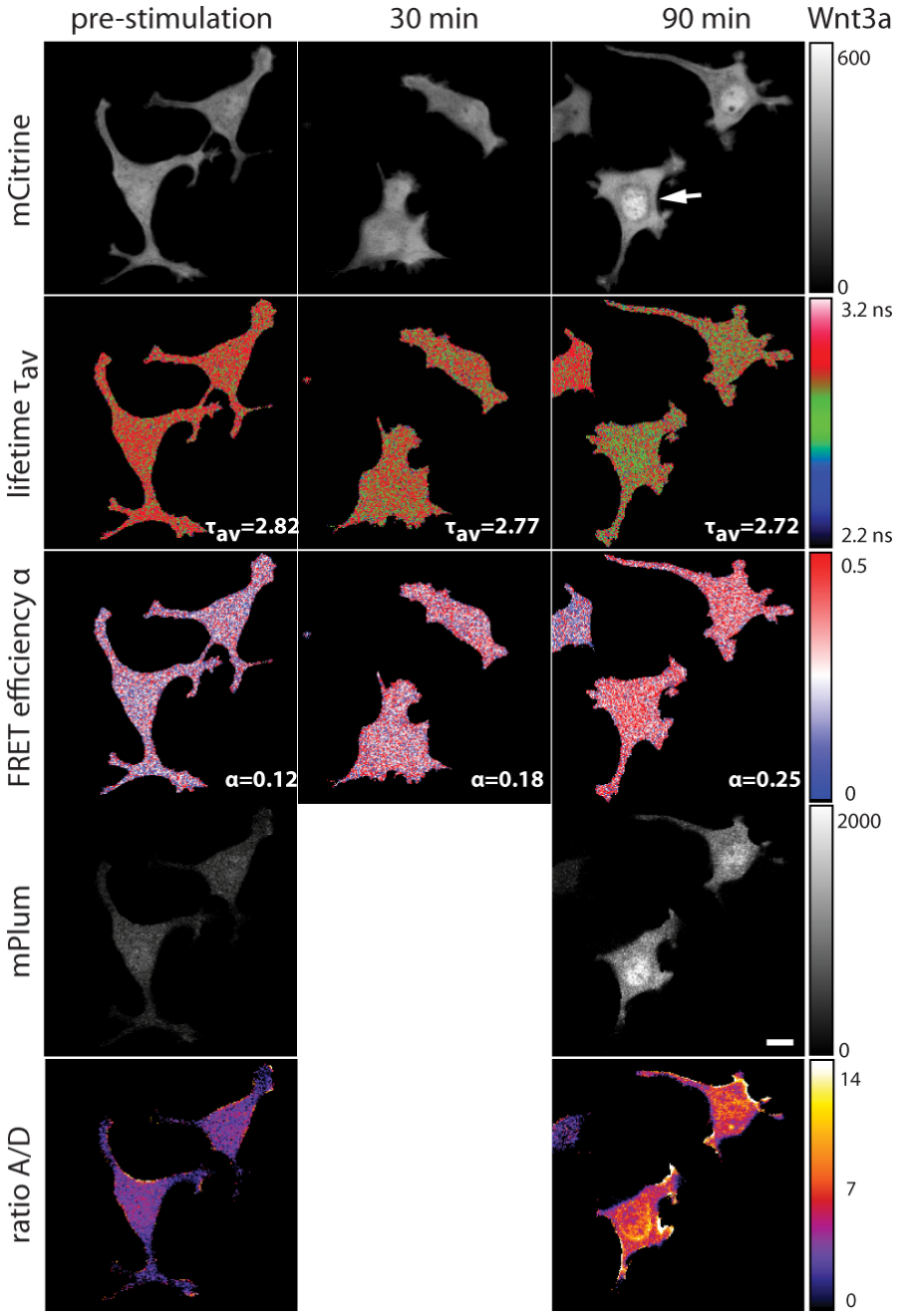

Figure 20: **Single–cell Wnt response of MCF7 cells transfected with mCitrine-mPlum-β-catenin^{WT}.** Time-domain FLIM of MCF7 cells stimulated with 150 ng/ml Wnt3a. The mCitrine lifetime (τ_{AV}) was reduced upon Wnt3a stimulation in presence of the acceptor and the sensor molecule accumulated in the nucleus after 90 min. Increase in donor intensity reflects new protein synthesis, while degradation was reduced. The increase in acceptor intensity indicated the stabilization of already existent sensor protein. As expected, the change in the ratio of acceptor over donor fluorescence intensity (A/D) and the drop in mCitrine lifetime report a prolonged half-lifetime of β-catenin upon stimulation. Scale bar 10 µm.

In order to overcome the problem of increased cell death through overexpression of β-catenin within the sensor, the β-catenin sequence of the sensor had to be mutated to prevent as many as possible downstream interactions with other proteins or DNA leading to a cellular response. Optimally, the final sensor monitors only β-catenin stability, but is inert in all other cellular contexts. The first step towards an optimized sensor was the mutation of the β-catenin/TCF interaction site (H470A), because transcriptional hyper activation is known to induce apoptosis. Until now, there was no evidence for an altered stability of the β-catenin^{H470A}. In FLIM experiments, mCitrine-mPlum-β-catenin^{H470A} was stabilized upon Wnt stimulation in some cells, similar to the sensor with β-catenin wildtype (Figure 21). Transient transfection of the transcriptionally inactive sensor variant led to a better survival of transfected cells over 48 h. However, the nuclear translocation upon Wnt3a stimulation was no longer observed, due to the lack of retention of β-catenin within the nucleus upon the interruption of interaction with the TCF/Lef family of transcription factors and could therefore no longer be used to identify responding single cells.

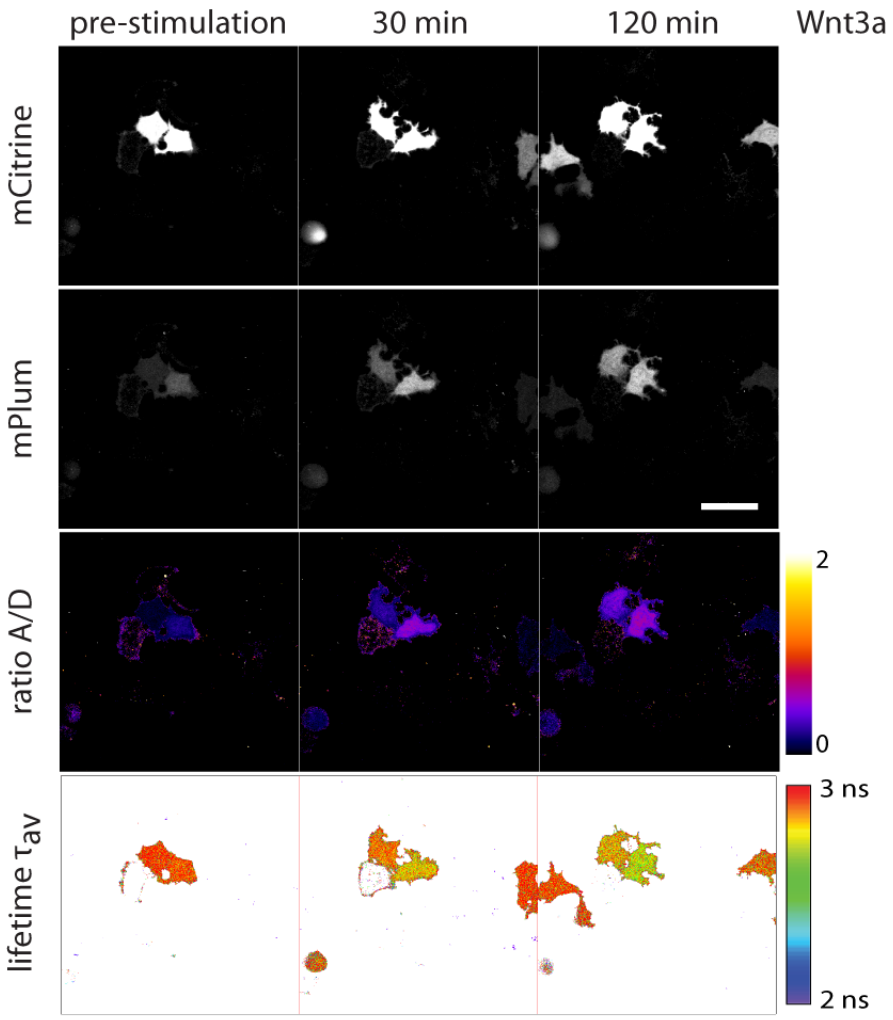

Figure 21: **Single-cell Wnt response of MCF7 cells transfected with mCitrine-mPlum-β-catenin^{H470A}.** Time-domain FLIM of MCF7 cells stimulated with 150 ng/ml Wnt3a. The mCitrine lifetime (τ_{AV}) was reduced upon Wnt3a stimulation in presence of the acceptor and the sensor molecule accumulated in the nucleus after 120 min. Increase in donor intensity reflects new protein synthesis, while degradation was reduced. The increase in acceptor intensity indicated the stabilization of already existent sensor protein. As expected, the change in the ratio of acceptor over donor fluorescence intensity (A/D) and the drop in mCitrine lifetime report a prolonged half-lifetime of β-catenin upon stimulation. Scale bar 10 µm.

To summarise, a sensor was successfully developed, which monitors β-catenin stability by Wnt3a-dependent stabilization and acceptor maturation. FLIM measurements are appropriate as a read-out for this stability sensor. However, challenges of sensor optimisation are the dynamic range of the lifetime and the reproducibility between cells. Furthermore, an optimised model system has to be identified, which does not depend on autocrine Wnt signalling.

6.1.4 Modulation of the Wnt response

The stabilization of the sensor was investigated biochemically, to determine whether the stability of the sensor was matching the stability of endogenous β-catenin or whether overexpression of the β-catenin sensor caused an overload of the degradation machinery. Stimulation with Wnt3a did not stabilize endogenous β-catenin compared to control in MCF7 cells (data not shown), due to an already high stability of β-catenin in the absence of exogenous Wnt. Other options to modulate the Wnt/β-catenin signalling pathway for a proof-of-principle of the β-catenin stabilization were small molecule inhibitors. Inhibition of GSK3β using SB2166763 should result in β-catenin accumulation upon stabilization, while inhibition of Tankyrase with IWR-1-endo would have the opposite effect, due to inhibition of axin degradation. Since Wnt/β-catenin signalling is cell density dependent, subconfluent and confluent cultures of MCF7 cells were compared (Figure 22). Treatment with the GSK3β inhibitor SB216763 increased the amount of total as well as active β-catenin (β-catenin that is not phosphorylated at S33/S37 and T41) in sub-confluent but not in confluent MCF7 cells, without affecting the ratio of active/total β-catenin. The Tankyrase inhibitor IWR-1-endo prevents Axin degradation and should therefore decrease β-catenin stability. In sub-confluent MCF7 cells IWR-1-endo did not reduce β-catenin levels, but in confluent cultures β-catenin was destabilized.

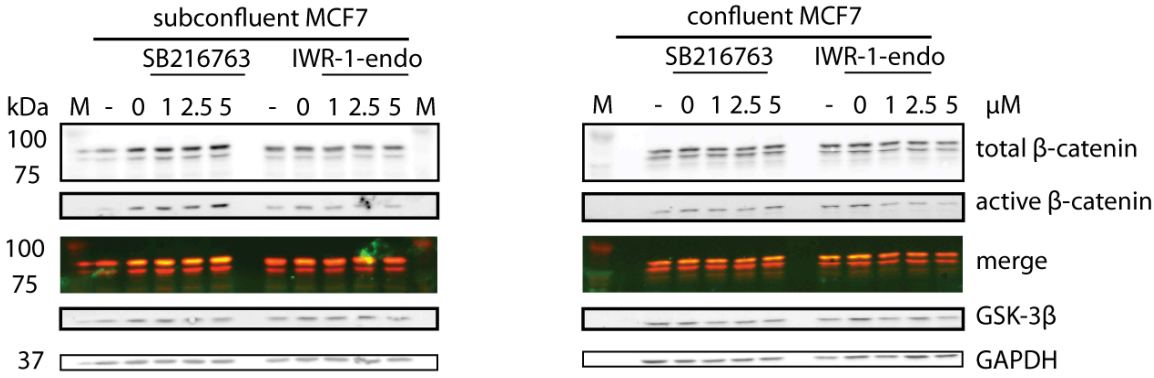

Figure 22: **Wnt/β-catenin pathway modulation by small molecule inhibitors in MCF 7 cells is cell density dependent.** Western blot analysis of endogenous β-catenin upon application of GSK3β inhibitor SB216763 or Tankyrase inhibitor IWR-1-endo for 3 h on sub-confluent and confluent MCF7 cells. Representative western blots of 2 independent experiments. Repetitions were done by F. Dietrich.

In western blots, the levels of β-catenin fused to mCitrine or the sensor variants were elevated, independent of the Wnt stimulation status in HEK293 (data not

shown) and MCF7 cells (Figure 23). mCitrine-β-catenin^{H470A} was stabilised in MCF7 cells independent of stimulation with Wnt3a and not destabilized following addition of IWR-1-endo. mCitrine-mPlum-β-catenin^{H470A} stability was not enhanced after stimulation with Wnt3a. The inhibition of GSK3β and Tankyrase failed to modulate the β-catenin levels efficiently, both on endogenous as well as ectopic level. The Axin1 expression level was not affected by IWR-1-endo treatment.

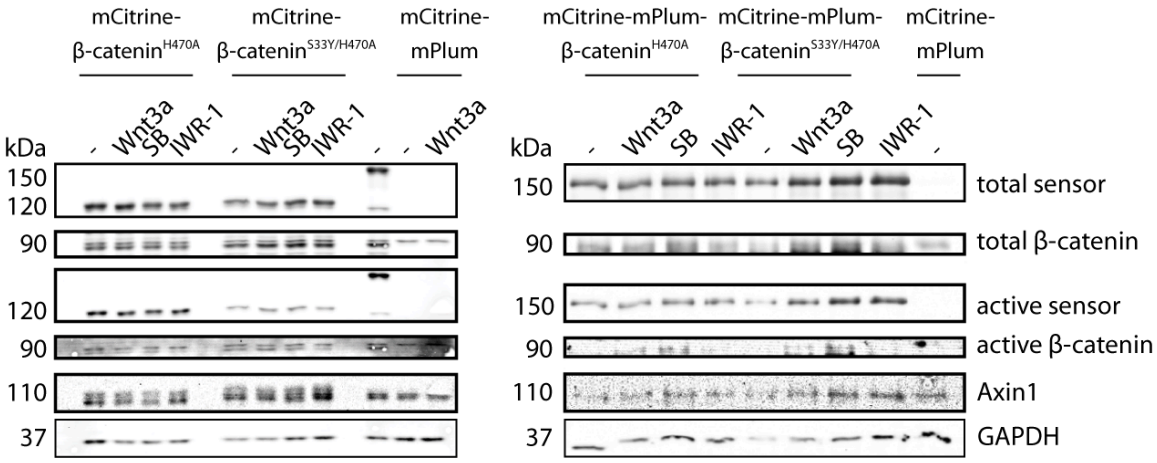

Figure 23: **Biochemical investigation of β-catenin stability sensor in correlation with endogenous β-catenin in sub-confluent MCF7 cells**. Western blot analysis of endogenous and ectopic β-catenin upon application of Wnt3a, GSK3β inhibitor SB216763 or Tankyrase inhibitor IWR-1-endo for 3 h on sub-confluent MCF7 cells. 10 µg protein/lane from whole cell lysates after treatment with 0.5 % DMSO(-) control, 150 ng/ml mWnt3a, 5 µM SB216763, 5 µM IWR-1-endo.

To investigate whether culture conditions can be changed to reset the MCF7 cells to an Wnt "OFF" state, western blot analysis of MCF7 cells treated with a known antagonist of Wnt signalling, *Wnt inhibitory factor* (WIF), was performed (Figure 24). Short (1 h) as well as long term (19 h) incubation with WIF in a concentration series did not reveal any efficient inhibition of β-catenin stabilization in MCF7 cells, as determined by the level of active β-catenin in relation to the total β-catenin level.

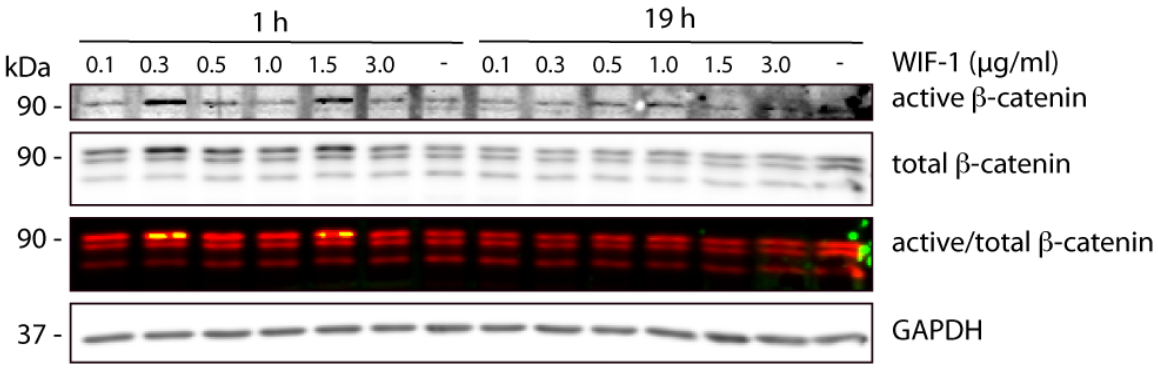

Figure 24: **WIF-1 failed to efficiently reset sub-confluent MCF7 cells to a Wnt "OFF" state.** MCF7 whole cell lysates of cells treated with WIF-1 (in DMEM+ 0.1 % FBS) for 1 h (left) and 19 h (right) with increasing concentration in comparison to untreated control cells (-). GAPDH was used as internal loading control. 10 µg protein/lane.

6.1.5 Model system for the β-catenin stability sensor

Most cancer cell lines exhibit abnormal Wnt signalling due to frequent mutations in Wnt signalling-related genes like β-catenin, APC, Axin1, Conductin and WIF-1 as well as general deregulation of cell proliferation and survival[4,124]. In order to find a cell line with low β-catenin levels and activation in absence of Wnt, as well as stabilization upon Wnt3a stimulation, examination of different cell lines towards the cellular Wnt response was performed (Figure 25). The human cell lines MCF7, A431, Caco-2 as well as the mouse cell line mPDAC were investigated for their response towards Wnt3a ligand stimulation or small molecule inhibition of GSK3β or Tankyrase. Beforehand HEK293 had been tested previously (data not shown). Due to the conserved canonical Wnt pathway, Wnt ligands show species-cross reactivity between human and murine cells[4] (see sequence alignments in attachment**).** MCF7 epithelial cells were previously isolated from a mamma carcinoma, A431 epithelial cells from an epidermis carcinoma with high chromosome instability and hypertriploidy, exhibiting a high EGFR expression level (Giard et al 1973). Caco2 are colorectal adenocarcinoma derived epithelial cancer cells. mPDAC mouse pancreatic ductual adenocarcinoma cells were induced and immortalized by an oncogenic KRas knock in (G12D). Caco2 and mPDAC cells showed a high initial activation level of β-catenin, while A431 cells were responding dependent on Wnt3a stimulation with activation and stabilization of β-catenin in 4 independent experiments (Figure 25).

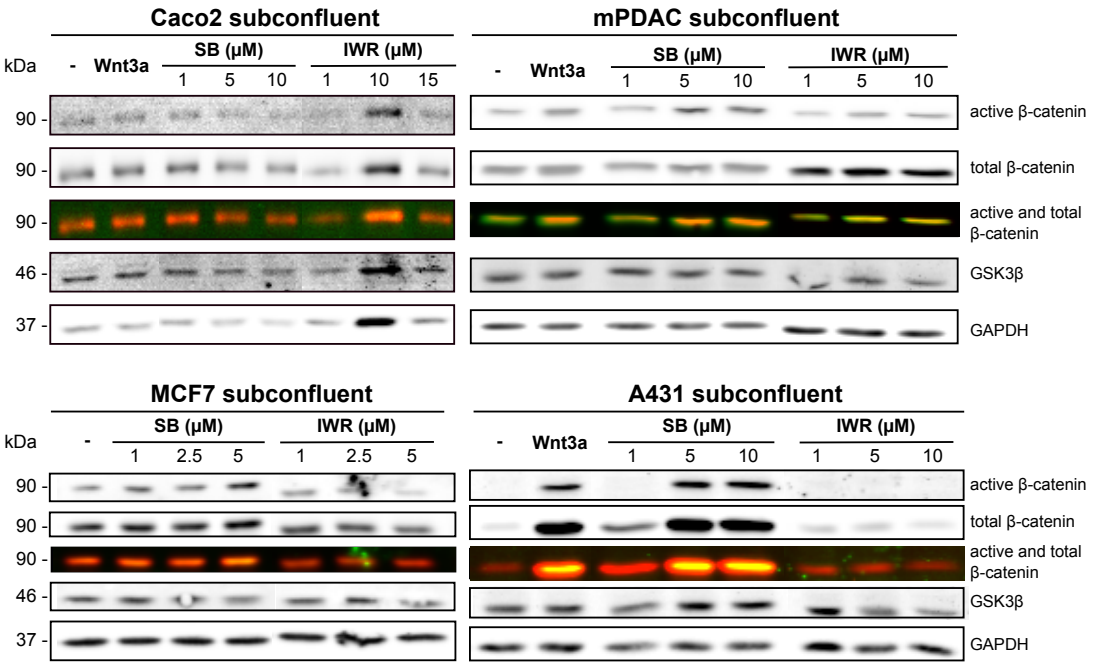

Figure 25: **Comparison of the Wnt modulation response in different cell lines.** Specific cell line responses of Caco2, mPDAC, MCF7 and A431 cells to 3 h stimulation with 150 ng/ml recombinant mWnt3a (0.1 % BSA in PBS), 1-10 µM SB216763 and IWR-1-endo (DMSO). Whole cell lysate immunoblots with 15 µg protein/lane, control (-) was incubated with respective amount of DMSO and 0.1 % BSA in PBS for 3 h. GAPDH was used as internal loading control Representative WB of 2 independent experiments. Adapted from F. Dietrich, Master thesis.

In WB analysis, A431 cells transfected with mCitrine-β-catenin^{WT} or mCitrine-β-catenin^{H470A} revealed stability changes upon Wnt stimulation on the endogenous β-catenin level, but the ectopically expressed sensor constructs were stabilized even without Wnt3a stimulation (Figure 26). The mCitrine-β-catenin^{WT} did not respond to Wnt response modulation by Wnt3a or the small molecule inhibitors, while mCitrine-β-catenin^{H470A} was stabilized upon Wnt3a and SB216763 treatment and destabilized by IWR-1-endo. Stability changes were visualized by the overlay of active and total β-catenin signal as well as active and total sensor signal.

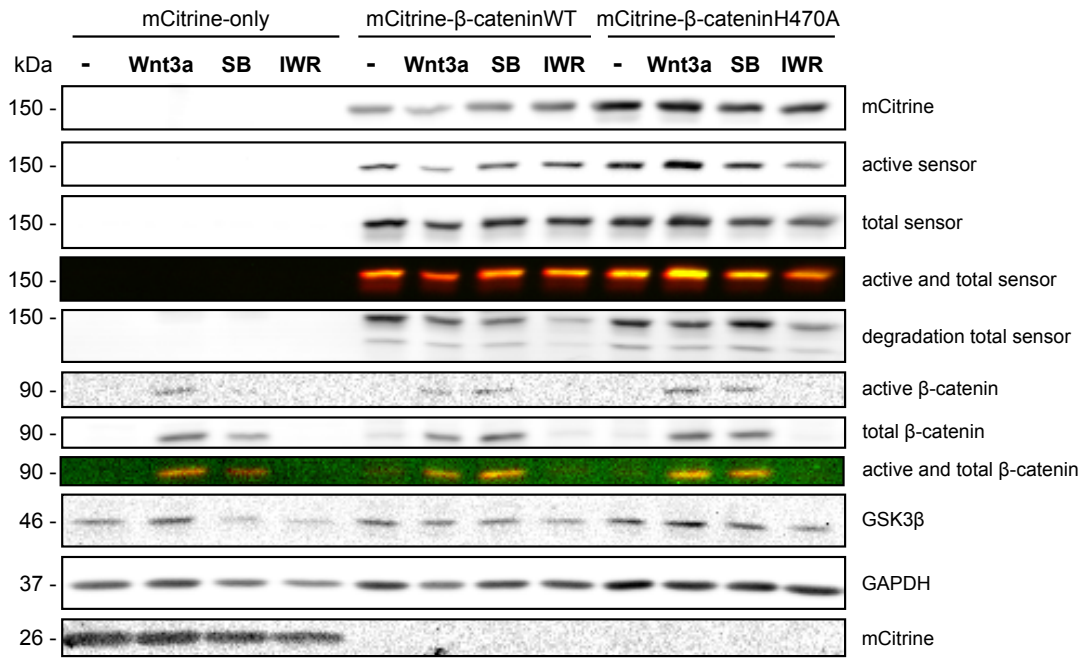

Figure 26: **Sensor response to Wnt signalling in A431 cells.** A431 were transfected with mCitrine, mCitrine-β-catenin^{WT}, mCitrine-β-catenin^{H470A} 48 h pre-stimulation. Western Blot analysis of whole cell lystaes upon stimulation with 150 ng/ml mWnt3a (0.1 % BSA in PBS), 10 µM SB216763 and IWR-1-endo (DMSO) for 3 h. Control (-) was incubated with respective amount of DMSO and 0.1 % BSA in PBS for 3 h. GAPDH was used as internal loading control. 20 µg protein/lane.

A431 cells were transfected with mCitrine-β-catenin^{WT} and mCitrine-β-catenin^{H470A} as well as corresponding mCitrine-acceptor-β-catenin combinations with mKate2, mCherry and mPlum (Figure 27). β-catenin fusion constructs localized at the plasma membrane, especially at sites of cell-cell contact. Soluble cytosolic β-catenin increased with expression level and mCitrine-mKate2-β-catenin tended to accumulate in the nuclei of cells. β-catenin^{H470A} did not accumulate within the nucleus, even in cells with high expression level.

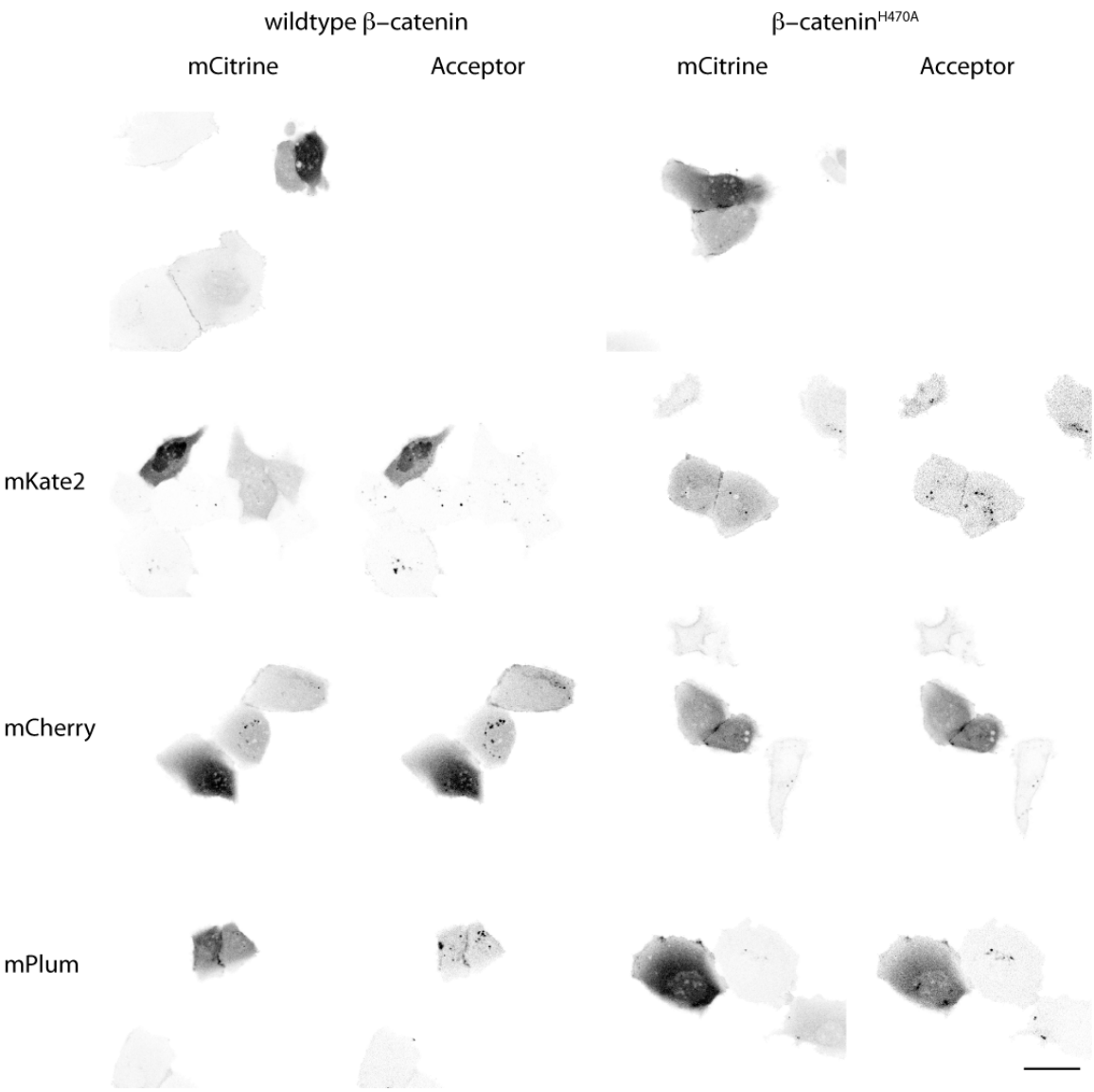

Figure 27: **Localization of β-catenin sensor constructs in A431 cells.** A431 cells transfected with mCitrine or mCitrine-acceptor fused β-catenin constructs, starved for 3 h. β-catenin localized to the plasmamembrane, especially to sides of cell-cell contact, as well as the cytosol. In addition, β-catenin^{WT} localized to the nuclei of A431 cells at high expression levels. Left: β-catenin^{WT} right: β-catenin^{H470A}. upper row: mCitrine without acceptor. Acceptors were mKate2, mCherry, mPlum. Scale bar 50 µm.

Since a high fraction of β-catenin is bound in the membranous pool by E-cadherin, once cells build cell-cell contact via adherens junctions, A431D cells, derived by dexamethasone treatment of A431 cells, were used[125]. It was shown, that A431D exhibit very low levels of E-cadherin and β-catenin and therefore changes in β-catenin protein level and activation upon Wnt stimulation should be dominant. In A431D cells, the sensor variants were not localized to the plasma membrane but distributed in the cytosol and the nucleus (Figure 28).

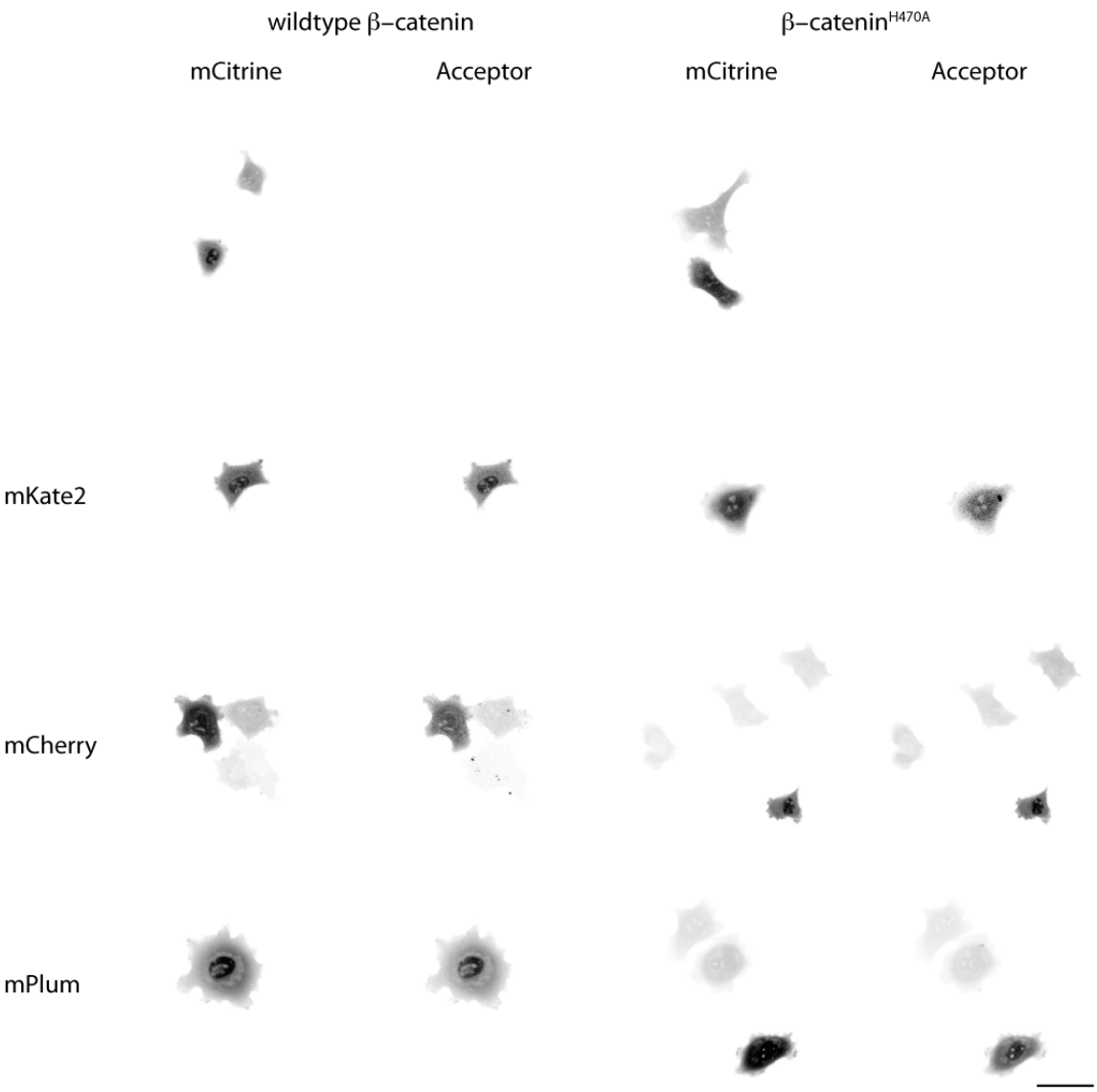

Figure 28: **Localization of β-catenin sensor constructs in starved A431D cells.** A431D cells transfected with mCitrine or mCitrine-acceptor fused β-catenin constructs, starved for 3 h. β-catenin localized to the cytosol and to the nuclei of A431D cells at high expression levels. Left: β-catenin^{WT} right: β-catenin^{H470A}. upper row: mCitrine without acceptor. Acceptors were mKate2, mCherry, mPlum. Scale bar 50 µm.

In starved A431D cells, wild type β-catenin was localized in the cytosol and the nucleus. In case of high expression levels, soluble β-catenin was increased and nuclear accumulation of wild type β-catenin was more prominent. β-catenin^{H470A} was less accumulated within the nucleus, likely because the reduced binding of the transcriptionally inactive mutant to TCF/Lef transcription factors, causes less retention of the β-catenin mutant in the nucleus[126].

6.2 Investigation of Wnt/β-catenin signalling in primary mouse hepatocytes

As the first step towards investigation of the Wnt/β-catenin activation during liver regeneration, the Wnt/β-catenin signalling in hepatocytes was investigated. Primary mouse hepatocytes (pmHep) were isolated and the Wnt response characterized in immunohistochemistry and immunoblots. During the isolation pmHeps were mechanically stressed and thereby already primed for regeneration[127,128]. Since Wnt signalling occurs during the priming phase of liver regeneration, it will most likely be present even without any stimulation[129]. Thus, it will be difficult to find an "OFF" state of Wnt signalling in primary hepatocytes.

Primary mouse hepatocytes were stained for total β-catenin and active β-catenin in collagen monolayer cultures (Figure 29). In unstimulated pmHep, total β-catenin was predominantly localized at sites of cell-cell contacts. A low level of cytosolic active β-catenin was detected. Upon stimulation with recombinant mWnt3a, active β-catenin translocated into the nuclei of pmHep. Total as well as active β-catenin level in the perinuclear area increased and β-catenin seemed to be localized to endomembranes.

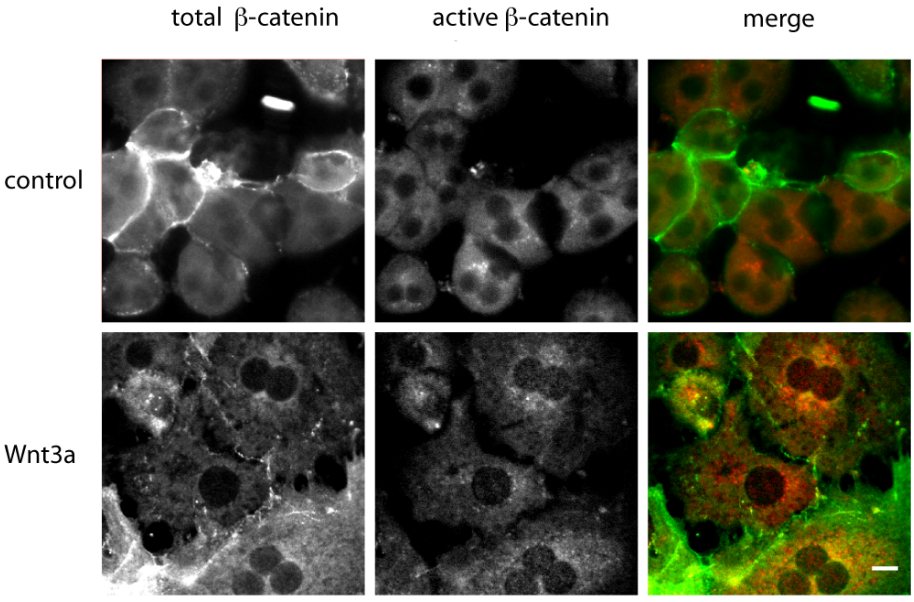

Figure 29: **Localization of endogenous β-catenin in primary mouse hepatocytes.** Active β-catenin translocated into the nuclei of primary mouse hepatocytes upon stimulation with recombinant mouse Wnt3a for 60 min. Immunohistochemistry of primary mouse hepatocytes on collagen monolayer, fixed with MeOH/Acetone and stained with rabbit anti total β-catenin (green) and mouse anti active β-catenin (red). Nuclei were stained using Hoechst dye. Scale bar 10 µm.

In WB analysis, pmHep on collagen monolayer were responding to Wnt stimulation and inhibition of GSK3β 24 h after isolation by an increase in active/total β-catenin (Figure 30). 48 h post isolation the Wnt3a response was diminished. In collagen sandwich cultures cells responded to Wnt3a stimulation as well as GSK3β inhibition by stabilization of β-catenin and to IWR-1-endo inhibition of Tankyrase by destabilization 48 h post isolation.

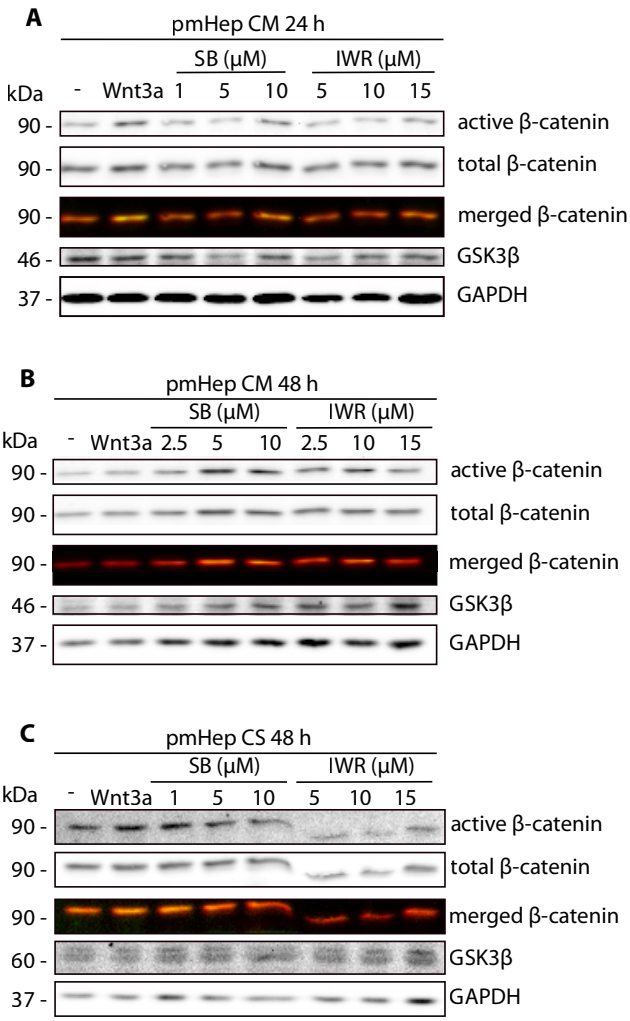

Figure 30: **Comparison of the modulation of the pmHep Wnt response under different culture conditions.** pmHep response to stimulation with 150 ng/ml recombinant murine Wnt3a (0.1 % BSA in PBS), 1-10 µM SB216763 and IWR-1-endo (DMSO) for 3 h. Collagen monolayer cultured pmHeps A. 24h or B. 48h post-isolation. C. Collagen sandwich cultured pmHeps 48h post-isolation. 30 µg (A.+B.) or 60 µg protein/lane (C) of whole cell lysates were immunoblotted. Control (-) was incubated with respective amount of DMSO and 0.1 % BSA in PBS for 3 h. GAPDH was used as an internal loading control.

Considering that primary hepatocytes de-differentiate and proliferate in collagen monolayer cultures and stay for a longer time resting and differentiated in collagen sandwich cultures, these two culture conditions canbe chosen as proliferative and

post-mitotic conditions of primary mouse hepatocytes when the β-catenin stability sensor would be applied.

6.3 Independent confirmation of the cellular Wnt response

As an independent reference for the cellular Wnt response, a published transcriptional reporter for Wnt induction, TCF/Lef:H2B-GFP, was selected. The reporter with nuclear localization was chosen, to spatially separate the transcriptional reporter from the sensor. The original construct harbours a GFP-fused Histone 2B under control of a minimal heat shock protein 68 promoter and a 4x TCF/Lef binding site[101]. GFP was exchanged against mTagBFP, for spectral separation from the β-catenin sensor. To see modulations in the reporter induction with a better temporal resolution a reporter with a C-terminal PEST sequence destabilized mTagBFP (d1mTagBFP) TCF/Lef:H2B-(d1)mTagBFP was created. Under Wnt stimulated conditions, the H2B-(d1)mTagBFP expression is facilitated and due to this, nuclear mTagBFP fluorescence intensity rises. The localization was not affected by the exchange of the fluorophore, but the distribution throughout the nucleus was different for the destabilized version (Figure 31), likely due to the reduced stability and therefore less condensed packaging of the tagged histones.

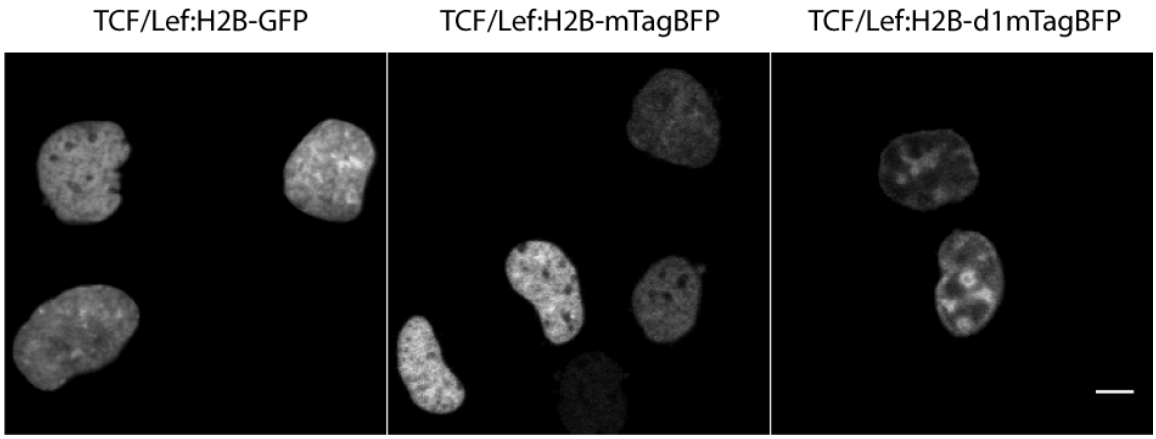

Figure 31: **Localization of TCF/Lef reporter constructs.** Under a TCF/Lef binding motif, an H2B-fusion protein is expressed upon transcription factor binding. GFP was exchanged to mTagBFP for spectral separation from the β-catenin sensor. mTagBFP was tagged with a C-terminal PEST sequence (d1mTagBFP) in order to destabilize H2B fusion proteins. Scale bar 10µm.

A431D cells were transfected with the transcriptional reporter TCF/Lef:H2B-mTagBFP and TCF/Lef:H2B-d1mTagBFP. Single cell traces were quantified for a

period of 2 h pre and 8 h post-stimulation, calculating the nuclear integrated density per time point per cell (Figure 32). Within this timeframe there was no significant difference between temporal profiles of carrier control (A/C) and recombinant mWnt3a (B/D) stimulated cells. The destabilization of the H2B at least reduced the variance of the control measurement (C), and under mWnt3a stimulation the slope of the average destabilized reporter response was steeper (D).

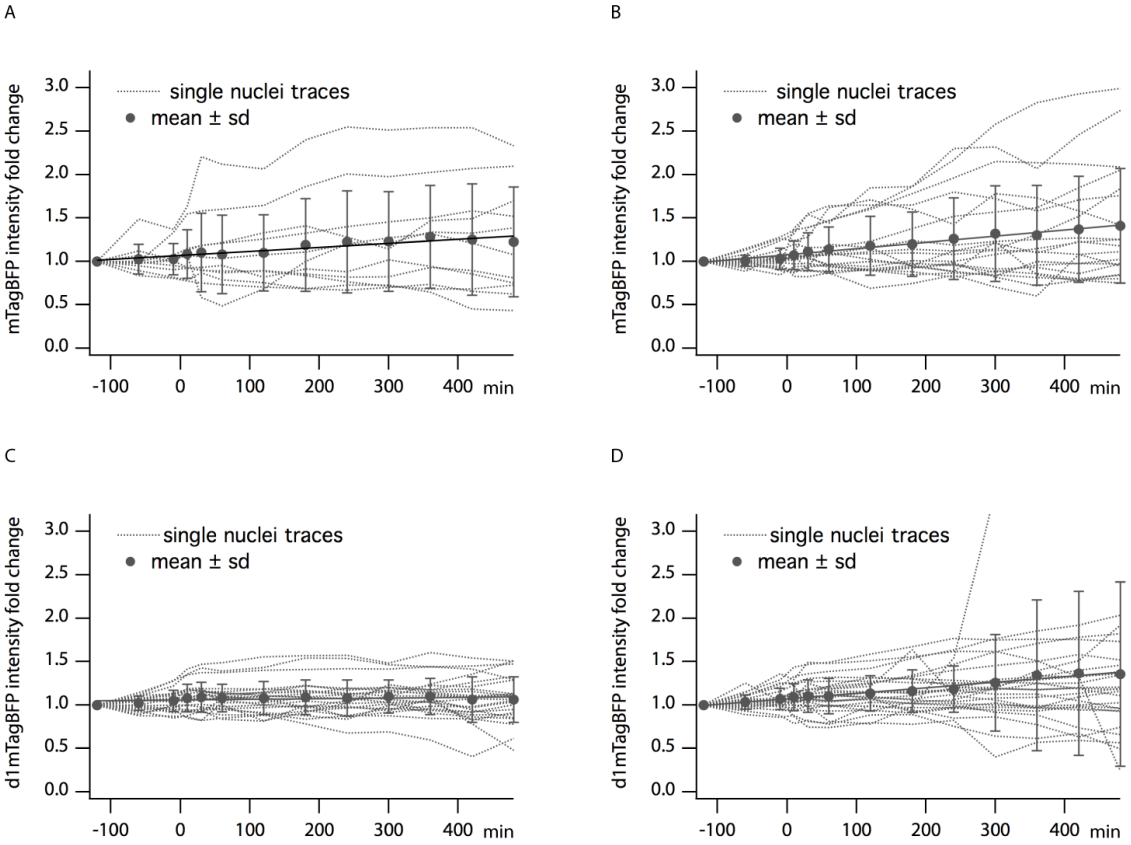

Figure 32: **TCF/Lef reporter response to recombinant mWnt3a stimulation in A431D cells.** Under a TCF/Lef binding motif, an H2B-fusion protein is expressed upon transcription factor binding. A. Basal TCF/Lef induction measured with the reporter construct TCF/Lef:H2B-mTagBFP (n=11). B. Wnt ligand dependent TCF/Lef induction measured with the reporter construct TCF/Lef:H2B-mTagBFP (n=19). C. Basal TCF/Lef induction measured with the destabilized reporter construct TCF/Lef:H2B-d1mTagBFP (n=25) D. Wnt ligand dependent TCF/Lef induction measured with the reporter construct TCF/Lef:H2B-d1mTagBFP (n=25). Data from 3 independent experiments.

In most studies using a transcriptional reporter, the whole population of cells was quantified independent of single cell fate. In contrast to that, the correlation of single cell transcriptional induction with stimulation was addressed in this experiment. Since Wnt stimulation causes cell cycle progression, the single cell analysis was reduced to a certain subset of cells. Over a time series of 10 h Wnt

stimulation led to cell division of the responding cells and reduced the number of cells left for analysis. The question is how to correlate the increase in reporter intensity with stimulation, if the signal becomes diluted after cell division? The more delayed a read out is from the signal induction; the more cells were excluded from single cell analysis in order not to monitor mitotic β-catenin signalling. To take later time points after stimulation into account to see a significant difference would therefore not solve the problem. In addition, it was shown that β-catenin/TCF interaction peaks in the late G2/M phase directly before mitosis[130]. This peak might bias the Wnt induced effect. Therefore all mitotic cells were excluded from the analysis, if mitosis occurred earlier than 8 h post-stimulation, reasoning that this cell cycle progression might not be Wnt induced.

The high variance in unstimulated control profiles of the transcriptional reporter strengthens the point, that due to the time delay in transcriptional induction, single cell Wnt response could not be resolved by this reporter efficiently. The idea to shorten the lifetime of the fluorophore to have a better temporal resolution of the transcriptional reporter was in principle correct, as the standard deviation in the control measurement of the d1mTagBFP intensity is lower than for mTagBFP. Still the stimulation with Wnt3a did not increase the temporal profile in a statistically significant manner.

6.4 β-catenin biosensor optimization

The overexpression of β-catenin^{WT} constructs as well as the stabilized S33Y mutants caused severe effects in most cell lines. Although the localization of β-catenin was unaffected, the activation of Wnt/β-catenin signalling led to induction of apoptosis. To prevent downstream effects of the sensor expression, further modifications of protein binding sites on β-catenin followed. Mutation of the TCF/Lef interaction site H470A led to a reduced transcriptionally active variant (<3 % of TCF/Lef interaction compared to wild type)[4].

This down modulation of transcriptional activity did not affect the stability or localization of overexpressed β-catenin (Figure 18). As described before, a lot of post-translational modifications and related functions on β-catenin have been

identified until now (Figure 4)[4]. Most of them are related to the degradation machinery or signalling. But there are also some connected to adherens junctions via E-cadherin or α-catenin binding.

In order to create a sensor that is exclusively reporting changes in β-catenin stability due to Wnt signalling, several additional mutations were introduced in the β-catenin sequence. Growth factor induced activation of c-src leads to phosphorylation of β-catenin at tyrosine 333. Pyruvate kinase M2 (PKM2) binding to phosphorylated Y333- β-catenin in the nucleus facilitates CyclinD1 expression[14]. Mutation of Y333 to phenylalanine (β-catenin^{Y333F}) inhibits the interaction of β-catenin with PKM2 and therefore abolishes the EGFR-induced CyclinD1 expression. In pulse-chase experiments, β-catenin^{Y333F} did not show altered stability as compared to the wild type protein[14]. Consequently, an effect of the mutation on the stabilization of the sensor independent of Wnt signalling would not be expected. Subsequent to Kras induction, the Rac1 effector p21-activated kinase 1 (PAK-1) interacts with β-catenin and phosphorylates it at serine 675 in the c-terminal domain, stabilizing it and promoting transcriptional activation[15]. The mutation S675A did not reduce β-catenin stability or interfere with β-Trcp binding and ubiquitination. It also did not interfere with binding to TCF/Lef promoter sequences, but reduced CyclinD1 induction and TOP/Flash activation in colorectal cancer cells[15]. Implementing S675A in the stability sensor would therefore reduce the Kras induced transcriptional activation, but not cause Wnt independent changes in stability. Another residue that was mutated was serine 552, since it becomes directly phosphorylated by Akt-1/PKB independent of Wnt signalling. This S552A mutation nearly abolishes the AKT/PKB mediated non-canonical stabilization and nuclear translocation of β-catenin[16]. Whether it affects the Wnt dependent stabilization of β-catenin was not yet addressed. E-cadherin binds to β-catenin in adherens junctions at the plasma membrane. Upon growth factor stimulation, β-catenin is phosphorylated at tyrosine 654 by RTKs and released from the E-cadherin complex. The phospho-mimetic mutant β-catenin^{Y654E} was shown not to localize at the plasma membrane, but in the cytosol in MDCK cells[17], thereby reducing the non-canonical activation of β-catenin translocation and transcription. In order to optimize the Wnt response of the

sensor, all non-Wnt induced pools of the β-catenin stability sensor should be reduced to a minimum. A high fraction of endogenous β-catenin is localized to the plasma membrane in complex with E-cadherin and released upon growth factor stimulation. This release causes a massive and abrupt relative increase in soluble cytosolic β-catenin levels, mimicking β-catenin stabilization and thereby also influencing downstream signalling. β-catenin Y654E mutation in the stability sensor would reduce this Wnt independent influence on β-catenin stabilization.

Complementary to the inhibition of non-canonical β-catenin stabilization by disruption of interaction using mutations, the stability of β-catenin can be modified by C- or N-terminal truncations. While N-terminal truncations lead to stabilization, similar to the mutations in the GSK3β motif (β-catenin^{S33Y}), reduced half-lifetimes have been shown for C-terminally truncated β-catenin, like $\partial 664$ β-catenin[12]. In addition and in consistence with data for β-catenin^{S675A}, expression of 108 AA C-terminal truncated β-catenin $\partial 675$ reduced transcriptional activity by a factor of 10 compared to overexpressed full-length protein[13].

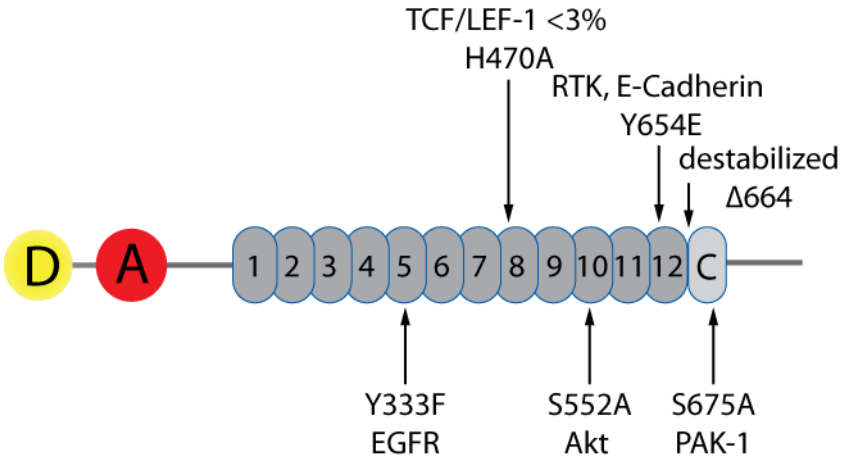

Figure 33: **Optimized β-catenin stability sensor.** Mutations to limit signalling activity of the sensor construct to a minimum and to reduce non-canonical Wnt response. D: donor fluorophore, A: acceptor fluorophore, 1-12: ARM repeats, C: c-terminal α-helix.

The reduction of overall stability by the c-terminal truncations would probably fit better to the maturation times of the acceptor fluorophores that were available. Therefore the dynamic range of the sensor could be maximized. Although there are multiple other sites, the suggested mutations hit the major non-canonical pathways affecting β-catenin stability and down stream effects. The full-mutated

sensor bears the following point mutations: β-catenin$^{Y333F/H470A/S552/Y654E/S675A}$, and will be referred to as β-catenin^{FM}. The stabilized version β-catenin$^{S33Y/FM}$ was used as a reference. In an attempt to better match the turn-over rate of the sensor with the maturation time of the fluorophores a truncated β-catenin^{FM}, β-catenin$^{FM\text{-}\partial CTD}$ was tested.

6.5 Characterization of the intramolecular β-catenin biosensor

6.5.1 Biochemical analysis of the β-catenin sensor

A431D cells were transfected with empty pcDNA3.1S+ (mock), TCF/Lef:H2B-d1mTagBFP (TCF/Lef reporter), mCitrine-β-catenin^{FM} (mCitrine-β-catenin^{FM}) as the donor only control used for FLIM, the sensor mCitrine-mPlum-β-catenin^{FM} (sensor^{FM}), the stabilized mutants of the sensor^{FM} constructs with an additional S33Y mutation and the mCitrine-β-catenin$^{FM\text{-}\partial CTD}$ as well as sensor$^{FM\text{-}\partial CTD}$. 32 h post-transfection A431D were starved over night in medium containing 0.1% FCS. After stimulation with 150 ng/ml Wnt3a for 0 (ctrl), 90 or 180 min, whole cell lysates were prepared. On WB, active β-catenin antibody (ABC) recognizes N-terminally non-phosphorylated (active) β-catenin (Figure 34). Endogenous β-catenin was stabilized and active β-catenin detected after stimulation with Wnt for 90 and 180 min. The fraction of active/total β-catenin increased upon stimulation, indicating an inhibition of the degradation complex. The endogenous Wnt response was similar in the samples with the transcriptional reporter, sensor or mock-transfected cells. Due to an unspecific band at the size of the sensor, ectopic ABC level was not quantified for the sensor-transfected cells. Upon stimulation, protein level of the sensor was not increased when compared to pre-stimulation levels (Figure 34). C-myc protein level increased upon Wnt3a induced β-catenin activation and stabilization, but basal c-myc levels were not elevated in sensor-transfected cells compared to mock transfected cells (Figure 35). This indicates that an efficient block of the transcriptional activity of the sensor has been achieved.

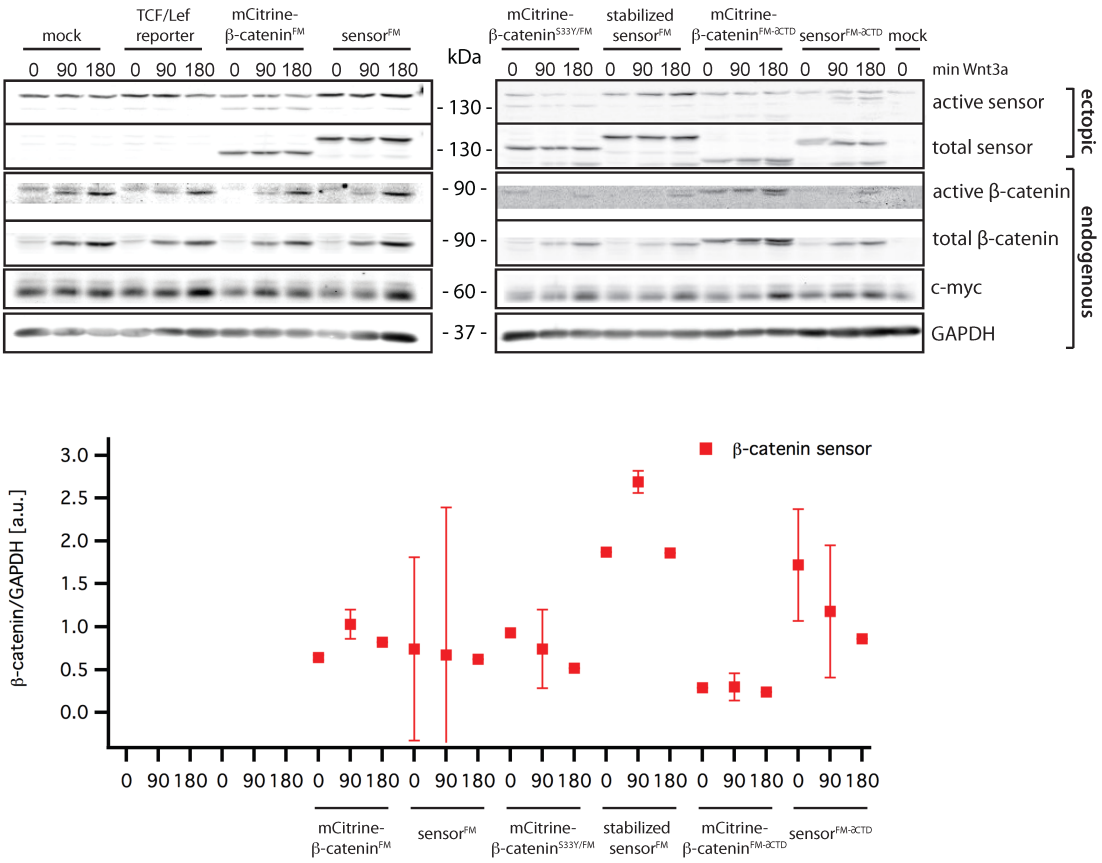

Figure 34: **Biochemical characterization of the stability sensor β-catenin^{FM} and β-catenin$^{FM-\partial CTD}$.** β-catenin protein level in A431D cells upon stimulation with 150ng/ml recombinant Wnt3a. Comparison of cells transfected with empty plasmid (mock), a TCF/Lef reporter with H2B-d1TagBFP expression under control of a TCF/Lef responsive element (TCF/Lef reporter), mCitrine-β-catenin^{FM}, the biosensor mCitrine-mPlum-β-catenin^{FM} (sensor^{FM}), the stabilized mutants mCitrine-β-catenin$^{S33Y/FM}$, sensor$^{S33Y/FM}$, mCitrine-β-catenin$^{FM-\partial CTD}$ and sensor$^{FM-\partial CTD}$. Due to the unspecific band at the size of the sensor, ectopic ABC level was not quantified for the sensor transfected cells. Protein levels were normalized to GAPDH. Mean ± standard deviation, N=3.

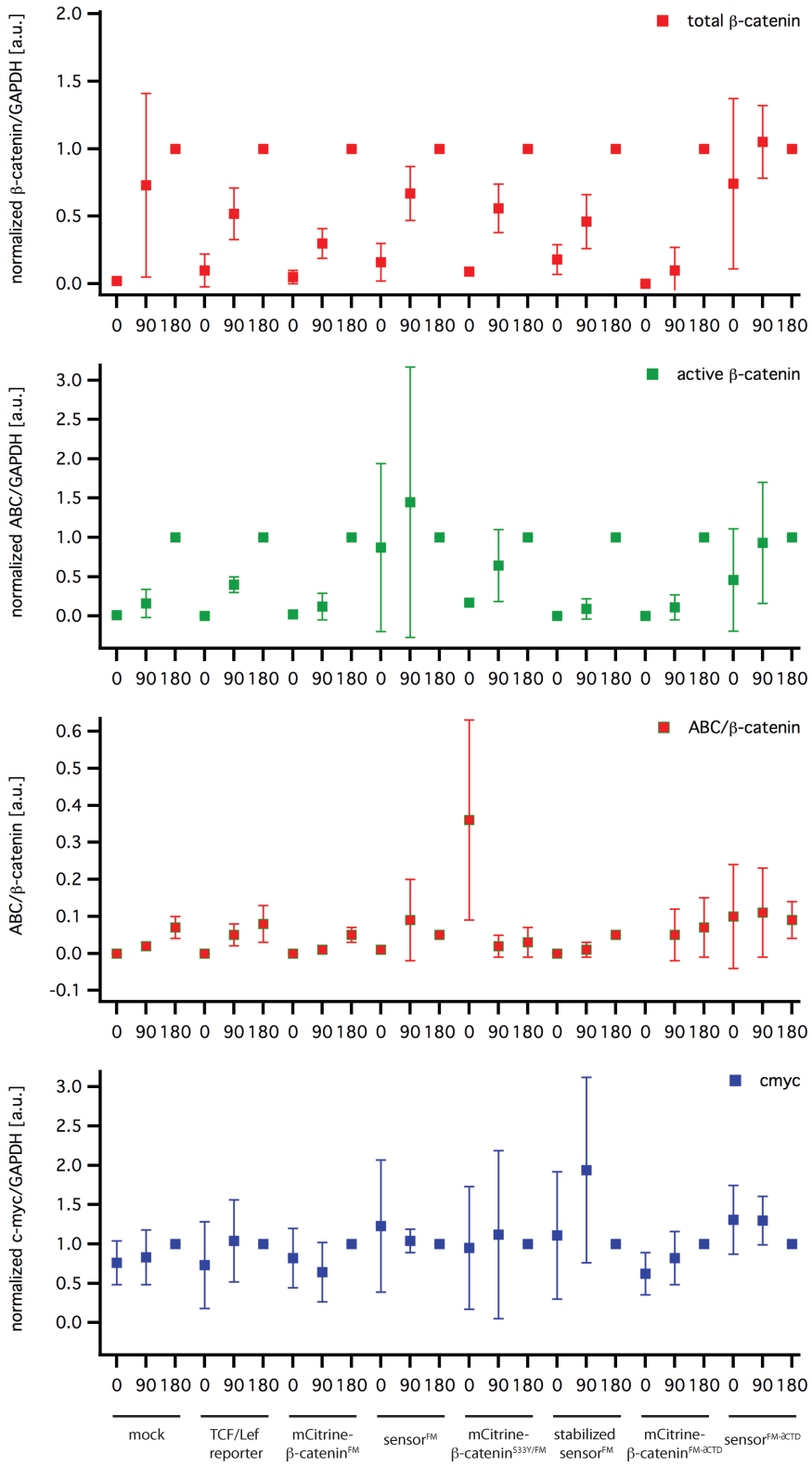

Figure 35: **Biochemical characterization of the stability sensor β-catenin^{FM} and β-catenin$^{FM-\partial CTD}$.** β-catenin protein level in A431D cells upon stimulation with 150ng/ml recombinant Wnt3a. Comparison of cells transfected with empty plasmid (mock), a TCF/Lef reporter with H2B-d1TagBFP expression under control of a TCF/Lef responsive element (TCF/Lef reporter), mCitrine-β-catenin^{FM}, the biosensor mCitrine-mPlum-β-catenin^{FM} (sensor^{FM}), the stabilized mutants mCitrine-β-catenin$^{S33Y/FM}$, sensor$^{S33Y/FM}$, mCitrine-β-catenin$^{FM-\partial CTD}$ and sensor$^{FM-\partial CTD}$. Protein levels were normalized to GAPDH and the 180 min stimulation time point. Mean ± standard deviation, N=3.

The β-catenin stability sensor^{FM} and sensor$^{FM\text{-}\partial CTD}$ did not accumulate upon recombinant Wnt3a stimulation in whole cell lysates of A431D cells. The endogenous Wnt response was not hyper activated by the expression of the stability sensor, neither on the level of β-catenin stabilization, nor on transcriptional activation level.

6.5.2 Correlating the β-catenin sensor response with cellular Wnt response using ratiometric imaging

Alternatively to the lifetime measurement, the ratio between the mCitrine and mPlum intensity in the sensor was analysed as a measure of protein stability. For this approach no specialized equipment is needed, except a conventional inverted widefield microscope with a high NA objective and a filter set for YFP/RFP spectral separation. When β-catenin is stabilized within the cell, the sensor protein half-lifetime is prolonged and mPlum maturation more probable. Consequently, the ratio of A/D should be higher after Wnt stimulation and subsequent β-catenin stabilization.

WB analysis of stimulated A431D cells (Figure 34) and imaging experiments showed a response of β-catenin accumulation within 3 h post-stimulation. Considering that Wnt3a promotes cell cycle progression, and in turn, it is known that cell cycle progression changes β-catenin concentration within the cell, stabilization profiles were recorded 1 h pre-stimulation until 6 h post-stimulation. All cells that divided within that timeframe were excluded from the analysis. A representative example of β-catenin stability sensor^{FM} showed an increase in mCitrine over mPlum (D/A) intensity ratio upon Wnt3a stimulation within 90 min (Figure 36). While mCitrine intensity peaks at 90 min post-stimulation, mPlum intensity was maximal after 3 h.

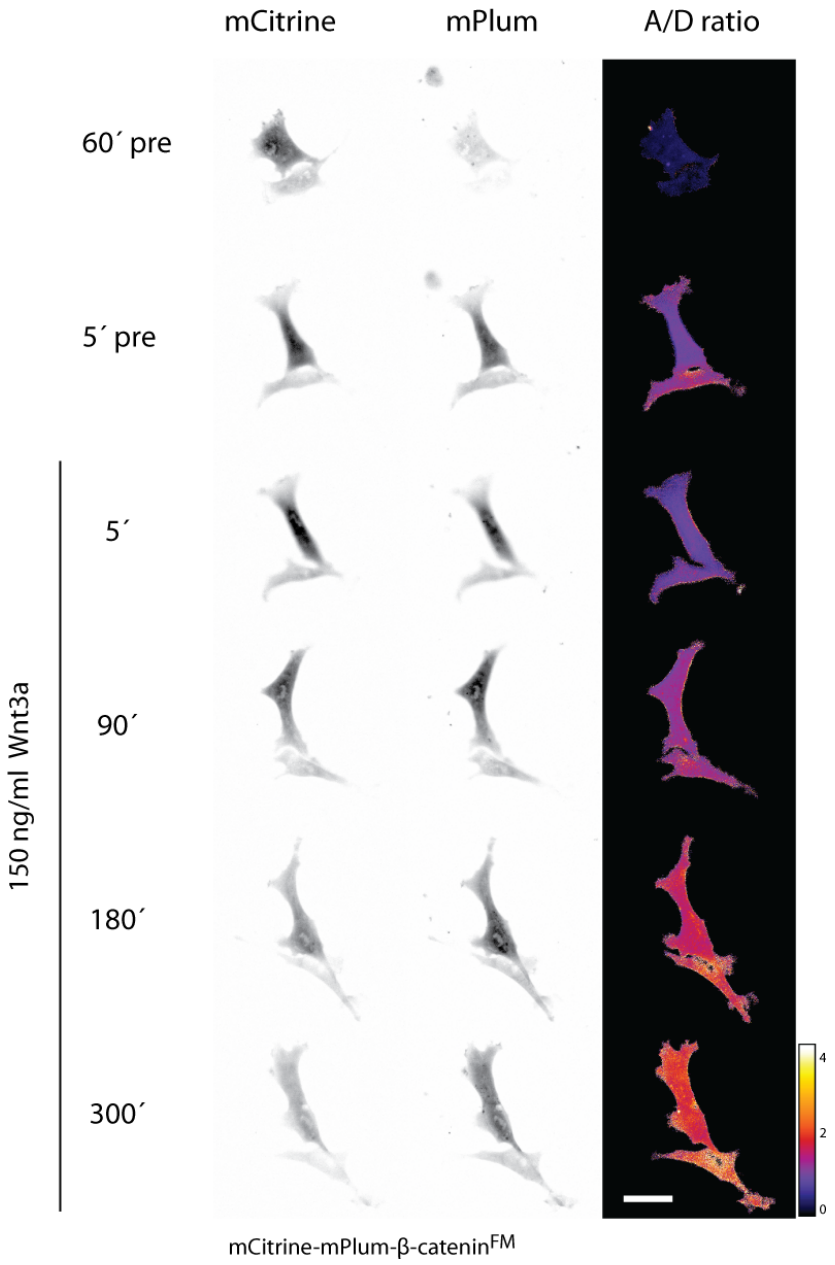

Figure 36: **Ratiometric imaging of the optimized β-catenin sensor in A431D cells.** A representative example of a responding cell upon 150 ng/ml Wnt3a stimulation. Scale bar 50 µm.

These results indicate that the β-catenin stability sensor^{FM} monitors the accumulation of endogenous β-catenin early (within 2 hours) after Wnt induction by an increase of the donor intensity and indeed, due to longer protein-half-lifetime, reports stabilization by an increase of mPlum intensity.

Different variants of the sensor were tested for their temporal profiles of D/A ratio to Wnt stimulation. For the control, without Wnt, flat temporal profiles of D/A intensity were expected.

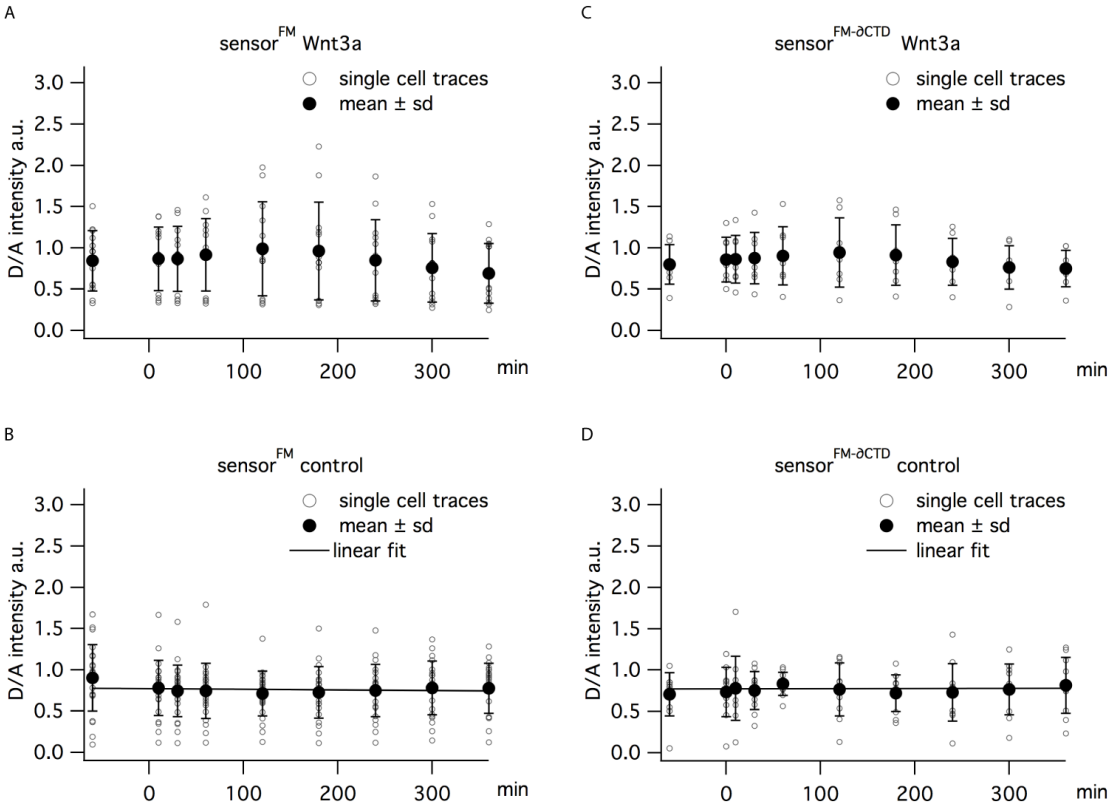

Figure 37: **Single-cell profiles of full mutated sensor constructs in A431D cells.** Quantification of β-catenin^{FM} sensor or β-catenin$^{FM\text{-}\partial CTD}$ transfected A431D cells upon stimulation with recombinant mWnt3a (150 ng/ml) or carrier control. Plots show single-cell traces and average profiles +/- sd from N=3 independent experiments with different cell passages on different days.

The D/A intensity ratio was highly diverse for single cell analysis, since a lot of parameters influence the stability of β-catenin and the copy number of the β-catenin sensor plasmid for example could not be controlled. Hence, amplitude-based clustering to classify responders and non-responders was performed using an affinity propagation test provided and computed by Dr. habil. A. Koseska. The affinity propagation algorithm[105] takes the set of real-valued similarities (s(i,k)) calculated between all pairs of β-catenin sensor stability profiles after Wnt3a stimulation as an input. With this affinity propagation assay the temporal profiles of β-catenin^{FM} sensor were clustered into active and inactive ones (Figure 38). The fraction of responders in the analysed cells was 26 %. Considering that all fast responders could not be clustered because they divided within the 6 h post-stimulation, this fraction was expected. In the control situation, where the Wnt pathway is inactive and cells were starved but not stimulated, very few cells were excluded. Most of these cells were dying or moving out of the field of view. In the

control situation, cells with a comparably stable β-catenin^{FM} sensor (shifted basal D/A intensity ratio) and a flat temporal profile were observed. The difference in temporal profiles proved that stabilization does not occur simply due to an overload of the degradation machinery in sensor-transfected cells, but due to Wnt stimulation. Otherwise these profiles would occur also in the control measurement.

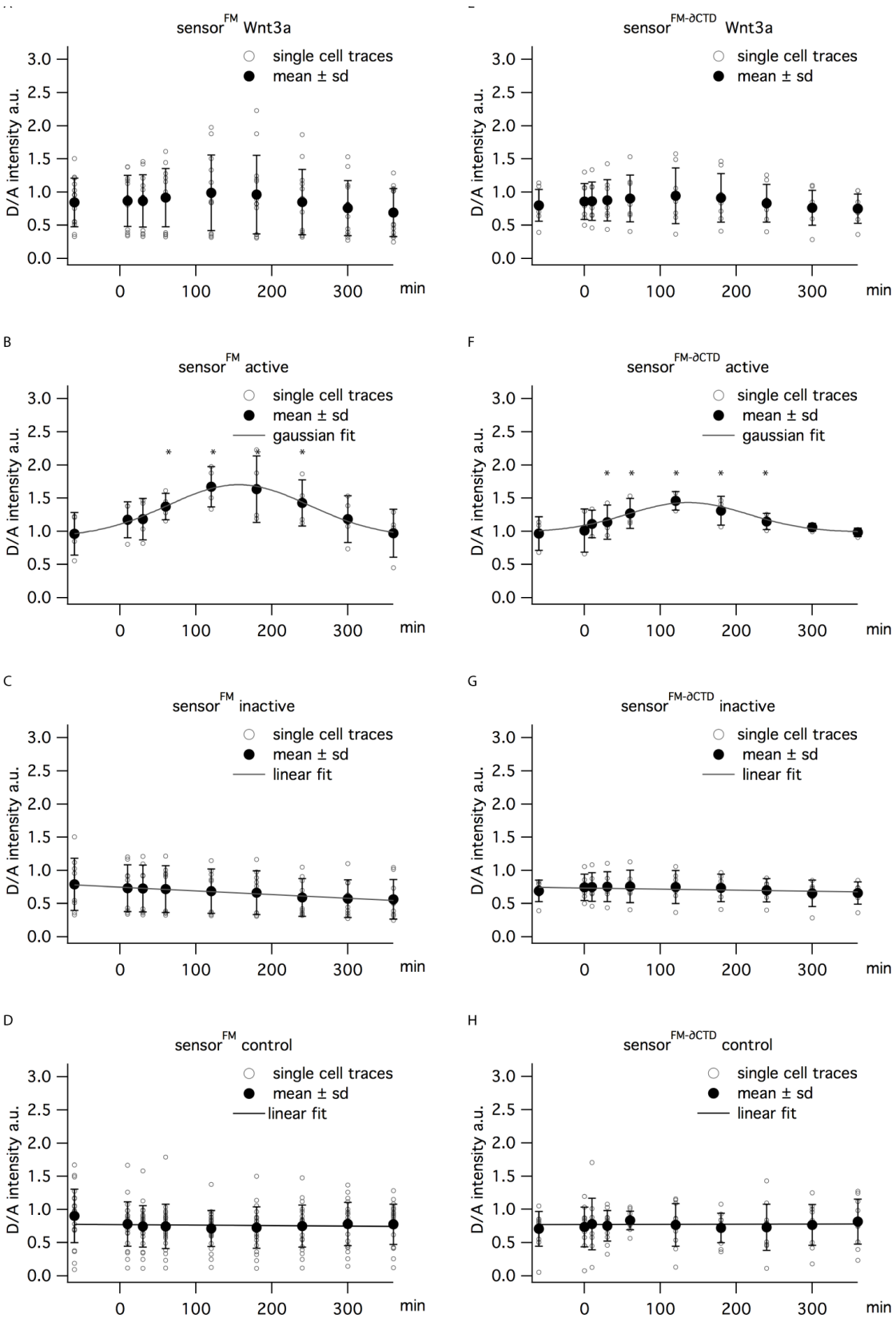

Figure 38: **Affinity propagation clustered single-cell profiles of β-catenin sensor^{FM} (A-D) and sensor$^{FM-\delta CTD}$ (E-H) in A431D cells**. Single-cell and average ± sd temporal profiles upon stimulation with recombinant mWnt3a (150 ng/ml) or carrier control. A+E. Wnt3a stimulated cells before affinity propagation test. B+F. active (responder) C+G. inactive (non-responder) and D+H. control cell temporal profiles. * significant difference to non-responders and control (Wilcoxon Rank Test). N=3 independent

experiments with different cell passages on different days. Affinity propagation test for classification of profiles provided and computed by Dr. habil A. Koseska.

The comparison of the gaussian fits of the average active sensor profiles showed different response properties of the full-length and the CTD-truncated variant (Figure 39). In agreement with the published data about a destabilization of β-catenin after C-terminal truncation, the sensor$^{FM\text{-}\delta CTD}$ was reaching the peak of it's D/A ratio (136±25 min) faster than the sensor^{FM} (156±30 min). In addition, the peak width was shorter (112±42 min) in case of sensor$^{FM\text{-}\delta CTD}$ than for sensor^{FM} (131±93 min). Considering that also the standard deviation for the peak amplitude was reduced for the truncated version, sensor$^{FM\text{-}\delta CTD}$ would probably be the better sensor.

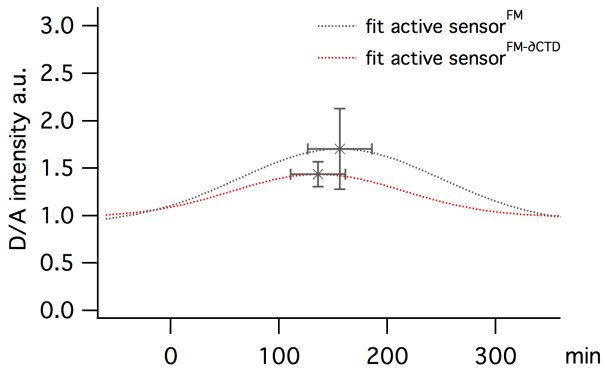

Figure 39: **Comparison of the full-mutated sensor variants and their response properties.** From the Gaussian fit of the active sensor^{FM} and active sensor$^{FM\text{-}\delta CTD}$ the maximal response time point for the two variants was calculated and indicated as markers with sd.

In order to cross-correlate the sensor response with an independent measure of cellular stimulation, the transcriptional reporter (TCF/Lef:H2B-d1mTagBFP) was co-expressed (Figure 40). In case of the β-catenin^{FM} sensor, active and inactive temporal profiles of the sensor could be separated by affinity propagation, but were not significantly different from the control. The cross-correlation of the stability sensor and the TCF/Lef reporter was not possible, since the normalized fold-change of the transcriptional reporter was independent of Wnt stimulation. Probably, the reporter with H2B fusion constructs is not suitable to report short-term changes in transcriptional activation, due to the relatively stable protein H2B.

The peak of the temporal profiles of Wnt-responding cells is shifted towards later time points in presence of the transcriptional reporter, as compared to the temporal profiles without co-expression of the transcriptional reporter (Figure 38 Figure 41). During long-term experiments, a lot of the responders divided or died, while the non-responders just stayed. As mentioned before, it might be an effect of the transcriptional reporter, that endogenous β-catenin binds to the repetitive TCF/Lef motif on the reporter, rather than endogenous TCF/Lef motifs in the promoter region of target genes. If target genes are not induced, feedback loops of Wnt signalling, like an increase in Conductin, leading to a shut down of β-catenin stabilization will not occur. That could cause a hyper activation of Wnt responsive cells and lead to apoptosis.

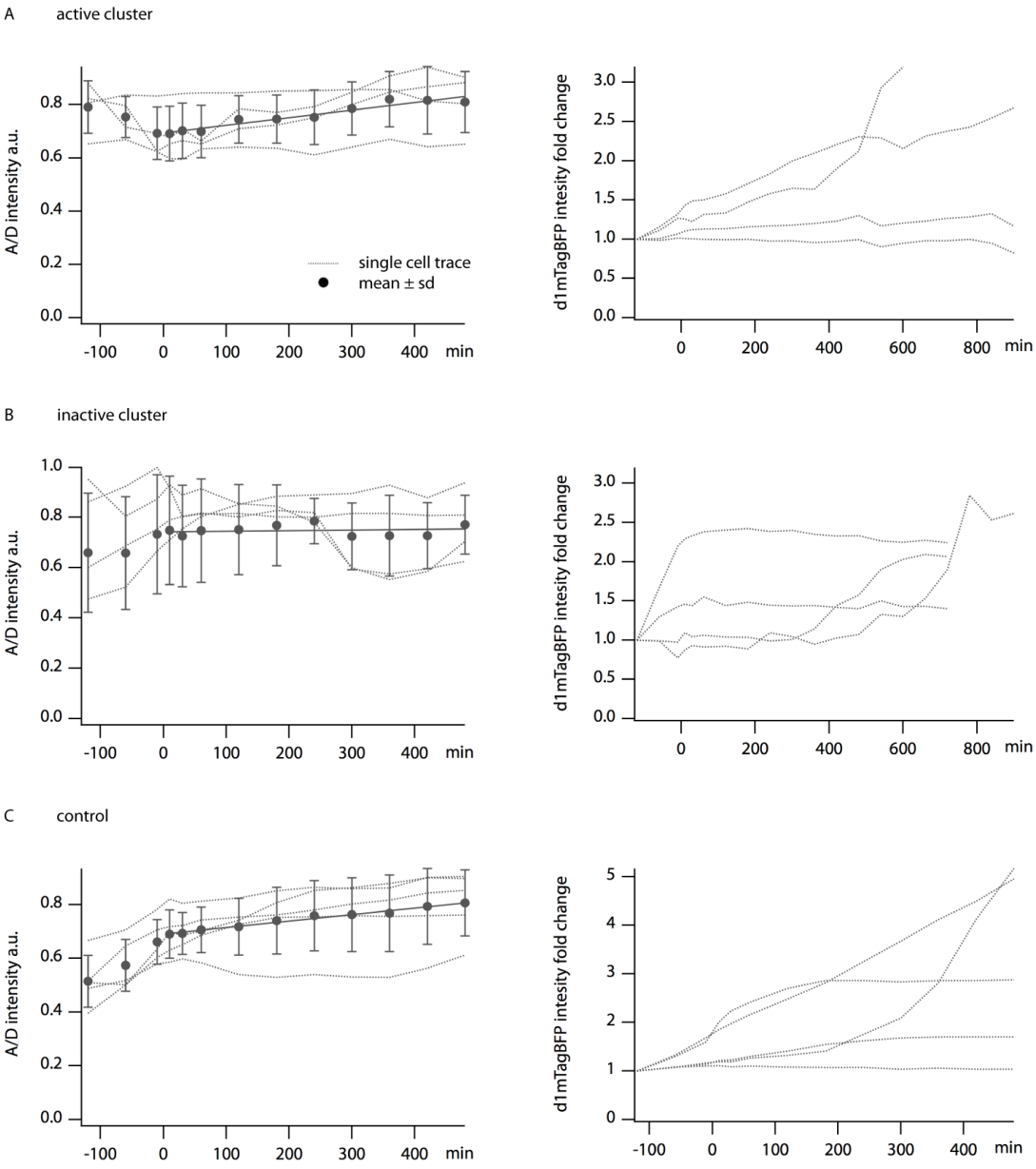

Figure 40: **Affinity propagation clustered single-cell profiles of β-catenin^{FM} sensor and correlation with the transcriptional reporter in A431D cells**. Affinity propagation clustered single-cell and average +/-sd temporal profiles of β-catenin^{FM} sensor in A431D cells co-transfected with TCF/Lef:H2B-d1mTagBFP reporter upon stimulation with mWnt3a (150 ng/ml) or carrier control. Temporal response of A. active B. inactive C. control. N=4 independent experiments with different cell passages on different days.

For the stabilized sensor$^{S33Y\text{-}FM}$, the affinity propagation test identified responders, which showed a good cross-correlation with the transcriptional reporter (Figure 41). The classified non-responders did not show a fold change in the intensity of the transcriptional reporter signal. In the control situation the same two groups of responders and non-responders were present. The artificial stabilization by the S33Y mutation could have induced a chronic autonomous activation of the Wnt signalling cascade, since the H470A mutation reduced the interaction with TCF/Lef

family of transcription factors to 3 % but did not completely abolish it. The remaining low affinity of the stabilized construct for the binding to TCF/Lef transcription factors might have been sufficient for induction of the transcriptional reporter. This conclusion was also supported by the increase in the reporter intensity already observed for the pre-stimulation time points.

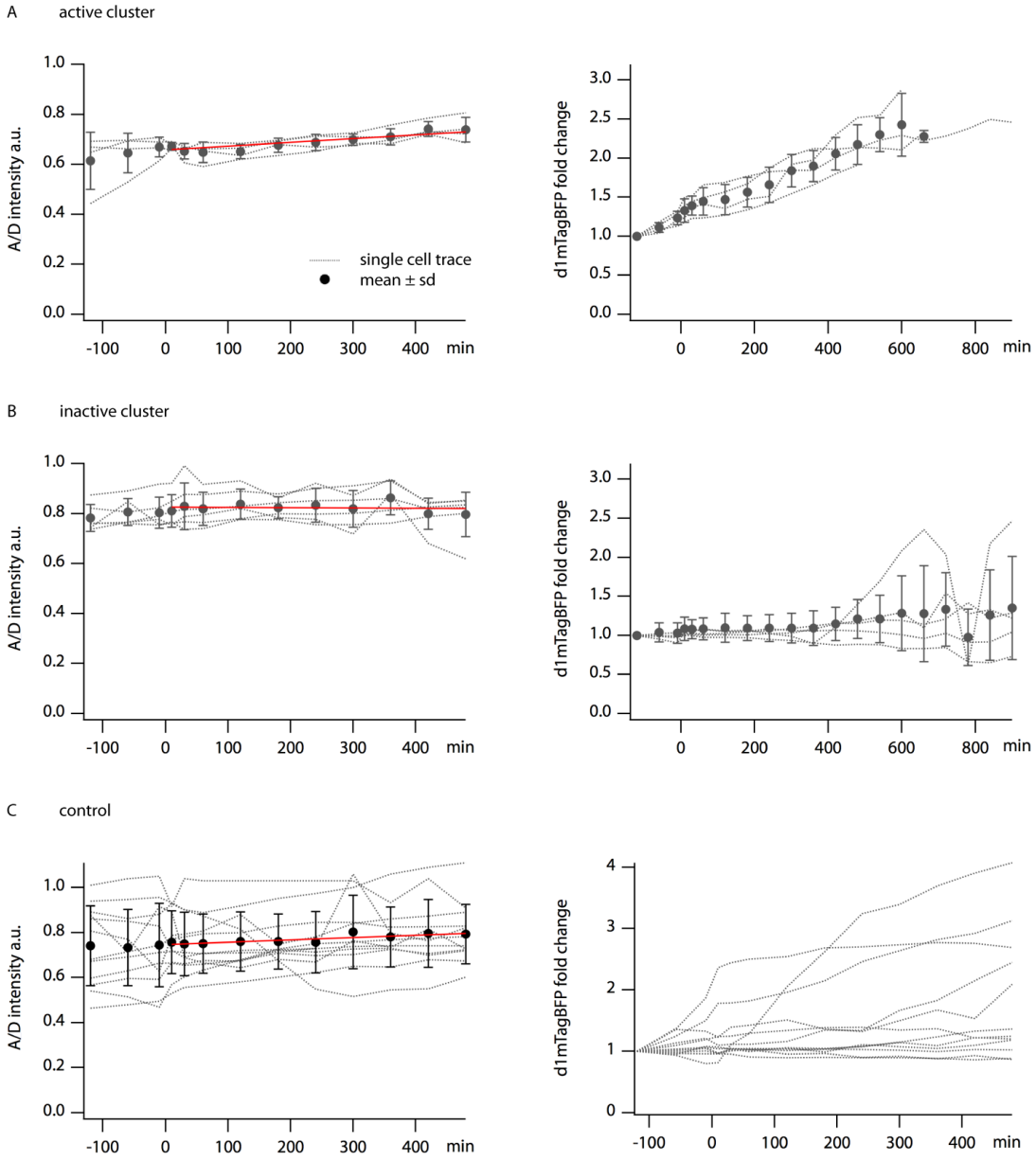

Figure 41: **Affinity propagation clustered single-cell profiles of β-catenin$^{S33Y-FM}$ sensor and correlation with the transcriptional reporter in A431D cells**. Affinity propagation clustered single-cell and average +/-sd temporal profiles of β-catenin$^{S33Y-FM}$ sensor in A431D cells co-transfected with TCF/Lef:H2B-d1mTagBFP reporter upon stimulation with mWnt3a (150 ng/ml) or carrier control. Temporal response of A. active B. inactive C. control. N=4 independent experiments with different cell passages on different days.

7 Discussion

7.1 The current status of the toolbox to analyse Wnt/β-catenin signalling

Investigations of Wnt signalling have been mostly done with chronic or long-term perturbation of the systems. The read-out was typically population-based, rather than at the single-cell level, partially due to a lack of methods allowing single-cell analysis over the long period of time Wnt/β-catenin signalling needs to be observed to correlate input and output of the signalling pathway. Different approaches have been performed to investigate Wnt/β-catenin signalling so far:

- Transciptional reporter systems

The transcriptional responses upon Wnt induction typically reported by the transcriptional reporter system TOPflash or its derivatives. Theses are luciferase- or GFP-based reporters of β-catenin mediated transcription activation and therefore report changes with a time delay. Such transcriptional reporter systems cannot discriminate between Wnt dependent and Wnt independent transcriptional β-catenin activation.

- GSK3β activity sensor

In the context of Wnt signalling, a GSK3β activity sensor based on the intensity increase of destabilized fast folding eGFP was introduced in 2010[131]. Although there is a correlation between the GSK3β sensor response and β-catenin activity, the GSK3β sensor addresses the whole group of GSK3β regulating signalling pathways and the stability of the down stream effectors (approx. 20% of the protein mass in the cell).

- A FRET sensor based on β-catenin truncated mutant

A FRET sensor based on truncated β-catenin N-terminally tagged with a CFP and C-terminally tagged with a YFP was used to show that the CTD is folding back on the ARM domains, therefore allowing FRET to occur[12]. Nevertheless, the authors admit that they could not observe FRET between CFP/YFP fused to full-length β-catenin. They used a N-terminally truncated version, overriding the degradation complex control of β-catenin levels in the cell. Consequently, the conformational change of active β-catenin upon binding to the degradation complex can be addressed but not stability changes. Since β-catenin is per default active, unless it is

phosphorylated at the N-terminus, this N-terminally truncated conformational sensor can not address the Wnt induced stabilization and accumulation, because without its degradation motif it is per default stabilized. In addition, there is no way to discriminate between unbound but phosphorylated and unbound non-phosphorylated species, which would have a different protein half-lifetime.

In this thesis a novel sensor for Wnt/β-catenin signalling that accurately reports early events of Wnt/β-catenin activation was presented, which can be used to monitor the temporal and spatial profile of β-catenin at the singe cell level.
This β-catenin stability sensor was modified to disentangle β-catenin/Wnt signalling from non-canonical Wnt signalling pathways. Further, downstream transcriptional activation was inhibited, so that the biosensor neither interferes with the degradation kinetics of the endogenous β-catenin nor the downstream effectors or the induction of feedback loops. To address the decision point in Wnt/β-catenin signalling, which is the inhibition of β-catenin degradation, leading to accumulation and transcriptional activation, β-catenin stability itself was chosen as the read-out of the sensor. Since intensity based approaches are very sensitive to changes in expression level, transfection efficiency, penetration depth of light into the sample and other factors, the design of the sensor was intended to be intensity independent. The fluorescence lifetime of a fluorophore is independent of its intensity, but changes upon FRET with an acceptor in close proximity.
With the development of timer fluorophores, which change their spectral properties during maturation, it is possible to gather information about the lifetime of proteins in living cells using one fluorescent tag[106]. Due to improvements of genetically encoded fluorescent tags, the better characterization of maturation times and spectral properties, combinations of fluorophores can be used as stabilization timers[132].

7.2 Characterising the new biosensor

Biochemical investigations of the β-catenin stability sensor were performed to confirm that the endogenous Wnt signalling response was not overwritten by the expression of the β-catenin stability sensor (Figure 35). As a result, endogenous

β-catenin was not pre-stabilized in sensor transfected cells and the target gene expression was not elevated in comparison to the control, this aim was reached. Strikingly, the protein level of the sensor molecule itself was not enhanced after Wnt stimulation (Figure 34). In context of literature data about the protein half-life time of endogenous β-catenin, ectopic β-catenin half-life time was always higher. In combination with the fact that the expression level of ectopic β-catenin was already high, even without any stimulation, further accumulation of the sensor molecule upon Wnt stimulation might occur only after longer stimulation time. Additionally, the high expression level might to a certain degree overload the degradation machinery. The fact, that the endogenous β-catenin was degraded in the presence of the sensor, points to a less efficient binding of fluorescently tagged β-catenin to the degradation complex due to steric hindrance in the degradation complex, rather than an overload of the degradation machinery. Considering that a change in relative levels is more important for β-catenin activity than absolute levels within the cell[133], it is also likely that a stable expression will be even less perturbing for the cellular system than the transient transfection used during the development of the sensor. FLIM measurements of the β-catenin stability sensor in MCF7 cells revealed a Wnt dependent decrease of the donor lifetime, but with a very limited dynamic range (Figure 21).

Besides FLIM, the ratiometric analysis of the FRET-pair fluorescence over time is also concentration-independent. Due to the acceptors slow chromophore maturation, the fraction of acceptor over donor rises upon β-catenin stabilization (Figure 37). Affinity propagation testing was performed in order to cluster defined temporal response profiles of the β-catenin stability sensor upon Wnt stimulation (Figure 38). Two classes of temporal profiles were identified and the Wnt stimulated cells were divided into active and inactive or responder and non-responder by their temporal profile. The temporal profile of sensor^{FM} revealed a maximum in donor over acceptor intensity around 2.5 h post-stimulation (156 ± 30 min), as well as a decrease to the basal stability level after 5-6 h post-stimulation (Figure 38). The decrease of the stabilization is a combination of acceptor maturation and degradation and points to an unbiased endogenous negative feedback on β-catenin stabilization in accordance with published data for transcriptional activation of e.g. Conductin[134]. In the case of the β-catenin

sensor$^{FM\text{-}\partial CTD}$ the peak in donor over acceptor ratio occurred even earlier and with a lower standard deviation, after already 136 ± 25 min (Figure 38).

The usual time frame of treatment in order to observe changes in Wnt signalling with the transcriptional reporters is 12-24 h[135]. Changes from baseline were published for optimized reporter systems after a minimal response time of 4 h. Considering that the β-catenin stability sensor peaks at 2.5 h already, but exhibits significant difference from baseline after as little as 60 min, the temporal resolution improvement is 2-4 fold (Figure 38). In protein expression studies it was shown for L cells and HEK293T, that feedback induction and degradation occurs in Wnt stimulated state after as little as 2 h[136]. This matches with the temporal profile of the β-catenin stability sensor in A431D cells, which returns to basal A/D intensity ratio after 5-6 h, indicating that Wnt induced stabilization is counteracted by feedback mechanisms.

With the novel sensor developed here, it is now possible to address early events as well as cell fate in Wnt signalling in live cell imaging.

7.3 Assessing spatio-temporal activation of Wnt/β-catenin signalling

In A431D cells with low expression level of the β-catenin^{WT} stability sensors, the sensors were localized at the plasma membrane; consistent with the Wnt independent E-cadherin bound pool within the cells (Figure 27). High levels of overexpression caused a shift of the sensor towards the soluble cytoplasmic pool. These findings fit to an E-cadherin bound pool of β-catenin in non-stimulated cells, while in Wnt stimulation β-catenin is stabilized and solubilized. This high overexpression in some β-catenin^{WT} transfected cells results from an artificially high synthesis rate of ectopic compared to endogenous β-catenin (Figure 23). In combination with an overload of the degradation machinery this led to an apparent stabilization of the protein. In cell culture of immortalized cells, constitutively active Wnt signalling was a major issue and overexpression of β-catenin often lead to apoptosis induction, due to hyper activation and -proliferation[137]. The Wnt response of several cell lines was investigated in order to find an optimal culture system to develop and optimize the β-catenin stability sensor. Optimal is a cell line expressing low levels of endogenous

β-catenin and lacking autocrine Wnt stimulation. In addition, the β-catenin sensor constructs were modified to prevent hyper activation of the Wnt pathway due to an elevated β-catenin level, induced by ectopic expression of the sensor. The insertion of the H470A mutation reduced the interaction with TCF/Lef transcription factors to a minimum (<3%)[122]. These constructs revealed a lower nuclear accumulation compared to the wild type constructs, due to the lack of interaction with the TCF/Lef transcription factors and less cytotoxic effects (Figure 27).

Further modifications in the β-catenin domain within the sensor were done to inhibit non-canonical Wnt and growth factor induced RTK mediated β-catenin accumulation and target gene regulation (section 6.4, Figure 33). The kinase c-src phosphorylates β-catenin at tyrosine 333, in an EGFR dependent manner. This in turn induces pyruvate kinase M2 (PKM2) binding to β-catenin in the nucleus[14] leading to facilitated CyclinD1 expression. This interaction was so far only reported for EGFR-promoted β-catenin transactivation in proliferation and tumorigenesis of cancer tissue, but could as well be a general mechanism of Wnt independent or non-canonical β-catenin signalling. Exchange of the tyrosine 333 against phenylalanine prevents β-catenin interaction with PKM2 and therefore EGFR-promoted CyclinD1 expression. It is highly likely, that this mechanism is not restricted to EGFR but would occur with other RTK activation as well, since c-src is not an exclusive down stream effector of EGFR. The phosphorylation of β-catenin serine 552, as a direct target of Akt-1/PKB, also depends on growth factor stimulation and is mediated through PI3K activation. The S552A mutation was reported to nearly abolish stabilization and nuclear translocation after non-canonical activation of Akt-1/PKB[16]. In addition to growth factor stimulated effects on cytosolic and nuclear β-catenin, the membranous pool of β-catenin bound to E-cadherin via α-catenin can be released and induce a fold-change in transcriptionally active β-catenin. β-catenin binds to E-cadherin at the site of adherens junctions. Upon growth factor stimulation, β-catenin is phosphorylated at tyrosine 654 by RTKs and released from the E-cadherin complex, feeding into the soluble cytosolic and nuclear pool of β-catenin. The phospho-mimicking mutant β-catenin^{Y654E} was shown not to localize at the plasma membrane, but in

the cytosol in MDCK cells[17], reducing the non-canonical activation of β-catenin translocation and transcription. Another pathway that leads to stabilization and transcriptional activation via the c-terminal domain of β-catenin is Rac/ROR. The Rac1 effector p21-activated kinase 1 (PAK-1) interacts with β-catenin and phosphorylates it at serine 675 in the c-terminal domain[15]. This activation occurs subsequent to K-ras induction in colorectal cancer in a Wnt independent manner. The S675A mutation did not reduce β-catenin stability or interfere with β-Trcp binding and ubiquitination. The binding to TCF/Lef promotor sequences itself was not inhibited by the S675A mutation, but subsequent transcriptional activation was reduced. Therefore a reduction in CyclinD1 expression and TOP/Flash activation was measured in colorectal cancer cells[15]. Although there are multiple other reported posttranslational modifications on β-catenin (Figure 4), the optimized sensor (β-catenin^{FM}) bears the essential mutations that reduce Wnt independent signalling pathway effects on β-catenin stability and transcriptional activation independent of Wnt (Figure 42).

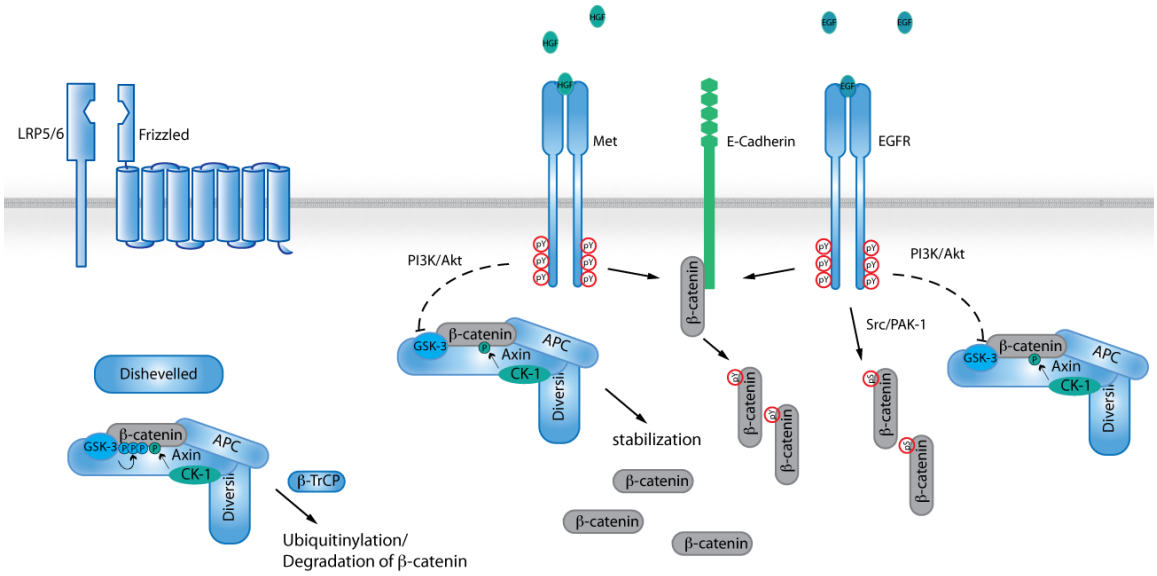

Figure 42: **Wnt-independent β-catenin stabilization.** Upon growth factor binding to RTKs, β-catenin stability can be affected by direct phosphorylation and re-localisation from the E-cadherin bound pool at the plasma membrane to the cytosol. Indirectly growth factor dependent GSK3β inhibition through PI3K/Akt activation can inhibit β-catenin degradation independent of Wnt and induce stabilization. Besides this, growth factor induced Src/PAK-1 activation and β-catenin phosphorylation contributes to a higher transcriptional activation and nuclear retention causing stabilization.

In an attempt to better match the turn-over rate of the sensor with the maturation time of the fluorophores a truncated version, β-catenin$^{FM\text{-}\partial CTD}$ was tested. It has been previously reported, that C-terminally truncated β-catenin, like ∂664

β-catenin[12] have a reduced half-lifetime. In addition and in consistence with data for β-catenin^{S675A}, expression of 108 AA C-terminal truncated β-catenin *∂*675 reduced transcriptional activity by a factor of 10 compared to overexpressed full-length protein[13]. The truncated optimized sensor β-catenin$^{FM\text{-}\partial CTD}$ was indeed destabilized in comparison to its full-length pendant. In temporal profiles of the A/D ratio after Wnt stimulation, the truncation led to a faster maximal response time (136 vs 156 min) and a faster recovery after Wnt stimulation (Figure 39).

The measurement of the sensor stabilization depends on the maturation kinetics of the FRET pair fluorophores. The donor molecule of choice was the YFP derivative mCitrine, since it is a monomeric fluorophore with a very fast maturation time[110]. This should ensure, that all β-catenin sensor within the cell is recorded at any time of its persistence. The acceptor fluorophore was chosen from a group of red shifted fluorophores that still have a spectral overlap with the emission profile of mCitrine, which were mKate2, mCherry, mPlum and mRaspberry. All of these fluorophores exhibit a different maturation time, ranging from 30 min (mCherry) to 100 min (mPlum) in vitro[113]. It turned out, that due to its very slow maturation, mPlum was the most suitable acceptor in the β-catenin^{FM} sensor, although the FRET efficiency between mCitrine and mCherry was much better (Figure 16). Considering that, the maximal amplitude of the temporal D/A intensity ratio profile of β-catenin$^{FM\text{-}\partial CTD}$ was reduced compared to the full-length construct, the acceptor maturation time is probably too slow. Therefore, using a different acceptor fluorophore might raise the amplitude of the β-catenin$^{FM\text{-}\partial CTD}$ temporal profile. The red fluorophore mRaspberry, with a reported *in vitro* maturation time of 55 min would be a promising candidate. Since the *in vitro* determination of the fluorophore maturation is based on the final oxidation step and neglects the time needed for the first 2 maturation steps as well as the , the *in vivo* chromophore maturation might be extended. Keeping this in mind, the maturation time of mRaspberry could probably fit the shift in the temporal profile peak between β-catenin^{FM} and β-catenin$^{FM\text{-}\partial CTD}$.

Both β-catenin sensor^{FM} and sensor$^{FM\text{-}\partial CTD}$ respond earlier to Wnt stimulation as compared to the TOPflash system. In an attempt to directly correlate this, a TCF/Lef:H2B reporter was co-expressed in order to confirm the Wnt response independently in live single cells. After testing the transcriptional reporter

previously (Figure 31-33), the modified destabilized version TCF/Lef:H2B-d1mTagBFP was identified as a faster read-out than the original construct. Cross-correlations with this reporter were not successful, because the transcriptional reporter response time was longer than the time until cells divided. This made single-cell analysis using the reporter, even the one expressing destabilized H2B-d1mTagBFP, essentially impossible. The temporal profiles of the sensors in cells co-transfected with the transcriptional reporter systems points to delay in β-catenin accumulation. A competition of the TCF/Lef motifs in the reporter system with endogenous motifs, might cause side effects in downstream transcriptional regulation and therefore bias the negative feedback loops from target gene induction on β-catenin stability like Conductin expression and recovered degradation.

7.4 Correlations between β-catenin stabilization and cell cycle progression

The interdependence of Wnt signalling and cell cycle progression is regulated on multiple levels. Wnt/β-catenin signalling regulates transcriptional regulation of cell cycle promoting proteins, including c-myc and CyclinD1. The effect on CyclinD1 is indirect via Wnt dependent GSK3β inhibition, but also mediated via β-catenin induced c-myc. Either way, CyclinD1 expression results in G1 cell cycle progression[82-85]. Besides CyclinD1 expression, c-myc represses p21 and p27, two proteins that inhibit Cyclin E and thereby G1/S transition[84,85]. Thus c-myc inhibition causes G1/S progression. GSK3β destabilizes cell cycle effectors by phosphorylation and priming for proteasomal degradation. After Wnt stimulation, GSK3β inhibition leads to stabilization of its target proteins, among others are c-myc, CyclinD1 and Cyclin E1, further promoting cell cycle progression.

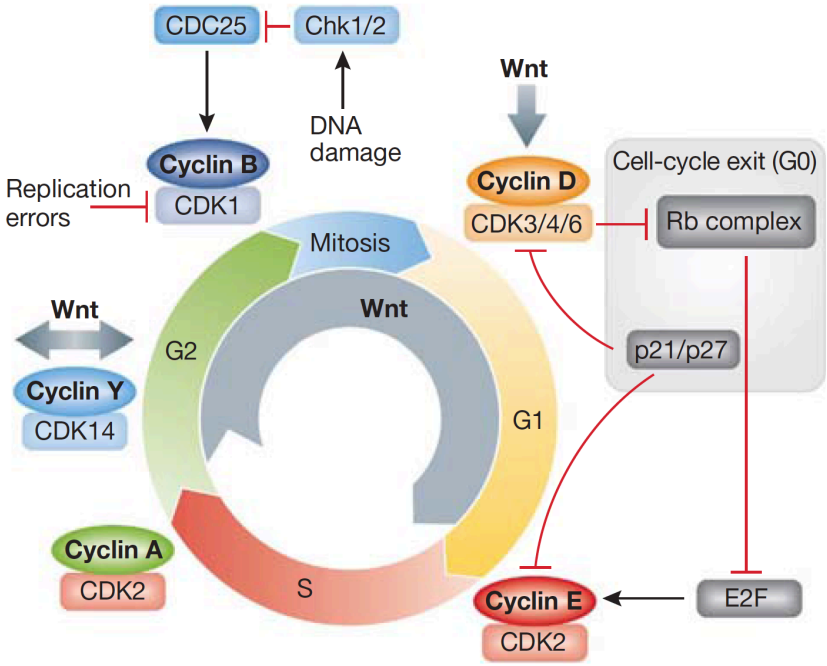

Figure 43: **Overview of Wnt in cell-cycle regulation.** Wnt feeds into the cell cycle by promotion of Cyclin D in early G1. In addition CDK14 expression in G2 and priming of LRP5/6 through receptor phosphorylation by CDK14 favours Wnt signalling induction[86].

In turn, some components of the Wnt/β-catenin pathway are expressed in an oscillating fashion with the cell cycle, e.g β-catenin and its target genes Lgr5 and Conductin in G2/M[90,92]. This is explained by priming of LRP5/6 for Wnt signalling by phosphorylation of its PPPSP motif through cyclin-dependent kinase 14 (CDK14). CDK14 itself is associated with cyclin Y, therefore expressed in the G2/M phase of the cell cycle[91]. This oscillations in priming of Wnt/β-catenin pathway components lead to a probably lower activation threshold and thus a facilitation of cell cycle progression.

In the context of the tight correlation between Wnt signalling and the cell cycle, the question arose, whether the stabilization observed could be a cell cycle dependent effect. Indeed, cells that are stimulated with Wnt exhibit a faster cell cycle progression, leading to a high number of cells that divide within the response time of 8 h. We had to exclude cells that proliferated from the analysis to exclude cell cycle dependent protein stabilization. The fact that D/A intensity ratio of the remaining analysed cells returned to the initial level (Figure 38), showed a Wnt dependent β-catenin stabilization independent of the cell cycle progression. In sub confluent and confluent cultures of MCF7 cells, a different response to small molecule inhibitors could be observed (Figure 22). The GSK3β inhibitor SB216763

increased the amount of total as well as active β-catenin in sub-confluent but not in confluent MCF7 cells, while the Tankyrase inhibitor IWR-1-endo, which inhibits Axin degradation, reduced the β-catenin levels only in confluent cultures. Considering, that MCF7 cells had a high initial level of active β-catenin, this difference might be due to a higher proportion of confluent culture cells in resting state G_0, while the sub confluent cells were still proliferating and therefore throughout the cell cycle proned for Wnt signalling. In future experiments using flow cytometry (FACS) experiments of synchronized, sensor transfected cells, the question of cell-cycle dependence in the sensor response and *vice versa* the impact of Wnt dependent β-catenin stabilization reported by the sensor on cell cycle progression remains to be addressed and quantified.

8 Outlook

The developed β-catenin sensor, as presented here, opens up new possibilities to investigate β-catenin activation in space and time and correlate Wnt signalling with cell fate decisions in live cell imaging.

A number of potential applications for the β-catenin stability sensor can be identified, such as monitoring the β-catenin activity in cancer development, in stem cell differentiation or during liver regeneration. This sensor has the potential of being used *in vivo*, since it has been shown recently, that lifetime imaging in living mice is possible using a FRET biosensor with red fluorophores[138].

How is cancer development in the small intestine correlated to Wnt pathway induction, more specifically to β-catenin stability changes?

With small intestinal organoids, that establish a Wnt gradient from the bottom of the crypt to the neck upon differentiation, the dynamic range of the sensor could be explored in non-cancerous 3D cell culture (Figure 44, right). The crypt stem cells are surrounded by Wnt producing Paneth as well as stromal cells, receiving pro proliferative signals, while differentiating cells towards the neck do not. Induction of APC mutations and their relevance for the activation of the Wnt pathways could be temporally and spatially well localized in very early stages to investigate cancer emerging from a single cell, since proto-oncogenic mutations and truncations in APC lead to β-catenin stabilization. The β-catenin stability sensor would be an option to visualize this stabilization on single cell level already. Similar to this idea, Jarde *et al.* have developed an assay using a Conductin-β-galactosidase construct (Figure 44, left). Under the promotor of the direct Wnt target Conductin, a β-cgalactosidase gene was induced in case of Wnt stimulation. In lineage tracing studies this approach gives an overview over the history of the cell, emerging from a parental cell with β-catenin activation but it does not resolve the actual β-catenin activation state at a given time, especially not if Wnt signalling dynamically regulated.

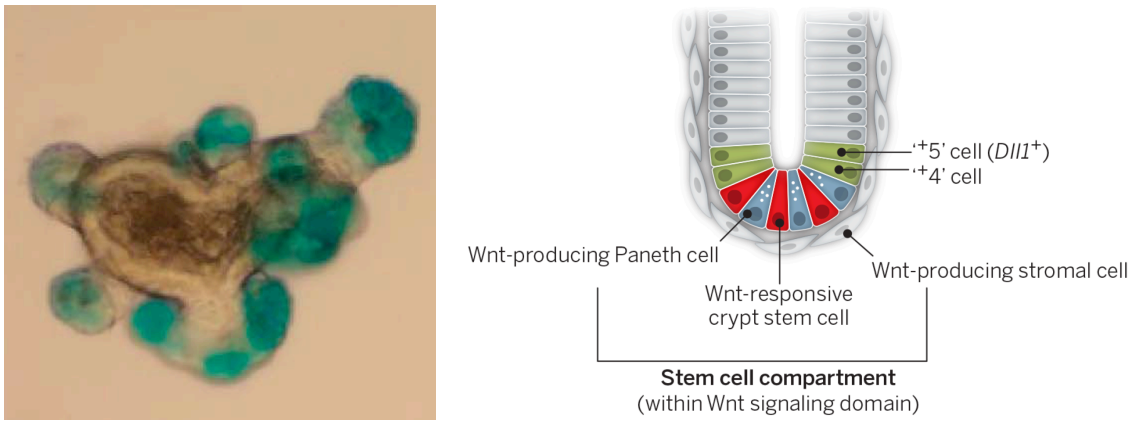

Figure 44: **Left: Conductin-β-galactosidase expression in Tet-OΔN89-β-catenin organoids of the small intestine.** Organoids were cultured with R-spondin, but in absence of Doxycylcine[139]. **Right: The intestinal stem cell compartement.** Wnt responding and secreting cell populations in the basal crypt of small intestine[140].

In liver regeneration, the Wnt/β-catenin pathway activation is one of the very early responses. Hence, measurements of β-catenin stabilization with high spatio-temporal resolution would provide new and valuable information on the mechanism of hepatocyte cell cycle entry.

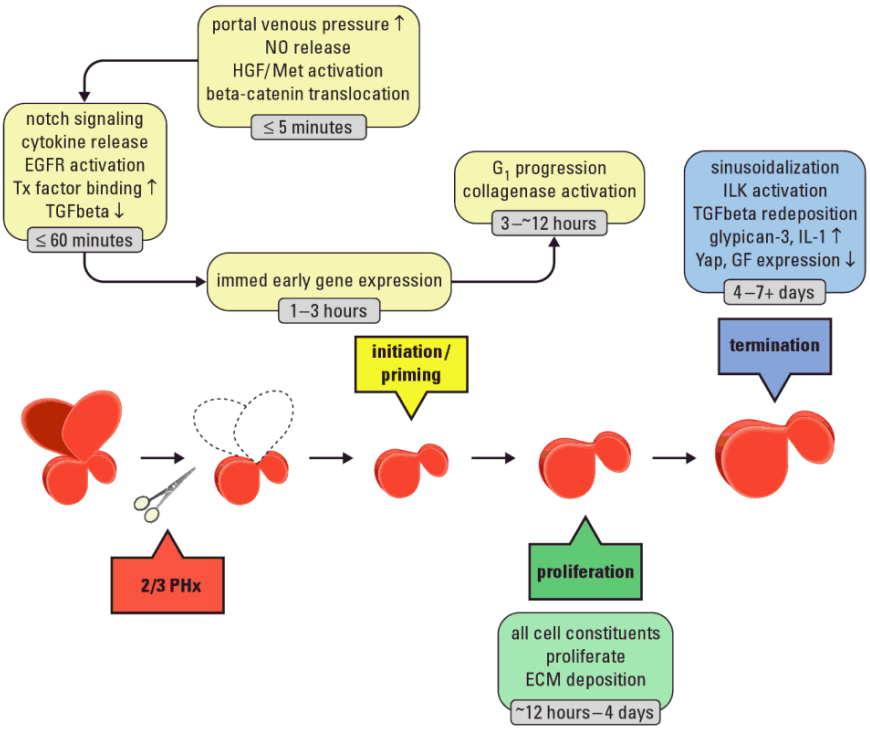

Figure 45: **Cellular response induced by 2/3 PHx in mice**[129]. β-catenin translocation to the nucleus is an immediate effect during priming for liver regeneration. G1 cell cycle progression follows with a delay of 3-12 h. Both events may be Wnt signalling induced and therefore addressed by the new β-catenin stability sensor.

How does cell fate and history in terms of β-catenin stability correlate to proliferation or differentiation processes during liver regeneration?

Studying the liver regeneration process using the β-catenin stability sensor would provide insight into the context dependent cross-talk between signalling pathways, since different growth factor dependent pathways become activated during proliferation after liver injury[129,141,142] (Figure 45). Studies have shown, that proliferation of hepatocytes but also recruitment of progenitor and liver specific stem cells are responsible for liver restoration after injury[129]. This restoration is induced by a set of growth factors, cytokines and metabolic networks[143]. These studies were performed using end-point analysis in vitro like immunoblots and other population-based experiments. Although these help to understand molecular effects in liver regeneration, they cannot provide a good spatial or temporal resolution in correlation with cell history and fate. This can only be addressed by measurements of dynamic response in live cells. Correlating sensor activity with cell history and fate might be a major step in understanding the mechanisms of proliferation versus differentiation in regenerative processes and thus in influencing these processes in cases of abnormal regulation e.g fibrosis or cancer by using the physiological context provided by transgenic animals. In such model systems, also the following questions could be directly addressed:

How does this stabilization correspond to the entrance into the cell cycle? Does stabilization persist during proliferation? Do spatial redistribution, elevated expression or higher activation levels of β-catenin play a role in the G_1 entry, or are they a result of GSK3β inhibition during cell cycle progression?

The relationship between β-catenin levels within a cell and the activation state of canonical Wnt signalling is well described in various cell types within the liver at steady-state. Although highly context-dependent, stabilized β-catenin has a general tendency to translocate to the nucleus and act as a transcriptional activator through binding to TCF/Lef. Making use of the sensor, we can resolve the connection between spatio-temporal stabilization of β-catenin and cell fate decisions in vivo and with subcellular resolution.

Which cell type secretes the Wnt ligands involved in hepatic canonical Wnt signalling?

In hepatic organoids this question could be addressed by cell type specific knockout of Wnt ligand secretion (cell type specific WL-KO). Hepatic organoids emerge from isolated liver specific stem cells under Wnt3a stimulation, but don't need Wnt ligand addition during cultivation for maintenance or proliferation[144]. Correlation of organoid growth or maintenance of hepatic organoids isolated from cell type specific WL-KO mice and the β-catenin stabilization within the hepatic organoid might answer this question. In liver specific β-catenin knockout mice a delayed regeneration after partial hepatectomy was observed[145]. The underlying mechanisms and contribution of different β-catenin stabilizing pathways was not yet solved. The Wnt/β-catenin signalling dependent effects could be determined by the β-catenin stability sensor. Apart from Wnt/β-catenin signalling, β-catenin resists in complex with cMet at the plasma membrane in resting hepatocytes, where it becomes phosphorylated upon EGF or HGF treatment. β-catenin dissociates from cMet and translocates to the nucleus[93]. In addition, cMet activation by HGF leads to inhibition of GSK3β and subsequent β-catenin stabilization through PI3K/Akt signalling. Both activation mechanisms are Wnt independent, therefore the sensor would have to be further modified, as discussed below.

What is the contribution of other β-catenin stabilizing signalling pathways?

The developed β-catenin stability sensor is a tool to investigate Wnt dependent β-catenin stabilization in live cells with a far better temporal resolution than the transcriptional reporters used before. In addition, the β-catenin sensor provides the option to see oscillations in on/off states of Wnt signalling. The spatial activity of β-catenin, as well as potential other mechanisms of β-catenin stabilization than Wnt induction could be addressed by functionalizing the β-catenin stability sensor with mutations of binding sites, truncations of the protein and so on. Functionalized sensors reporting β-catenin stabilization induced by other pathways than Wnt signalling would help to understand the intracellular organization of the β-catenin pool with regard to localization as well as stabilization. By mutating single sites for specific interaction partners like E-cadherin (Y654), the sensor could be applied to dissect the contribution of RTK dependent E-cadherin release from overall β-catenin stability in liver regeneration.

Further it could be used to monitor other β-catenin stabilizing signalling activities, like growth factor binding and subsequent PI3K activity in other cellular contexts.

9 Table of figures

10 Table of abbreviations

aa	amino acid
Ab	antibody
ABC	active β-catenin
APC	*adenomatous polyposis coli*
ARM	armadillo
BisTris	Bis-(2-hydroxyethyl) aminotris (hydroxymethyl) methane
bp	base pair
BSA	bovine serum albumin
C57/Bl6N	inbred mouse strain
CAAX-GID	membrane tethered GSK3β inhibitory domain
cDNA	complementary DNA
CIP	calf intestinal phosphatase
CK1	casein kinase 1
CM	collagen monolayer
cMet	hepatocyte growth factor receptor
CS	collagen sandwich
CTD	C-terminal domain
CTTA	C-Terminal Transcriptional Activators
ddNTP	di-deoxynucleotide tri-phosphate
DMEM	Dulbecco's minimal essential medium
DNA	deoxyribonucleic acid
dNTP	deoxynucleotide tri-phosphate
dsDNA	double stranded DNA
DTT	dithiothreitol
Dvl	Dishevelled
EB	elution buffer
EDTA	ethylene diamine tetraacetic acid
EF	suffix: endotoxin free
EGF	epithelial growth factor
EGFR	epithelial growth factor receptor
EGTA	ethylene glycol tetraacetic acid
ER	endoplasmatic reticulum
EtOH	ethanol
FGM	full growth medium
FLIM	fluorescence lifetime imaging microscopy
FOXO	forkhead box protein
FRET	Förster resonance energy transfer
Fz	Frizzled receptor
GSK3β	glycogen synthase kinase 3-β
HGF	hepatocyte growth factor
IR	infrared
kb	kilo base pair
kD	kilo dalton
KH buffer	Krebs-Henseleit buffer
L-Glu	L-glutamine
LB	lysogeny broth
Lef	lymphoid enhancing factor
LRP	low-density lipoprotein receptor related protein
MACF1	microtubule actin cross-linking factor 1
MeOH	methanol

MOPS	3-(N-morpholino)propanesulfonic acid
mRNA	messenger RNA
NEAA	non-essential amino acid solution
NTD	N-terminal domain
NTTA	N-Terminal Transcriptional Activators
o.n.	over night
P/S	penicillin/streptomycin
PAGE	polyacrylamide gel electrophoresis
PAK-1	p21-activated kinase 1
PBS	phosphate buffered saline
PCR	polymerase chain reaction
pDNA	plasmid-DNA
PHx	partial hepatectomy
PI3K	phosphoinositide-3-kinase
PKB	protein kinase B
PKM2	pyruvate kinase M2
PM	plasma membrane
pmHep	primary mouse hepatocytes
PP1	protein phosphatase 1
PP2A	protein phosphatase 2A
PVDF	polyvinylidene difluoride
RNA	ribonucleic acid
ROI	region of interest
ROR	Receptor tyrosine kinase-like orphan receptor
rpm	rounds per minute
RT	room temperature
RTK	receptor tyrosine kinase
RYK	related to receptor tyrosine kinase
SDS	sodium dodecyl sulphate
sFRP	secreted Frizzled related proteins
T_a	annealing temperature
TAE	Tris-acetate-EDTA
TBS	Tris buffered saline
TCF	T-cell factor
TCF/Lef	T-cell factor/lymphoid enhancing factor
TE	Tris-EDTA
T_m	melting temperature
Tris	2-Amino-2-hydroxymethyl-propane-1,3-diol
τ	lifetime
τ_{AV}	average lifetime
U	units
UV	ultraviolet light
VIS	visible light
WCL	whole cell lysate
WIF	Wnt inhibitory factor
WLS	Wntless
x g	fold gravitational force
β-Trcp	β-transducin repeat containing E3 ubiquitin protein ligase

If not otherwise described, units were abbreviated according to the International system of Units (1960) and their derivatives.
Amino acid nomenclature was used according to the IUPAC-IUB Commission on Biochemical Nomenclature (1971).

11 References

1 Schneider, S. Q., Finnerty, J. R. & Martindale, M. Q. Protein evolution: structure-function relationships of the oncogene beta-catenin in the evolution of multicellular animals. *Journal of experimental zoology. Part B, Molecular and developmental evolution* **295**, 25-44, doi:10.1002/jez.b.6 (2003).

2 Clevers, H. & Nusse, R. Wnt/beta-catenin signaling and disease. *Cell* **149**, 1192-1205, doi:10.1016/j.cell.2012.05.012 (2012).

3 van Amerongen, R. & Berns, A. Knockout mouse models to study Wnt signal transduction. *Trends in genetics : TIG* **22**, 678-689, doi:10.1016/j.tig.2006.10.001 (2006).

4 Valenta, T., Hausmann, G. & Basler, K. The many faces and functions of beta-catenin. *The EMBO journal* **31**, 2714-2736, doi:10.1038/emboj.2012.150 (2012).

5 Xing, Y. *et al.* Crystal structure of a full-length beta-catenin. *Structure* **16**, 478-487, doi:10.1016/j.str.2007.12.021 (2008).

6 Huber, A. H., Nelson, W. J. & Weis, W. I. Three-dimensional structure of the armadillo repeat region of beta-catenin. *Cell* **90**, 871-882 (1997).

7 Wu, G. *et al.* Structure of a beta-TrCP1-Skp1-beta-catenin complex: destruction motif binding and lysine specificity of the SCF(beta-TrCP1) ubiquitin ligase. *Molecular cell* **11**, 1445-1456 (2003).

8 Jiang, J. & Struhl, G. Regulation of the Hedgehog and Wingless signalling pathways by the F-box/WD40-repeat protein Slimb. *Nature* **391**, 493-496, doi:10.1038/35154 (1998).

9 Nagafuchi, A. Molecular architecture of adherens junctions. *Current opinion in cell biology* **13**, 600-603 (2001).

10 Drees, F., Pokutta, S., Yamada, S., Nelson, W. J. & Weis, W. I. Alpha-catenin is a molecular switch that binds E-cadherin-beta-catenin and regulates actin-filament assembly. *Cell* **123**, 903-915, doi:10.1016/j.cell.2005.09.021 (2005).

11 Yamada, S., Pokutta, S., Drees, F., Weis, W. I. & Nelson, W. J. Deconstructing the cadherin-catenin-actin complex. *Cell* **123**, 889-901, doi:10.1016/j.cell.2005.09.020 (2005).

12 Mo, R. *et al.* The terminal region of beta-catenin promotes stability by shielding the Armadillo repeats from the axin-scaffold destruction complex. *The Journal of biological chemistry* **284**, 28222-28231, doi:10.1074/jbc.M109.045039 (2009).

13 Cong, F., Schweizer, L., Chamorro, M. & Varmus, H. Requirement for a nuclear function of beta-catenin in Wnt signaling. *Molecular and cellular biology* **23**, 8462-8470 (2003).

14 Yang, W. *et al.* Nuclear PKM2 regulates beta-catenin transactivation upon EGFR activation. *Nature* **480**, 118-122, doi:10.1038/nature10598 (2011).

15 Zhu, G. *et al.* A Rac1/PAK1 cascade controls beta-catenin activation in colon cancer cells. *Oncogene* **31**, 1001-1012, doi:10.1038/onc.2011.294 (2012).

16 Fang, D. *et al.* Phosphorylation of beta-catenin by AKT promotes beta-catenin transcriptional activity. *The Journal of biological chemistry* **282**, 11221-11229, doi:10.1074/jbc.M611871200 (2007).

17 Howard, S., Deroo, T., Fujita, Y. & Itasaki, N. A positive role of cadherin in Wnt/beta-catenin signalling during epithelial-mesenchymal transition. *PloS one* **6**, e23899, doi:10.1371/journal.pone.0023899 (2011).
18 van Amerongen, R., Mikels, A. & Nusse, R. Alternative wnt signaling is initiated by distinct receptors. *Science signaling* **1**, re9, doi:10.1126/scisignal.135re9 (2008).
19 Willert, K. *et al.* Wnt proteins are lipid-modified and can act as stem cell growth factors. *Nature* **423**, 448-452, doi:10.1038/nature01611 (2003).
20 Takada, R. *et al.* Monounsaturated fatty acid modification of Wnt protein: its role in Wnt secretion. *Developmental cell* **11**, 791-801, doi:10.1016/j.devcel.2006.10.003 (2006).
21 Komekado, H., Yamamoto, H., Chiba, T. & Kikuchi, A. Glycosylation and palmitoylation of Wnt-3a are coupled to produce an active form of Wnt-3a. *Genes to cells : devoted to molecular & cellular mechanisms* **12**, 521-534, doi:10.1111/j.1365-2443.2007.01068.x (2007).
22 MacDonald, B. T., Tamai, K. & He, X. Wnt/beta-catenin signaling: components, mechanisms, and diseases. *Developmental cell* **17**, 9-26, doi:10.1016/j.devcel.2009.06.016 (2009).
23 Tang, X. F., Fan, X. L. & Lin, X. H. Regulation of Wnt Secretion and Distribution. *Targeting the Wnt Pathway in Cancer*, 19-33, doi:Doi 10.1007/978-1-4419-8023-6_2 (2011).
24 Lin, X. Functions of heparan sulfate proteoglycans in cell signaling during development. *Development* **131**, 6009-6021, doi:10.1242/dev.01522 (2004).
25 Morrell, N. T. *et al.* Liposomal packaging generates Wnt protein with in vivo biological activity. *PloS one* **3**, e2930, doi:10.1371/journal.pone.0002930 (2008).
26 Logan, C. Y. & Nusse, R. The Wnt signaling pathway in development and disease. *Annual review of cell and developmental biology* **20**, 781-810, doi:10.1146/annurev.cellbio.20.010403.113126 (2004).
27 He, X., Semenov, M., Tamai, K. & Zeng, X. LDL receptor-related proteins 5 and 6 in Wnt/beta-catenin signaling: arrows point the way. *Development* **131**, 1663-1677, doi:10.1242/dev.01117 (2004).
28 Binnerts, M. E. *et al.* R-Spondin1 regulates Wnt signaling by inhibiting internalization of LRP6. *Proceedings of the National Academy of Sciences of the United States of America* **104**, 14700-14705, doi:10.1073/pnas.0702305104 (2007).
29 Cong, F., Schweizer, L. & Varmus, H. Wnt signals across the plasma membrane to activate the beta-catenin pathway by forming oligomers containing its receptors, Frizzled and LRP. *Development* **131**, 5103-5115, doi:10.1242/dev.01318 (2004).
30 Bryja, V. *et al.* The extracellular domain of Lrp5/6 inhibits noncanonical Wnt signaling in vivo. *Molecular biology of the cell* **20**, 924-936, doi:10.1091/mbc.E08-07-0711 (2009).
31 Green, J., Nusse, R. & van Amerongen, R. The role of Ryk and Ror receptor tyrosine kinases in Wnt signal transduction. *Cold Spring Harbor perspectives in biology* **6**, doi:10.1101/cshperspect.a009175 (2014).
32 Kroiher, M., Miller, M. A. & Steele, R. E. Deceiving appearances: signaling by "dead" and "fractured" receptor protein-tyrosine kinases. *BioEssays : news*

and reviews in molecular, cellular and developmental biology **23**, 69-76, doi:10.1002/1521-1878(200101)23:1<69::AID-BIES1009>3.0.CO;2-K (2001).
33 Hsieh, J. C. *et al.* A new secreted protein that binds to Wnt proteins and inhibits their activities. *Nature* **398**, 431-436, doi:10.1038/18899 (1999).
34 Inoue, T. *et al.* C-elegans LIN-18 is a Ryk ortholog in parallel to LIN-17/frizzled in Wnt and functions signaling. *Cell* **118**, 795-806, doi:Doi 10.1016/J.Cell.2004.09.001 (2004).
35 Yoshikawa, S., Bonkowsky, J. L., Kokel, M., Shyn, S. & Thomas, J. B. The Derailed guidance receptor does not require kinase activity in vivo. *J Neurosci* **21**, art. no.-RC119 (2001).
36 Taillebourg, E., Moreau-Fauvarque, C., Delaval, K. & Dura, J. M. In vivo evidence for a regulatory role of the kinase activity of the linotte/derailed receptor tyrosine kinase, a Drosophila Ryk ortholog. *Dev Genes Evol* **215**, 158-163, doi:Doi 10.1007/S00427-004-0457-6 (2005).
37 Lu, W. G., Yamamoto, V., Ortega, B. & Baltimore, D. Mammalian Ryk is a Wnt coreceptor required for stimulation of neurite outgrowth. *Cell* **119**, 97-108, doi:Doi 10.1016/J.Cell.2004.09.019 (2004).
38 Berndt, J. D. *et al.* Mindbomb 1, an E3 ubiquitin ligase, forms a complex with RYK to activate Wnt/beta-catenin signaling. *Journal of Cell Biology* **194**, 737-750, doi:Doi 10.1083/Jcb.201107021 (2011).
39 Saldanha, J., Singh, J. & Mahadevan, D. Identification of a Frizzled-like cysteine rich domain in the extracellular region of developmental receptor tyrosine kinases. *Protein science : a publication of the Protein Society* **7**, 1632-1635, doi:10.1002/pro.5560070718 (1998).
40 Mikels, A. J. & Nusse, R. Purified Wnt5a protein activates or inhibits beta-catenin-TCF signaling depending on receptor context. *PLoS biology* **4**, e115, doi:10.1371/journal.pbio.0040115 (2006).
41 Oishi, I. *et al.* The receptor tyrosine kinase Ror2 is involved in non-canonical Wnt5a/JNK signalling pathway. *Genes to cells : devoted to molecular & cellular mechanisms* **8**, 645-654 (2003).
42 Al-Shawi, R., Ashton, S. V., Underwood, C. & Simons, J. P. Expression of the Ror1 and Ror2 receptor tyrosine kinase genes during mouse development. *Dev Genes Evol* **211**, 161-171 (2001).
43 Grumolato, L. *et al.* Canonical and noncanonical Wnts use a common mechanism to activate completely unrelated coreceptors. *Genes & development* **24**, 2517-2530, doi:10.1101/gad.1957710 (2010).
44 Kazanskaya, O. *et al.* R-Spondin2 is a secreted activator of Wnt/beta-catenin signaling and is required for Xenopus myogenesis. *Developmental cell* **7**, 525-534, doi:10.1016/j.devcel.2004.07.019 (2004).
45 Xu, Q. *et al.* Vascular development in the retina and inner ear: Control by Norrin and Frizzled-4, a high-affinity ligand-receptor pair. *Cell* **116**, 883-895, doi:Doi 10.1016/S0092-8674(04)00216-8 (2004).
46 Bovolenta, P., Esteve, P., Ruiz, J. M., Cisneros, E. & Lopez-Rios, J. Beyond Wnt inhibition: new functions of secreted Frizzled-related proteins in development and disease. *Journal of cell science* **121**, 737-746, doi:10.1242/jcs.026096 (2008).

47 Semenov, M., Tamai, K. & Xi, H. SOST is a ligand for LRP5/LRP6 and a Wnt signaling inhibitor. *Journal of Biological Chemistry* **280**, 26770-26775, doi:Doi 10.1074/Jbc.M504308200 (2005).
48 Semenov, M. V. *et al.* Head inducer Dickkopf-1 is a ligand for Wnt coreceptor LRP6. *Curr Biol* **11**, 951-961, doi:Doi 10.1016/S0960-9822(01)00290-1 (2001).
49 Itasaki, N. *et al.* Wise, a context-dependent activator and inhibitor of Wnt signalling. *Development* **130**, 4295-4305 (2003).
50 Li, X. *et al.* Sclerostin binds to LRP5/6 and antagonizes canonical Wnt signaling. *The Journal of biological chemistry* **280**, 19883-19887, doi:10.1074/jbc.M413274200 (2005).
51 Piccolo, S. *et al.* The head inducer Cerberus is a multifunctional antagonist of Nodal, BMP and Wnt signals. *Nature* **397**, 707-710, doi:10.1038/17820 (1999).
52 Zhu, W. *et al.* IGFBP-4 is an inhibitor of canonical Wnt signalling required for cardiogenesis. *Nature* **454**, 345-349, doi:10.1038/nature07027 (2008).
53 Kimelman, D. & Xu, W. beta-catenin destruction complex: insights and questions from a structural perspective. *Oncogene* **25**, 7482-7491, doi:10.1038/sj.onc.1210055 (2006).
54 Yang, J. *et al.* Adenomatous polyposis coli (APC) differentially regulates beta-catenin phosphorylation and ubiquitination in colon cancer cells. *The Journal of biological chemistry* **281**, 17751-17757, doi:10.1074/jbc.M600831200 (2006).
55 Polakis, P. Wnt signaling and cancer. *Genes & development* **14**, 1837-1851 (2000).
56 Huang, H. & He, X. Wnt/beta-catenin signaling: new (and old) players and new insights. *Current opinion in cell biology* **20**, 119-125, doi:10.1016/j.ceb.2008.01.009 (2008).
57 Major, M. B. *et al.* Wilms tumor suppressor WTX negatively regulates WNT/beta-catenin signaling. *Science* **316**, 1043-1046, doi:10.1126/science/1141515 (2007).
58 Schwarz-Romond, T. *et al.* The ankyrin repeat protein Diversin recruits Casein kinase Iepsilon to the beta-catenin degradation complex and acts in both canonical Wnt and Wnt/JNK signaling. *Genes & development* **16**, 2073-2084, doi:10.1101/gad.230402 (2002).
59 Luo, W. *et al.* Protein phosphatase 1 regulates assembly and function of the beta-catenin degradation complex. *The EMBO journal* **26**, 1511-1521, doi:10.1038/sj.emboj.7601607 (2007).
60 Su, Y. *et al.* APC is essential for targeting phosphorylated beta-catenin to the SCFbeta-TrCP ubiquitin ligase. *Molecular cell* **32**, 652-661, doi:10.1016/j.molcel.2008.10.023 (2008).
61 Xing, Y., Clements, W. K., Kimelman, D. & Xu, W. Crystal structure of a beta-catenin/axin complex suggests a mechanism for the beta-catenin destruction complex. *Genes & development* **17**, 2753-2764, doi:10.1101/gad.1142603 (2003).
62 Lee, E., Salic, A., Kruger, R., Heinrich, R. & Kirschner, M. W. The roles of APC and Axin derived from experimental and theoretical analysis of the Wnt pathway. *PLoS biology* **1**, E10, doi:10.1371/journal.pbio.0000010 (2003).

63 Takacs, C. M. *et al.* Dual positive and negative regulation of wingless signaling by adenomatous polyposis coli. *Science* **319**, 333-336, doi:10.1126/science.1151232 (2008).
64 Choi, J., Park, S. Y., Costantini, F., Jho, E. H. & Joo, C. K. Adenomatous polyposis coli is down-regulated by the ubiquitin-proteasome pathway in a process facilitated by Axin. *The Journal of biological chemistry* **279**, 49188-49198, doi:10.1074/jbc.M404655200 (2004).
65 Luo, J. *et al.* Wnt signaling and human diseases: what are the therapeutic implications? *Laboratory investigation; a journal of technical methods and pathology* **87**, 97-103, doi:10.1038/labinvest.3700509 (2007).
66 Davidson, G. *et al.* Casein kinase 1 gamma couples Wnt receptor activation to cytoplasmic signal transduction. *Nature* **438**, 867-872, doi:10.1038/nature04170 (2005).
67 Zeng, X. *et al.* A dual-kinase mechanism for Wnt co-receptor phosphorylation and activation. *Nature* **438**, 873-877, doi:10.1038/nature04185 (2005).
68 Pan, W. *et al.* Wnt3a-mediated formation of phosphatidylinositol 4,5-bisphosphate regulates LRP6 phosphorylation. *Science* **321**, 1350-1353, doi:10.1126/science.1160741 (2008).
69 Zeng, X. *et al.* Initiation of Wnt signaling: control of Wnt coreceptor Lrp6 phosphorylation/activation via frizzled, dishevelled and axin functions. *Development* **135**, 367-375, doi:10.1242/dev.013540 (2008).
70 Jorgensen, L. H. *et al.* Duplication in the microtubule-actin cross-linking factor 1 gene causes a novel neuromuscular condition. *Scientific reports* **4**, 5180, doi:10.1038/srep05180 (2014).
71 Chen, H. J. *et al.* The role of microtubule actin cross-linking factor 1 (MACF1) in the Wnt signaling pathway. *Genes & development* **20**, 1933-1945, doi:10.1101/gad.1411206 (2006).
72 Liu, X., Rubin, J. S. & Kimmel, A. R. Rapid, Wnt-induced changes in GSK3beta associations that regulate beta-catenin stabilization are mediated by Galpha proteins. *Curr Biol* **15**, 1989-1997, doi:10.1016/j.cub.2005.10.050 (2005).
73 Willert, K., Shibamoto, S. & Nusse, R. Wnt-induced dephosphorylation of axin releases beta-catenin from the axin complex. *Genes & development* **13**, 1768-1773 (1999).
74 Yamamoto, H. *et al.* Phosphorylation of axin, a Wnt signal negative regulator, by glycogen synthase kinase-3beta regulates its stability. *The Journal of biological chemistry* **274**, 10681-10684 (1999).
75 Doble, B. W. *et al.* Phosphorylation of serine 262 in the gap junction protein connexin-43 regulates DNA synthesis in cell-cell contact forming cardiomyocytes. *Journal of cell science* **117**, 507-514, doi:10.1242/jcs.00889 (2004).
76 Sharma, M., Jamieson, C., Johnson, M., Molloy, M. P. & Henderson, B. R. Specific armadillo repeat sequences facilitate beta-catenin nuclear transport in live cells via direct binding to nucleoporins Nup62, Nup153, and RanBP2/Nup358. *The Journal of biological chemistry* **287**, 819-831, doi:10.1074/jbc.M111.299099 (2012).
77 Olson, L. E. *et al.* Homeodomain-mediated beta-catenin-dependent switching events dictate cell-lineage determination. *Cell* **125**, 593-605, doi:10.1016/j.cell.2006.02.046 (2006).

78 Hendriksen, J. *et al.* RanBP3 enhances nuclear export of active (beta)-catenin independently of CRM1. *The Journal of cell biology* **171**, 785-797, doi:10.1083/jcb.200502141 (2005).
79 Roose, J. *et al.* Synergy between tumor suppressor APC and the beta-catenin-Tcf4 target Tcf1. *Science* **285**, 1923-1926, doi:Doi 10.1126/Science.285.5435.1923 (1999).
80 Jho, E. H. *et al.* Wnt/beta-catenin/Tcf signaling induces the transcription of Axin2, a negative regulator of the signaling pathway. *Molecular and cellular biology* **22**, 1172-1183, doi:Doi 10.1128/Mcb.22.4.1172-1183.2002 (2002).
81 Spiegelman, V. S. *et al.* Wnt/beta-catenin signaling induces the expression and activity of beta TrCP ubiquitin ligase receptor. *Molecular cell* **5**, 877-882, doi:Doi 10.1016/S1097-2765(00)80327-5 (2000).
82 Diehl, J. A., Cheng, M., Roussel, M. F. & Sherr, C. J. Glycogen synthase kinase-3beta regulates cyclin D1 proteolysis and subcellular localization. *Genes & development* **12**, 3499-3511 (1998).
83 He, T. C. *et al.* Identification of c-MYC as a target of the APC pathway. *Science* **281**, 1509-1512 (1998).
84 Welcker, M. *et al.* Multisite phosphorylation by Cdk2 and GSK3 controls cyclin E degradation. *Molecular cell* **12**, 381-392 (2003).
85 Welcker, M. *et al.* The Fbw7 tumor suppressor regulates glycogen synthase kinase 3 phosphorylation-dependent c-Myc protein degradation. *Proceedings of the National Academy of Sciences of the United States of America* **101**, 9085-9090, doi:10.1073/pnas.0402770101 (2004).
86 Niehrs, C. & Acebron, S. P. Mitotic and mitogenic Wnt signalling. *The EMBO journal* **31**, 2705-2713, doi:10.1038/emboj.2012.124 (2012).
87 Huang, P., Senga, T. & Hamaguchi, M. A novel role of phospho-beta-catenin in microtubule regrowth at centrosome. *Oncogene* **26**, 4357-4371, doi:10.1038/sj.onc.1210217 (2007).
88 Hadjihannas, M. V. *et al.* Aberrant Wnt/beta-catenin signaling can induce chromosomal instability in colon cancer. *Proceedings of the National Academy of Sciences of the United States of America* **103**, 10747-10752, doi:10.1073/pnas.0604206103 (2006).
89 Kikuchi, K., Niikura, Y., Kitagawa, K. & Kikuchi, A. Dishevelled, a Wnt signalling component, is involved in mitotic progression in cooperation with Plk1. *The EMBO journal* **29**, 3470-3483, doi:10.1038/emboj.2010.221 (2010).
90 Olmeda, D., Castel, S., Vilaro, S. & Cano, A. Beta-catenin regulation during the cell cycle: implications in G2/M and apoptosis. *Molecular biology of the cell* **14**, 2844-2860, doi:10.1091/mbc.E03-01-0865 (2003).
91 Davidson, G. *et al.* Cell cycle control of wnt receptor activation. *Developmental cell* **17**, 788-799, doi:10.1016/j.devcel.2009.11.006 (2009).
92 Hadjihannas, M. V., Bernkopf, D. B., Bruckner, M. & Behrens, J. Cell cycle control of Wnt/beta-catenin signalling by conductin/axin2 through CDC20. *EMBO reports* **13**, 347-354, doi:10.1038/embor.2012.12 (2012).
93 Monga, S. P. *et al.* Hepatocyte growth factor induces Wnt-independent nuclear translocation of beta-catenin after Met-beta-catenin dissociation in hepatocytes. *Cancer research* **62**, 2064-2071 (2002).

94 Pagano, M. A., Tibaldi, E., Gringeri, E. & Brunati, A. M. Tyrosine phosphorylation and liver regeneration: A glance at intracellular transducers. *IUBMB life* **64**, 27-35, doi:10.1002/iub.576 (2012).
95 Behari, J. The Wnt/beta-catenin signaling pathway in liver biology and disease. *Expert review of gastroenterology & hepatology* **4**, 745-756, doi:10.1586/egh.10.74 (2010).
96 Gougelet, A. & Colnot, S. A Complex Interplay between Wnt/beta-Catenin Signalling and the Cell Cycle in the Adult Liver. *International journal of hepatology* **2012**, 816125, doi:10.1155/2012/816125 (2012).
97 Yang, J. *et al.* Beta-catenin signaling in murine liver zonation and regeneration: A Wnt-Wnt situation! *Hepatology*, doi:10.1002/hep.27082 (2014).
98 Biechele, T. L. & Moon, R. T. Assaying beta-catenin/TCF transcription with beta-catenin/TCF transcription-based reporter constructs. *Methods Mol Biol* **468**, 99-110, doi:10.1007/978-1-59745-249-6_8 (2008).
99 van de Wetering, M., Oosterwegel, M., Dooijes, D. & Clevers, H. Identification and cloning of TCF-1, a T lymphocyte-specific transcription factor containing a sequence-specific HMG box. *The EMBO journal* **10**, 123-132 (1991).
100 Korinek, V. *et al.* Constitutive transcriptional activation by a beta-catenin-Tcf complex in APC-/- colon carcinoma. *Science* **275**, 1784-1787 (1997).
101 Ferrer-Vaquer, A. *et al.* A sensitive and bright single-cell resolution live imaging reporter of Wnt/ss-catenin signaling in the mouse. *BMC developmental biology* **10**, 121, doi:10.1186/1471-213X-10-121 (2010).
102 Hoogeboom, D. *et al.* Interaction of FOXO with beta-catenin inhibits beta-catenin/T cell factor activity. *The Journal of biological chemistry* **283**, 9224-9230, doi:10.1074/jbc.M706638200 (2008).
103 Klingmuller, U. *et al.* Primary mouse hepatocytes for systems biology approaches: a standardized in vitro system for modelling of signal transduction pathways. *Systems biology* **153**, 433-447, doi:Doi 10.1049/Ip-Syb:20050067 (2006).
104 *Advanced Fluorescence Microscopy*. (Humana Press, 2015).
105 Dueck, D. & Frey, B. J. Non-metric affinity propagation for unsupervised image categorization. *Ieee I Conf Comp Vis*, 198-205 (2007).
106 Subach, F. V. *et al.* Monomeric fluorescent timers that change color from blue to red report on cellular trafficking. *Nature chemical biology* **5**, 118-126, doi:10.1038/nchembio.138 (2009).
107 Munemitsu, S., Albert, I., Rubinfeld, B. & Polakis, P. Deletion of an amino-terminal sequence beta-catenin in vivo and promotes hyperphosporylation of the adenomatous polyposis coli tumor suppressor protein. *Molecular and cellular biology* **16**, 4088-4094 (1996).
108 Hernandez, A. R., Klein, A. M. & Kirschner, M. W. Kinetic Responses of beta-Catenin Specify the Sites of Wnt Control. *Science*, doi:10.1126/science.1228734 (2012).
109 Mak, B. C., Takemaru, K., Kenerson, H. L., Moon, R. T. & Yeung, R. S. The tuberin-hamartin complex negatively regulates beta-catenin signaling activity. *The Journal of biological chemistry* **278**, 5947-5951, doi:10.1074/jbc.C200473200 (2003).

110 Nagai, T. *et al.* A variant of yellow fluorescent protein with fast and efficient maturation for cell-biological applications. *Nature biotechnology* **20**, 87-90, doi:10.1038/nbt0102-87 (2002).
111 Iizuka, R., Yamagishi-Shirasaki, M. & Funatsu, T. Kinetic study of de novo chromophore maturation of fluorescent proteins. *Analytical biochemistry* **414**, 173-178, doi:10.1016/j.ab.2011.03.036 (2011).
112 Gordon, A. *et al.* Single-cell quantification of molecules and rates using open-source microscope-based cytometry. *Nature methods* **4**, 175-181, doi:10.1038/nmeth1008 (2007).
113 Shaner, N. C. *et al.* Improving the photostability of bright monomeric orange and red fluorescent proteins. *Nature methods* **5**, 545-551, doi:10.1038/nmeth.1209 (2008).
114 Khmelinskii, A. *et al.* Tandem fluorescent protein timers for in vivo analysis of protein dynamics. *Nature biotechnology* **30**, 708-714, doi:10.1038/nbt.2281 (2012).
115 Merzlyak, E. M. *et al.* Bright monomeric red fluorescent protein with an extended fluorescence lifetime. *Nature methods* **4**, 555-557, doi:10.1038/nmeth1062 (2007).
116 Shaner, N. C. *et al.* Improved monomeric red, orange and yellow fluorescent proteins derived from Discosoma sp. red fluorescent protein. *Nature biotechnology* **22**, 1567-1572, doi:10.1038/nbt1037 (2004).
117 Wang, L., Jackson, W. C., Steinbach, P. A. & Tsien, R. Y. Evolution of new nonantibody proteins via iterative somatic hypermutation. *Proceedings of the National Academy of Sciences of the United States of America* **101**, 16745-16749, doi:10.1073/pnas.0407752101 (2004).
118 Kishida, S. *et al.* Axin, a negative regulator of the wnt signaling pathway, directly interacts with adenomatous polyposis coli and regulates the stabilization of beta-catenin. *The Journal of biological chemistry* **273**, 10823-10826 (1998).
119 Liu, C. *et al.* Control of beta-catenin phosphorylation/degradation by a dual-kinase mechanism. *Cell* **108**, 837-847 (2002).
120 Morin, P. J. *et al.* Activation of beta-catenin-Tcf signaling in colon cancer by mutations in beta-catenin or APC. *Science* **275**, 1787-1790 (1997).
121 Walther, K. A., Papke, B., Sinn, M. B., Michel, K. & Kinkhabwala, A. Precise measurement of protein interacting fractions with fluorescence lifetime imaging microscopy. *Molecular bioSystems* **7**, 322-336, doi:10.1039/c0mb00132e (2011).
122 von Kries, J. P. *et al.* Hot spots in beta-catenin for interactions with LEF-1, conductin and APC. *Nature structural biology* **7**, 800-807, doi:10.1038/79039 (2000).
123 Schlange, T., Matsuda, Y., Lienhard, S., Huber, A. & Hynes, N. E. Autocrine WNT signaling contributes to breast cancer cell proliferation via the canonical WNT pathway and EGFR transactivation. *Breast cancer research : BCR* **9**, R63, doi:10.1186/bcr1769 (2007).
124 Taniguchi, H. *et al.* Frequent epigenetic inactivation of Wnt inhibitory factor-1 in human gastrointestinal cancers. *Oncogene* **24**, 7946-7952, doi:10.1038/sj.onc.1208910 (2005).

125 Lewis, J. E. *et al.* Cross-talk between adherens junctions and desmosomes depends on plakoglobin. *The Journal of cell biology* **136**, 919-934, doi:Doi 10.1083/Jcb.136.4.919 (1997).
126 Krieghoff, E., Behrens, J. & Mayr, B. Nucleo-cytoplasmic distribution of beta-catenin is regulated by retention. *Journal of cell science* **119**, 1453-1463, doi:10.1242/jcs.02864 (2006).
127 Godoy, P. *et al.* Recent advances in 2D and 3D in vitro systems using primary hepatocytes, alternative hepatocyte sources and non-parenchymal liver cells and their use in investigating mechanisms of hepatotoxicity, cell signaling and ADME. *Archives of toxicology* **87**, 1315-1530, doi:10.1007/s00204-013-1078-5 (2013).
128 Ramboer, E. *et al.* Strategies for immortalization of primary hepatocytes. *Journal of hepatology* **61**, 925-943, doi:10.1016/j.jhep.2014.05.046 (2014).
129 Häussinger, D. *Liver regeneration*. (de Gruyter, 2011).
130 Ding, Y. *et al.* Enrichment of the beta-catenin-TCF complex at the S and G2 phases ensures cell survival and cell cycle progression. *Journal of cell science* **127**, 4833-4845, doi:10.1242/jcs.146977 (2014).
131 Taelman, V. F. *et al.* Wnt signaling requires sequestration of glycogen synthase kinase 3 inside multivesicular endosomes. *Cell* **143**, 1136-1148, doi:10.1016/j.cell.2010.11.034 (2010).
132 Piatkevich, K. D. & Verkhusha, V. V. Guide to red fluorescent proteins and biosensors for flow cytometry. *Methods in cell biology* **102**, 431-461, doi:10.1016/B978-0-12-374912-3.00017-1 (2011).
133 Goentoro, L. & Kirschner, M. W. Evidence that fold-change, and not absolute level, of beta-catenin dictates Wnt signaling. *Molecular cell* **36**, 872-884, doi:10.1016/j.molcel.2009.11.017 (2009).
134 Lustig, B. *et al.* Negative feedback loop of Wnt signaling through upregulation of conductin/axin2 in colorectal and liver tumors. *Molecular and cellular biology* **22**, 1184-1193 (2002).
135 Biechele, T. L., Adams, A. M. & Moon, R. T. Transcription-based reporters of Wnt/beta-catenin signaling. *Cold Spring Harbor protocols* **2009**, pdb prot5223, doi:10.1101/pdb.prot5223 (2009).
136 Kim, S. E. *et al.* Wnt stabilization of beta-catenin reveals principles for morphogen receptor-scaffold assemblies. *Science* **340**, 867-870, doi:10.1126/science.1232389 (2013).
137 Kim, K., Pang, K. M., Evans, M. & Hay, E. D. Overexpression of beta-catenin induces apoptosis independent of its transactivation function with LEF-1 or the involvement of major G1 cell cycle regulators. *Molecular biology of the cell* **11**, 3509-3523 (2000).
138 Rusanov, A. L. *et al.* Lifetime imaging of FRET between red fluorescent proteins. *J Biophotonics* **3**, 774-783, doi:Doi 10.1002/Jbio.201000065 (2010).
139 Jarde, T. *et al.* In vivo and in vitro models for the therapeutic targeting of Wnt signaling using a Tet-ODeltaN89beta-catenin system. *Oncogene* **32**, 883-893, doi:10.1038/onc.2012.103 (2013).
140 Clevers, H., Loh, K. M. & Nusse, R. Stem cell signaling. An integral program for tissue renewal and regeneration: Wnt signaling and stem cell control. *Science* **346**, 1248012, doi:10.1126/science.1248012 (2014).

141 Michalopoulos, G. K. Liver regeneration. *Journal of cellular physiology* **213**, 286-300, doi:10.1002/jcp.21172 (2007).
142 Reinehr, R. & Haussinger, D. CD95 death receptor and epidermal growth factor receptor (EGFR) in liver cell apoptosis and regeneration. *Archives of biochemistry and biophysics* **518**, 2-7, doi:10.1016/j.abb.2011.12.004 (2012).
143 Riehle, K. J., Dan, Y. Y., Campbell, J. S. & Fausto, N. New concepts in liver regeneration. *Journal of gastroenterology and hepatology* **26 Suppl 1**, 203-212, doi:10.1111/j.1440-1746.2010.06539.x (2011).
144 Huch, M. *et al.* In vitro expansion of single Lgr5+ liver stem cells induced by Wnt-driven regeneration. *Nature* **494**, 247-250, doi:10.1038/nature11826 (2013).
145 Sekine, S., Gutierrez, P. J., Lan, B. Y., Feng, S. & Hebrok, M. Liver-specific loss of beta-catenin results in delayed hepatocyte proliferation after partial hepatectomy. *Hepatology* **45**, 361-368, doi:10.1002/hep.21523 (2007).

12 Acknowledgements

My special thanks goes to Prof. Dr. Philippe Bastiaens for his supervision and guidance in a challenging, yet exciting project.

I would like to thank Prof. Dr. Jan Hengstler for taking over the second supervisor position and for his expertise and advice. I also want to acknowledge his group's support when we set up the hepatocyte culture in our lab.

I want to acknowledge Dr. Astrid Krämers contribution, directly by proof-reading my thesis, but also indirectly because for her indispensable efforts in the department.

I really loved the time I spent being part of the "liver project", together with Kirstin Walther, Martin Masip, Sina Koch, Zeta Xouri, Rabea Stockert, Jana Mallah and Lisaweta Roßmannek. Sina, you have proven, that being a scientist and raising a family does not exclude each other. You have my deepest admiration. Zeta, my dear coffee-friend, besides your professional expertise, I miss our coffee-breaks with discussions about german safety guidelines, administration, politics and –of course- Chris. Lisaweta, my Ringberg room mate, we showed that sometimes different personalities are a perfect match.

In addition I want to thank:

Ola Sabet, for continuous support over the last 4 years including her corrections on my thesis and being solid as a rock, while I was freaking out the last month.

Yannick and Martin for calming down the “chicken” office. Dr. Sven Müller, the microscope expert, every company should be jealous for. He saved my life (at least my experiments) more than once and I really admire his patient and dedicated way to deal with us and the chaos we continuously cause. The technicians of the department II, past and present ones including our “lab soul” Nimetka Seloska for their continuous support. Dr. habil Aneta Koseska, for the affinity propagation assay performance and her patience with my deficits in statistical analysis. My practical students: Laura Burbaum, Lisa Niermann and Daniel Hilbig, and of course Franziska Dietrich, for solving the problem with the pre-activation of Wnt signalling during her master thesis. Thanks for your trust in my supervisor qualities. The past and present staff of the department II I met within the time I spent at the MPI, with special regards (but without order) to Jens, Björn, Klaus, Malte, Dina, Katja, Justine, Jenny, Ruth, Hernan, Marton, Jian, Peter, Angel and Tanja.

Walburga Hecker, Birgit’s Bistro, especially Birgit and Sandra, and the permanent employees at the MPI in the central units.

Thorsten, my family and friends for their support, patience and love, while I was absent minded. I hope there is a chance to pay back.